PACIFIC EARTHQUAKE ENGINEERING RESEARCH CENTER

Behavior of Reinforced Concrete Bridge Columns Having Varying Aspect Ratios and Varying Lengths of Confinement

Anthony J. Calderone
KGA Engineers, Inc.
Laguna Beach, California

Dawn E. Lehman
University of Washington, Seattle

and

Jack P. Moehle
University of California, Berkeley

A report on a research project funded by the Federal Highway Administration and the California Department of Transportation under grant no. RTA59X517

PEER 2000/08
JAN. 2001

Behavior of Reinforced Concrete Bridge Columns Having Varying Aspect Ratios and Varying Lengths of Confinement

Anthony J. Calderone
KGA Engineers, Inc.
Laguna Beach, California

Dawn E. Lehman
Department of Civil and Environmental Engineering
University of Washington, Seattle

Jack P. Moehle
Department of Civil and Environmental Engineering
University of California, Berkeley

A research project funded by the
Federal Highway Administration and the California Department of Transportation

PEER Report 2000/08
Pacific Earthquake Engineering Research Center
College of Engineering
University of California, Berkeley
January 2001

Technical Report Documentation Page

1. Report No.	2. Government Accession No.	3. Recipient's Catalog No.
2000/08		

4. Title and Subtitle Behavior of Reinforced Concrete Bridge Columns Having Varying Aspect Ratios and Varying Lengths of Confinement	5. Report Date January 2001 6. Performing Organization Code UCB/ENG-9374
7. Authors Anthony J. Calderone, Dawn E. Lehman, and Jack P. Moehle	8. Performing Organization Report No. UCB/PEER 2000/08
9. Performing Organization Name and Address Pacific Earthquake Engineering Research Center 1301 South 46th Street Richmond, CA 94804	10. Work Unit No. (TRAIS) 11. Contract or Grant No. RTA59X517
12. Sponsoring Agency Name and Address California Department of Transportation Engineering Service Center 1801 30th Street MS#9 Sacramento, CA 95816	13. Type of Report and Period Covered Research Report 7/1/1995 – 12/31/1998 14. Sponsoring Agency Code National Science Foundation

15. Supplementary Notes

16. Abstract

Experience and research on reinforced concrete bridges indicate that relatively stable response to strong ground motions can be obtained if the system is proportioned and detailed so that the predominant inelastic response is restricted to flexure in the column. In this case, it is important to know the strength of the column so that strengths of adjacent components can be set high enough to avoid inelastic action in those components. Details also are required that will enable the column to sustain the necessary inelastic deformations without disabling loss of resistance. Of interest are the configuration and amount of the transverse reinforcement required to sustain expected earthquake demands.

A research program is reported that examines the ductile flexural response of reinforced concrete columns of circular cross section reinforced with spiral reinforcement. The program involved laboratory tests on large-scale columns followed by analysis of the test results. The columns had longitudinal reinforcement ratio of 2.75 percent. Transverse reinforcement varied along the height, being closely spaced near the column ends where inelastic flexure was expected and less closely spaced outside that region. Materials were normal-weight aggregate concrete, with compressive strength around 5000 psi, A706 Grade 60 longitudinal reinforcement, and A82 spiral wire. The columns were tested as cantilevers subjected to constant axial load and cyclic lateral displacements in one plane. Analyses of the data led to conclusions regarding strength, effects of varying the transverse reinforcement along the column height, and deformation capacity including models for computing the deformation capacity.

17. Key Words	18. Distribution Statement
Reinforced concrete, bridges, earthquake engineering, experiments, tests, failure, flexure, strength, deformations, confinement, reinforcement	No restrictions

19. Security Classif. (of this report)	20. Security Classif. (of this page)	21. No. of Pages	22. Price
Unclassified	Unclassified	154	$20.00

Form DOT F 1700.7 (2-86)

ABSTRACT

Experience and research on reinforced concrete bridges indicate that relatively stable response to strong ground motions can be obtained if the system is proportioned and detailed so that the predominant inelastic response is restricted to flexure in the column. In this case, it is important to know the strength of the column so that strengths of adjacent components can be set high enough to avoid inelastic action in those components. Details also are required that will enable the column to sustain the necessary inelastic deformations without disabling loss of resistance. Of interest are the configuration and amount of the transverse reinforcement required to sustain expected earthquake demands.

A research program is reported that examines the ductile flexural response of reinforced concrete columns of circular cross section reinforced with spiral reinforcement. The program involved laboratory tests on large-scale columns followed by analysis of the test results. The columns had a longitudinal reinforcement ratio of 2.75 percent. Transverse reinforcement varied along the height, being closely spaced near the column ends where inelastic flexure was expected and less closely spaced outside that region. Materials were normal-weight aggregate concrete, with compressive strength around 5000 psi, A706 Grade 60 longitudinal reinforcement, and A82 spiral wire. The columns were tested as cantilevers subjected to constant axial load and cyclic lateral displacements in one plane. Analyses of the data led to conclusions regarding strength, effects of varying the transverse reinforcement along the column height, and deformation capacity including models for computing the deformation capacity.

ACKNOWLEDGMENTS

The authors wish to express their gratitude to the Federal Highway Administration (FHWA), Grant No. RTA-59X517, for sponsoring this project. Specifically, the contributions of Nancy Bobb and Phillip Yen are gratefully acknowledged. The project benefited greatly from day-to-day review and advice by Kelly Holden of the California Department of Transportation. Ray Zelinski of Caltrans provided valuable review comments. Opinions, findings, and conclusions expressed in this report are those of the authors and do not necessarily reflect the views of the project sponsors. This work was supported by the Pacific Earthquake Engineering Research Center through the Earthquake Engineering Research Centers Program of the National Science Foundation under Award number EEC-9701568.

In addition to the aforementioned, the authors wish to acknowledge the many individuals who contributed to the successful completion of this project: Silvia Mazzoni for her assistance in analytical modeling and patience in teaching use of software; the staff of undergraduate students for gaging the steel reinforcement; Jim Kirkwald of Canyon Construction for his attention to detail during the construction process; and Wesley Neighbour for his advice, support, and expertise during experimental testing. Special recognition is due to Adrian Nacamuli who worked beyond the call of duty and trained all of us in the preparation of the specimens for testing.

This report was prepared in partial fulfillment of the requirements for the Master of Engineering degree at the University of California, Berkeley, of the first author under the direction of the other authors. The first author thanks his family for their support and encouragement during the many late nights and weekends spent away from home while working toward the completion of this project.

CONTENTS

LIST OF FIGURES

LIST OF TABLES

LIST OF SYMBOLS

a	Column shear span
A_c	Area of concrete core, measured between centerlines of spiral reinforcement
A_e	Effective area of column cross section
A_g	Gross area of column cross section
A_{sp}	Nominal area of spiral reinforcement
b_w	Effective width of column cross section = D
c	Depth of compression zone in cross-sectional analysis
D	Gross diameter of column
d	Effective depth of column cross section = 0.8D
D'	Core diameter of column cross section measured between centerlines of spiral reinforcement
d_b	Diameter of longitudinal bar
d_{bl}	Nominal diameter of longitudinal bar
E_c	Elastic modulus of concrete
f'_c	Nominal or specified concrete compressive strength
f'_{cc}	Compression strength of confined concrete
f'_{ce}	Expected concrete compressive strength
F_{cr}	Cracking force demand
f_y	Nominal yield strength of longitudinal steel
f_{ye}	Expected yield strength of longitudinal steel
f_{yh}	Nominal yield strength of hoop reinforcement
G_c	Effective shear modulus of concrete
L	Column length
l_c	Length of column between point of maximum moment demand and point of zero moment
l_p	Plastic hinge length
M_{cr}	Cracking moment demand
M_n	Nominal moment strength of column cross section
M_p	Plastic moment demand
M_u	Ultimate moment strength of column cross section
M_y	Moment demand corresponding to first yield of the longitudinal steel
P_e	Expected column axial load
s	Spacing between spiral hoops
V_c	Shear strength of column cross section attributed to concrete
v_c	Unit shear strength of column cross section attributable to concrete
V_n	Column shear strength
	In Lehman model, shear demand corresponding to a compressive strain demand of 0.003 in
v_n	Unit shear strength of column cross section
V_p	Plastic shear demand
V_s	Shear strength attributed to spiral reinforcement
v_s	Unit shear strength of column cross section attributable to transverse steel
$V_{s\ req'd}$	Shear strength required of spiral reinforcement

Δ'_{fy}	Component deformation due to flexure at yield of column cross section
Δ'_{sy}	Component deformation due to slip at yield of column cross section
Δ'_{vy}	Component deformation due to shear at yield of column cross section
Δ'_{y}	Displacement of column at yield of column cross section
Δ_{cr}	Displacement of column at cracking of cover concrete
Δ_{fp}	Component plastic deformation due to flexure
Δ_{p}	Plastic displacement of column
Δ_{sp}	Component plastic deformation due to slip
Δ_{u}	Ultimate displacement of column
ε_{cu}	Ultimate compressive strain of confined concrete
ϕ'_{y}	Effective yield curvature of column cross section
ϕ_{cr}	Curvature of column cross-section at cracking of cover concrete
ϕ_{u}	Ultimate curvature of column cross section
ϕ_{y}	Yield curvature of column cross section
ρ_{l}	Longitudinal steel reinforcement ratio
ρ_{s}	Transverse steel reinforcement ratio

1 Introduction

1.1 BACKGROUND

Figure 1.1: Failed Bull Creek Column

The 1994 Northridge, California, earthquake exposed the seismic vulnerability of several reinforced concrete bridges. The Bull Creek Canyon Channel Bridge, constructed in 1976, was one example. The transverse reinforcement details within the concrete columns supporting the bridge consisted of two distinct zones of confinement. A well-confined zone (spacing of transverse steel equal to one-sixteenth of the column depth) was located at each column end, and a lightly confined zone (spacing of transverse steel equal to one-fourth of the column depth) was constructed between the column ends. These columns sustained significant damage in the vicinity of the transition between the well-confined and lightly confined regions. The observed distress included significant degradation of the column core, longitudinal reinforcement buckling, and fractured transverse reinforcement (Figure 1.1). Diagonal cracking and flexural cracking were also apparent. It has been suggested that a continuation of the smaller spiral spacing throughout the column height would have enhanced the ductile behavior of the column.

Since the 1989 Loma Prieta, California, earthquake, the Caltrans Bridge Design Specifications (BDS) [1993] have typically required continuous transverse steel at a constant spacing throughout the column height. In 1996, the Applied Technology Council (ATC) [ATC-32, 1996] proposed revisions and recommendations to the current BDS regarding the design and construction of bridges. For spirally reinforced circular-cross-section columns, the amount of transverse reinforcement required by ATC-32 inside the zone of potential plastic hinging is considerably greater than that required by the BDS. However, ATC-32 allows the transverse reinforcement spacing to be relaxed by one-half outside the zone of plastic hinging. Furthermore, for columns with an aspect ratio greater than 3.0, the plastic-hinge confinement length prescribed by ATC-32 is approximately 40 percent less than that required by the BDS.

1.2 STATEMENT OF PURPOSE

There has been considerable debate regarding whether changing the transverse reinforcement ratio within a column and prescribing a relatively short length of confinement for plastic hinging is a prudent design practice. Given the number of bridges constructed in the 1970s with details similar to those of the Bull Creek structure, as well as the ATC-32 [1996] recommendations, it is of interest to ascertain the behavioral effects of changing the transverse reinforcement ratio along the length of a column. Furthermore, while a considerable amount of experimental research has been performed regarding the behavior of reinforced concrete columns, very little research has been performed to study the behavior of slender columns. Of particular interest are the extent of inelasticity along the column height (and, hence, the length along which confinement is required), the achievable ductility under reversed cyclic loading, and the applicability of current design tools (which are largely based on the experimental results of short columns) toward predicting the load-displacement response of slender columns.

The objectives of this experimental research program were threefold:

1. To explore the ductile behavior of reinforced concrete columns designed with two distinct zones of confinement.
2. To compare the cyclic behavior of a reinforced concrete column designed with typical 1970s reinforcement details with that of a reinforced concrete column designed in accordance with current Caltrans design practice.

3. To observe the plastic hinging behavior of slender columns, and identify applicable design requirements.

To achieve these objectives, laboratory testing of four half-scale column specimens was conducted. This report describes the design procedures and test objectives of the four test specimens, reviews the data and observations obtained during experimental testing, and examines predictive models for assessing the shear strength and load-displacement response of reinforced concrete columns with varying aspect ratios and two zones of confinement.

2 Experimental Program

2.1 GENERAL DESCRIPTION OF TEST PROGRAM

The experimental program consisted of four test specimens intended to represent half-scale models of typical bridge columns. The design of each test specimen was based on a full-scale prototype bridge column. The cross-sectional dimensions, longitudinal reinforcement ratio, material properties, and column axial load ratio remained constant throughout the testing program; the Bull Creek columns were used as a reference for these parameters. The primary variables in the testing program were the column aspect ratio and the varied zones of confinement provided by the transverse steel. The test specimens were scaled down based on the final design of each prototype column.

The longitudinal reinforcement in each prototype column consisted of 50 No. 9 bars spaced evenly around the column perimeter. A No. 5 spiral and 2 inches of clear cover concrete confined the column core. The applied vertical load was determined to be approximately 9 percent of the gross cross-section strength of the column (0.092 $A_g f'_c$, where A_g is the gross cross-sectional area of the column and f'_c is the nominal concrete compressive strength). A sketch of the prototype column cross section is shown in Figure 2.1.

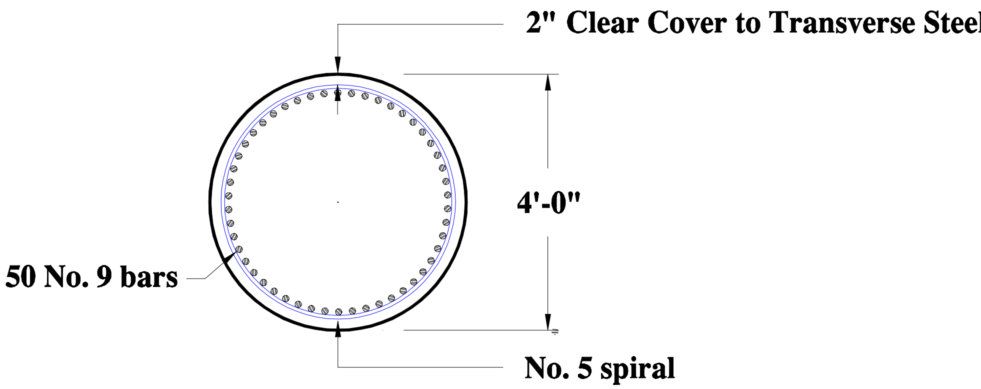

Figure 2.1: Prototype Cross Section of Column

Each column in the experimental program was given an identification number that denoted the column aspect ratio and longitudinal reinforcement ratio. Because each column contained a longtudinal reinforcement ratio of 2.75 percent, the last two digits in the identification number for each column are -28. The first digit(s) account for the column aspect ratio, 3, 8, and 10. The two columns with an aspect ratio of 3 were distinguished from each other by an additional "T" at the end of the identification number for Column 328T, which means that the column contained a transition in the amount of transverse steel provided. The identification numbers for the four columns in the experimental program were 328, 328T, 828, and 1028.

2.2 DESIGN OF PROTOTYPE COLUMNS

2.2.1 Design Criteria

Column 328 was designed in accordance with the provisions of the current Caltrans Bridge Design Specifications [BDS, 1993]. The transverse reinforcement for this column was provided at a constant spacing throughout the column height. This column served as a baseline for comparison for Column 328T, which was designed with transverse reinforcement details similar to those used in the 1970s. Specifically, two zones of confinement were prescribed for Column 328T.

The design of Columns 828 and 1028 was based on the requirements of the Applied Technology Council Improved Seismic Design Criteria for California Bridges — Provisional Recommendations [ATC-32, 1996]. ATC-32 prescribes two zones of confinement for slender columns. In both test specimens, the transverse steel required inside and outside the "plastic end region" of the column was based on the minimum requirements for achieving a curvature ductility of at least 13. Note that strength-reduction factors were not used in the design and evaluation of the test specimens because the controls placed on material strengths, workmanship, and dimensional tolerances were believed to be adequate to avoid understrength.

2.2.2 Material Strengths for Design

The BDS employ nominal (specified) material strengths in the analysis of bridge columns. ATC-32 also uses nominal material strengths in the analysis of bridge columns except when analyzing the design flexural strength; in that case, the "expected" material strengths are used. Table 2.1 summarizes the material properties used in the analysis and design of prototype Columns 328, 828, and 1028.

The design of Prototype Column 328T was based largely on the anticipated force demands determined from a moment-curvature analysis of the prototype column cross section. The effects of reinforcement strain hardening and confinement of the concrete core were considered in the analysis. Stress-strain relationships developed by Todeschini [1964] and Mander [1988] were used to model the unconfined and confined concrete, respectively. An assumed stress-strain history for the longitudinal reinforcement was based on the results of material testing performed by Mazzoni [1997]. The concrete and steel stress-strain relationships used in this analysis are shown in Figure A.1 of Appendix A. Note that the actual material properties of the test specimens differ from those used in design.

Table 2.1: Material Properties

Material	Specified (psi)	BDS (psi)	ATC-32 (psi)
Steel Reinforcement			
Longitudinal	$f_y = 60{,}000$	$f_y = 60{,}000$	$f_y = 66{,}000$ $f_{ye} = 66{,}000$
Transverse	$f_y = 60{,}000$	$f_y = 60{,}000$	$f_{yh} = 60{,}000$
Concrete	$f'_c = 4{,}000$	$f'_c = 4{,}000$	$f'_c = 4{,}000$ $f'_{ce} = 5{,}200$
Column Designation		328	828 and 1028

2.2.3 Design of Prototype 328

The nominal and plastic moment strengths of the prototype column for Specimen 328 were calculated in accordance with BDS Paragraphs 8.16.2 and 8.16.4 [1993]. In calculating the nominal flexural strength of the columns, the maximum allowable unconfined concrete strain was limited to 0.003. The nominal moment strength (M_n) was then factored by 1.3 to obtain the plastic moment strength (M_p). M_n and M_p for the prototype column of Specimen 328 were estimated to be 5050 kip-feet and 6565 kip-feet, respectively.

The ultimate shear demand (V_p) on the prototype column was determined by dividing M_p by the shear span, 12 feet. The following equations were used to estimate the shear strength contribution attributed to the concrete and the shear strength required of the transverse steel, in accordance with BDS Section 8.16.6.

$$V_{\mathrm{p}} = V_c + V_s \qquad \text{(Eq. 2-1)}$$

$$V_c = 2\left[1 + \frac{P_e}{2000 \cdot A_g}\right]\sqrt{f'_c} \cdot b_w d \qquad \text{(Eq. 2-2)}$$

$$V_{s \cdot req'd} = V_p - V_c \qquad \text{(Eq. 2-3)}$$

The values for V_p, V_c, $V_{s\,req'd}$ are 547 kips, 289 kips, and 258 kips, respectively.

The amount of transverse reinforcement provided in Columns 328 was based on the following minimum requirements determined from BDS Equation 8-53, Equation 8-62, and Paragraph 8.18.2.2.2 [1993], respectively:

$$V_{s \cdot req'd} = \frac{2A_{sp} f_y D'}{s} \qquad \text{(Eq. 2-4)}$$

$$\rho_s = 0.45\left(\frac{A_g}{A_c} - 1\right)\frac{f_c'}{f_y} \qquad \text{(Eq. 2-5)}$$

$$\rho_s = 0.12\frac{f_c'}{f_y}\left(0.5 + 1.25\frac{P_e}{f_c' A_g}\right) \qquad \text{(Eq. 2-6)}$$

Based on Equation 2-4, the controlling requirement, a minimum transverse reinforcement spacing of 5 inches was required.

2.2.4 Design of Prototype 328T

Prototype column 328T was designed with typical 1970s transverse reinforcement details, similar to those of the Bull Creek columns. The column was designed with two distinct zones of confinement, a well-confined zone within the plastic end region of the column and a lightly confined intermediate zone. The transverse reinforcement details within the well-confined zone, extending over a length of one column diameter, were the same as those of Specimen 328.

The design of the transverse reinforcement in the intermediate zone was based on achieving a shear demand-capacity ratio of one. The design objective was to achieve a theoretically balanced shear-flexure failure mechanism at the point of transition between the well-confined and lightly confined regions. The anticipated shear demand was determined from a moment-curvature analysis performed on the prototype column cross section. Given the design shear demand of 625 kips, the transverse reinforcement required inside the lightly confined region was determined using the BDS shear strength equations, neglecting minimum reinforcement requirements. The analysis was based on anticipated values of the compressive strength of the concrete (5200 psi) and yield strength of the transverse steel (85,000 psi).

Once the shear reinforcement was determined in the lightly confined region, an additional moment-curvature analysis of the cross section was performed to ensure that sufficient flexural strength was provided. Given the results of these analyses, it was determined that a spiral pitch of 9 inches in the intermediate zone of the prototype column would achieve the desired objective of a balanced failure mechanism at the transition of the spiral pitch.

2.2.5 Design of Prototypes 828 and 1028

The prototype columns for Specimens 828 and 1028 were designed in accordance with the provisions of ATC-32 [1996]. The nominal and plastic moment strengths of the prototype columns were calculated in accordance with Paragraphs 8.16.2 and 8.16.4. In calculating the nominal flexural strength of the columns, the maximum allowable unconfined concrete strain was limited to 0.004. The nominal moment strength (M_n) was factored by 1.4 to estimate the plastic moment strength (M_p). M_n and M_p for Columns 828 and 1028 were calculated to be 5800 kip-feet and 8120 kip-feet, respectively.

The ultimate shear demand on each prototype column (V_p) was determined by dividing M_p by the column shear span, 32 feet and 40 feet for Columns 828 and 1028, respectively. The ATC-32 equations listed below were used to calculate the concrete shear strength within each column. Nominal material strengths were used in the analysis of the column shear strength,

$$V_c = 2\left(0.5 + \frac{P_e}{2000A_g}\right)\sqrt{f_c'}A_e \quad \text{...inside } L_p \qquad \text{(Eq. 2-7)}$$

$$V_c = 2\left(1 + \frac{P_e}{2000A_g}\right)\sqrt{f_c'}A_e \quad \text{...outside } L_p \qquad \text{(Eq. 2-8)}$$

where $A_e = 0.8\ A_g$. Note that ATC-32 provides separate values for calculating the concrete shear strength inside and outside the zone of potential plastic hinging, defined above as length L_p. ATC-32 defines the plastic hinge zone for a column as being the greater of (a) the section dimension in the direction of loading considered and (b) that portion of the column over which the moment exceeds 80 percent of the maximum expected moment. Thus, for Specimens 828 and 1028, L_p was determined to be 36 inches and 48 inches, respectively.

The amount of transverse reinforcement required for shear strength in Columns 828 and 1028 was determined using the following equations:

$$V_{s\cdot req'd} = V_p - V_c \qquad \text{(Eq. 2-9)}$$

$$V_{s\cdot req'd} = \frac{\pi}{2}\frac{A_{sp} f_y D'}{s} \qquad \text{(Eq. 2-10)}$$

For Columns 828 and 1028, the curvature ductility requirements of ATC-32 Paragraphs 8.18.2.2.2 and 8.18.2.2.3 controlled the amount of transverse steel required inside and outside the column plastic end region. The minimum amount of transverse reinforcement required was determined as follows:

$$\rho_s = 0.16\frac{f'_{ce}}{f_{ye}}\left[0.5 + 1.25\frac{P_e}{f'_{ce}A_g}\right] + 0.13(\rho_l - 0.01) \quad \text{...inside } L_p \qquad \text{(Eq. 2-11)}$$

$$\rho_s = 0.5\left\{0.16\frac{f'_{ce}}{f_{ye}}\left[0.5 + 1.25\frac{P_e}{f'_{ce}A_g}\right] + 0.13(\rho_l - 0.01)\right\} \quad \text{...outside } L_p \qquad \text{(Eq. 2-12)}$$

With the exception of the second term, the equation for ρ_s inside the plastic hinge zone is similar to the provision in the current BDS Section 8.18.2.2.2 [1993]. This provision is intended to ensure that the column section will have a dependable section curvature ductility capacity (ϕ_u/ϕ_y) of at least 13.

Table 2.2 summarizes the transverse reinforcement required within the prototype columns based on the various requirements.

Table 2.2: Hoop Reinforcement Required

Column	Transverse Steel inside P.H. zone	Transverse Steel outside P.H. zone
328	No. 5 spiral @ 5" pitch	No. 5 spiral @ 5" pitch
328T	No. 5 spiral @ 5" pitch	No. 5 spiral @ 9" pitch
828	No. 5 spiral @ 3" pitch	No. 5 spiral @ 6" pitch
1028	No. 5 spiral @ 3" pitch	No. 5 spiral @ 6" pitch

Because the primary test objective was to determine the effects of varied zones of confinement and aspect ratio on column behavior, it was decided that the transverse reinforcement ratio should remain constant within the plastic hinge zone. Thus, a default spacing of 3 inches for the spiral was used in the plastic end region of each column, as well as throughout the height of Column 328. The transverse reinforcement provided in each prototype column is summarized in Table 2.3.

Table 2.3: Hoop Reinforcement Provided

Column	Transverse Steel inside P.H. zone	Transverse Steel outside P.H. zone
328	No. 5 spiral @ 3" pitch	No. 5 spiral @ 3" pitch
328T	No. 5 spiral @ 3" pitch	No. 5 spiral @ 9" pitch
828	No. 5 spiral @ 3" pitch	No. 5 spiral @ 6" pitch
1028	No. 5 spiral @ 3" pitch	No. 5 spiral @ 6" pitch

2.3 TEST SPECIMEN DESIGN DETAILS

The test specimens were one-half scale representations of the prototype columns. All geometries were scaled, as closely as practicable, by one half. The longitudinal and transverse reinforcement of the prototype columns consisted of No. 9 bars and No. 5 bars, respectively. In the test specimens, No. 6 bars and No. 2 spirals were used for the longitudinal and transverse steel, respectively. Although a No. 5 bar scales more closely by one-half relative to a No. 9 bar, the number of bars required created concerns regarding constructibility. Therefore, to reduce congestion of reinforcement around the critical section of the column, No. 6 bars were chosen instead. The number of bars was adjusted to achieve approximately the target longitudinal reinforcement ratio of 0.028.

A brief summary of the overall geometry and details of the column test specimens is presented in Table 2.4. The column test specimens have a nominal 1-inch-thick concrete cover surrounding the spiral hoop.

Table 2.4: Test Specimen Reinforcement

Column	Height	Diameter	Long. Bars	Transverse Steel inside P.H. zone	Transverse Steel outside P.H. zone
328	6'-0"	2'-0"	28 – No. 6	No. 2 @1" pitch	No 2 @ 1" pitch
328T	6'-0"	2'-0"	28 – No. 6	No. 2 @1" pitch	No 2 @ 3" pitch
828	16'-0"	2'-0"	28 – No. 6	No. 2 @1" pitch	No 2 @ 2" pitch
1028	20'-0"	2'-0"	28 – No. 6	No. 2 @1" pitch	No 2 @ 2" pitch

The test specimens were founded atop a reinforced concrete anchor block that was 4 feet by 8 feet in plan and 2 feet deep. The column longitudinal reinforcement was continuous into the anchor block, representing a rigid moment-resisting connection. The reinforcement details within the anchor block were designed to preclude primary inelastic action from occurring within the block. Construction drawings, details, and specifications used in the steel fabrication and construction of the test specimens are presented in the Appendix B.

2.4 MATERIALS USED IN CONSTRUCTION OF TEST SPECIMENS

2.4.1 Steel

With the exception of the spiral reinforcement, all reinforcing steel used to construct the test specimens consisted of Grade 60 deformed bar conforming to the American Society of Testing and Materials (ASTM) Designation A706. The spiral reinforcement consisted of smooth bar conforming to ASTM Designation A82. The use of smooth A82 bar in the test specimens was necessitated by two factors: (a) Caltrans Standard Specifications [CSS, 1992] require that spiral reinforcement in structures conform to the specifications of ASTM Designation A82 for wire or

ASTM Designation A615, Grade 60 for deformed bar and (b) No. 2, A615, Grade 60 rebar is readily available only in 20 foot lengths, requiring numerous, undesirable splices. The steel reinforcement for all four columns was ordered at the same time, and each steel type was manufactured from the same batch and heat to maintain consistency.

Three material samples each of the No. 6, A706, Grade 60 column longitudinal steel and the No. 2, A82 smooth bar spiral were supplied in addition to the steel reinforcement used to construct the test specimens. The material samples were manufactured from the same batch and heat as the reinforcement used in the columns. The samples were machined into coupons and tested in tension to obtain stress versus strain relationships. These relationships were subsequently used in a moment-curvature analysis to evaluate the behavior of the test specimens. The stress versus strain relationships for the test coupons are presented in Figure A.2 of Appendix A.

2.4.2 Concrete

Normal weight concrete was used to construct the test specimens. The target parameters of the design concrete mix are provided in Table 2.5. The quantities of the components in the target mix design are provided in Table 2.6.

Table 2.5: Concrete Mix Design Parameters

28-Day Strength	4000 psi, not to exceed 5500 psi
Water/Cement Ratio	0.530
Cement Type	ASTM C-150 Type II (6 sacks)
Slump	5" +/- 1"
Water-reducing Agent	ASTM C-494 Type A
Retarder	ASTM C-494 Type D
Maximum Aggregate Size	3/8"

Table 2.6: Target Mix Component Volumes and Weights

Material	Target Volume	Target Weight
3/8″ Coarse Aggregate	7.47 ft^3	1250 lbs
Regular Top Sand	8.25 ft^3	1374 lbs
Blend Sand	3.21 ft^3	521 lbs
Cement	2.87 ft^3	564 lbs
Water: 36 gallons	4.79 ft^3	299 lbs
Admixtures: Water-reducing Agent Retarder	0.41 ft^3	11.3 fl. oz. 16.9 fl. oz.
TOTAL:	27 ft^3	4009 lbs

For all concrete batches, standard compression testing of 6-inch by 12-inch concrete cylinders was performed at approximately 7-day intervals up to 28 days. Compression and split-tension tests were also performed on the concrete cylinders within a few days after the completion of a test; the stress versus strain relationships for the compression tests are presented in Figure A.3 of Appendix A.

The concrete cylinders were stored adjacent to the actual test specimens, ensuring that each cylinder would be exposed to the same external environmental conditions as the actual specimens during curing. The molds for the concrete cylinders of the column elements were removed from each cylinder after 7 days of curing, in conjunction with the removal of the column formwork of the actual test specimens. The concrete cylinders representative of the anchor block concrete remained in the cylinder molds until the time of material testing. This was done to represent the curing of the concrete inside the column-anchor block joint, which is heavily confined by the surrounding concrete and is not readily exposed to the environment.

2.5 CONSTRUCTION PROCEDURE

The steel used in the construction of the test specimens was cut and bent by a local steel fabricator before being delivered to the job site. A local contractor and the steel fabricator constructed the specimens at the Richmond Field Station, University of California, Berkeley.

Concrete formwork for the anchor blocks was constructed of dimensioned lumber and plywood. The assembly of the steel cages began with the placement of the bottom mat of reinforcing steel into the anchor block form. Next, the column cages were assembled on chairs (Figure 2.2) and were subsequently lifted to an upright position and placed atop the bottom mat of reinforcing steel within the anchor block. Once the column steel was aligned, plumbed, and secured in the anchor block, the top mat of anchor block reinforcing steel was woven through the column cage and tied into place. Lifting anchors were placed in the anchor block to enable moving of the specimens into the test bay. Concrete was placed into the anchor block formwork with the aid of a pump and mechanical vibrators. The exposed surface of the anchor block was finished with a smooth trowel and covered with saturated carpet and plastic for a period of seven days.

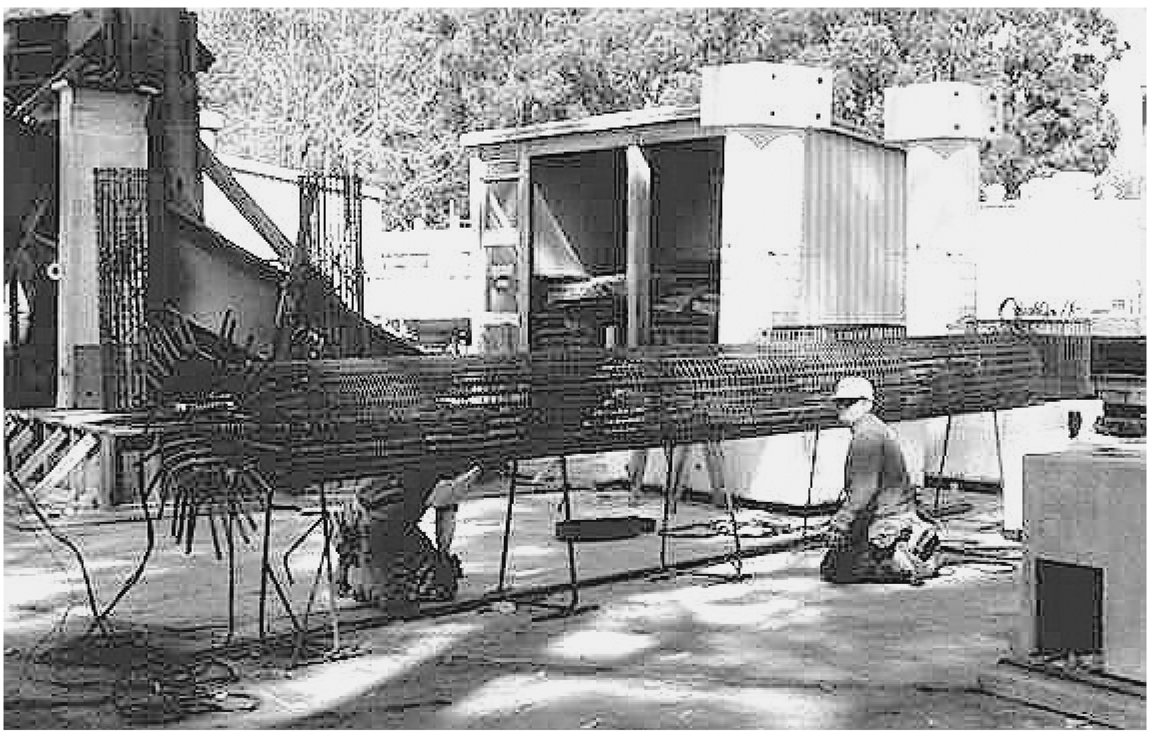

Figure 2.2: Assembly of Steel Cage for Column 1028 (note steel cages for Columns 328 and 328T in background)

A few days after placement of the anchor block concrete, a 2-foot diameter Burke heavy wall tube was placed over each column cage to serve as formwork. Prior to the installation of the Burke tubes, 1-inch-thick concrete dobies were tied to the exterior of the column cage to maintain a uniform cover over the column height. Holes were drilled into the tubes to allow for the insertion of the instrumentation rods. These holes were sealed with pipe insulation to prevent leakage during concrete placement. As a result, small impressions remained in the finished surface of the concrete at the location of each instrumentation rod. Each column form was reinforced with wood bracing and metal banding straps to resist hydrostatic pressure during placement of the concrete. Concrete was placed into the column forms with the aid of a pump and mechanical vibrators. The column formwork was removed after a curing period of seven days (Figure 2.3).

Figure 2.3: Anchor Block and Steel Cage for Columns 328 and 328T

2.6 INSTRUMENTATION OF TEST SPECIMENS

Each test specimen was instrumented with potentiometers and strain gages to monitor global, local, and internal deformations during testing. Internally, TML YFLA-5 electrical resistance strain gages with a gage factor of 2.14 were installed on the extreme longitudinal steel bar at the north and south faces of the column. These gages were placed on the side of the longitudinal bar parallel to the direction of loading.

TML FLK-1-11 electrical resistance strain gages with a gage factor of 2.11 were installed on the spiral reinforcement at the north, south, and east column faces. These gages were placed on the exterior face of the spiral. Prior to installation of the gages, the steel reinforcement was filed by hand to expose a smooth surface, free of mill scale, scratches, protrusions, and other imperfections. The strain gages were then attached to the steel reinforcement with adhesive. Electrical wire cable, running from the data acquisition system, was soldered to each gage terminal. All gages on the longitudinal bars were installed prior to the fabrication of the reinforcing cages. The spiral gages were installed after fabrication of the cages.

Externally, analog linear potentiometers with either a 1-inch or 2-inch stroke were installed to monitor vertical and shear deformations. The potentiometers were mounted on steel rods that passed horizontally through the column cross section and were cast into the column. The rods were encased in vinyl sleeves to inhibit bond with the surrounding concrete, although a 3-inch-long segment at the center of the rod remained exposed as necessary to fix the rods within the concrete and to prevent the rods from slipping during testing. In general, the location of the internal and external instrumentation coincided at the same level, which was determined to be a multiple of the column diameter. Figures 2.4 through 2.6 show the internal and external instrumentation layout for the four columns in the test series.

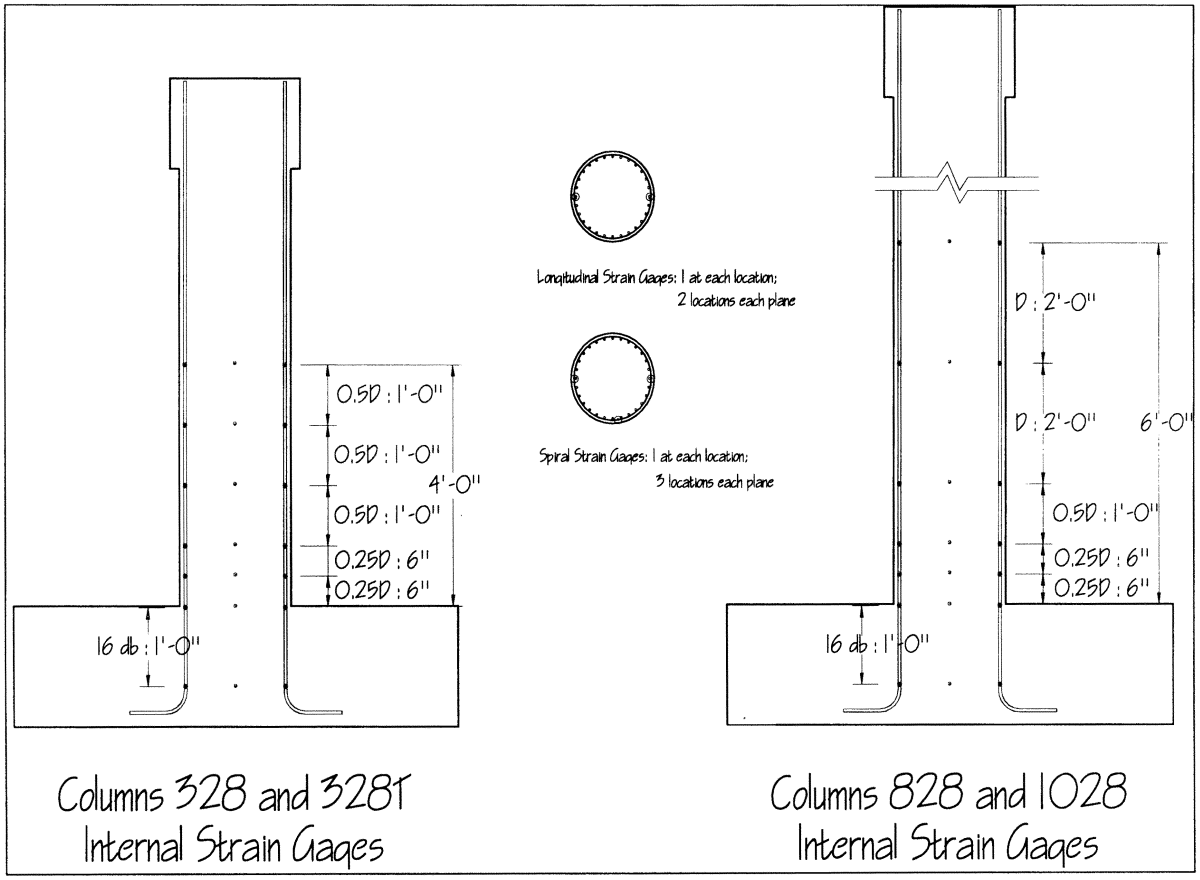

Figure 2.4: Internal Instrumentation

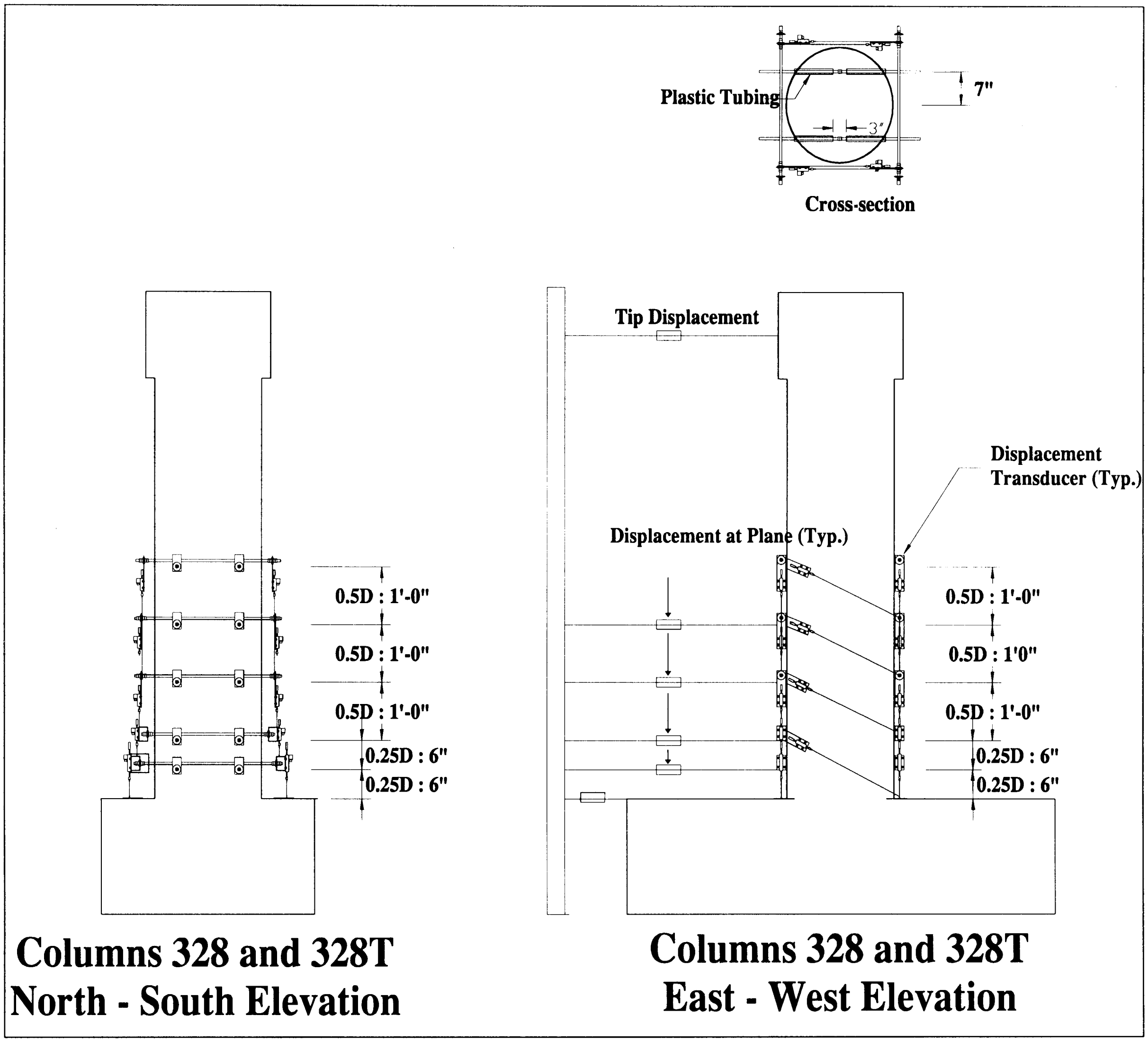

Figure 2.5: External Instrumentation for Columns 328 and 328T

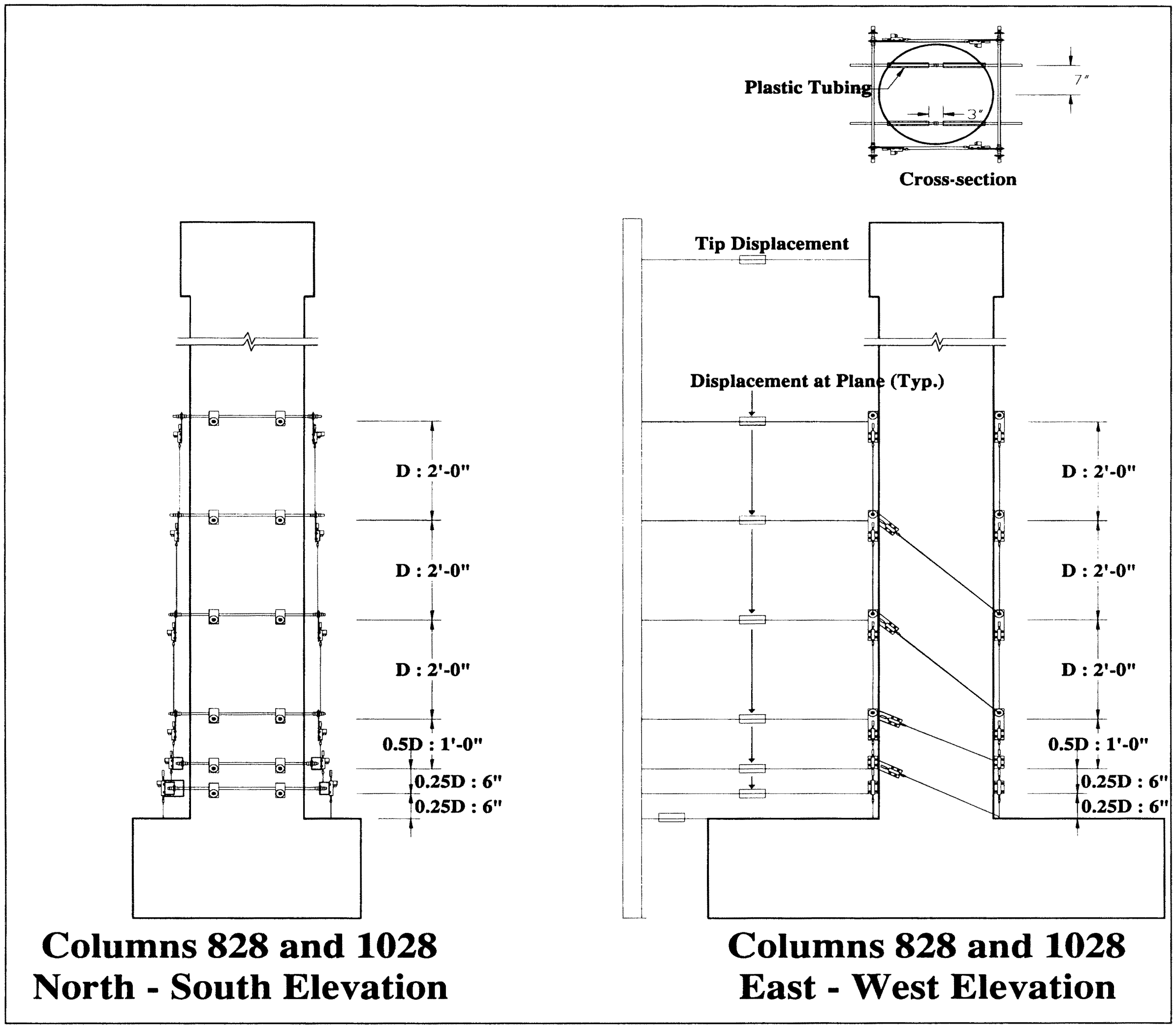

Figure 2.6: External Instrumentation for Columns 828 and 1028

The global horizontal displacement of the column tip was measured using either a linear variable differential transformer (LVDT) or a direct current differential transformer (DCDT) in the small displacements range; wire potentiometers were used in the large displacements range. These instruments were attached to an instrumentation column, isolated from the test specimen and the loading frame. An X-Y plotter was used to monitor the lateral load-displacement relationship of the column during testing. Global horizontal displacements were measured at various other levels of the column using linear and wire potentiometers mounted to the instrumentation column. Global rotation of the anchor block, column, and axial load spreader beam were measured using clinometers.

The Neff System 620 Data Acquisition System (Neff) was used to interpret the signals provided by each instrumentation channel and to convert the signals into digital information. A PC-type computer, interfaced with the Neff, was used to record the channel information during testing. DAS85, a DOS-based data acquisition software program, was used to process the incoming data. Utilizing this computer application, all data readings taken during testing were stored to a data file.

2.7 TEST SETUP

Prior to testing each column, the NEFF was used to calibrate the external and internal instrumentation. Calibration of the internal strain gages was accomplished by shunting a resistor across the strain gage channels and then verifying the corresponding strain value readings for each gage. By taking readings before and after this calibration process, it was possible to ascertain whether the strain gages were stable and operating properly. The channels that were determined to be unstable during calibration were removed from the system; thus, no data were recorded for the gages corresponding to the unstable channels.

Calibration of the linear and wire potentiometers was accomplished through a calibration process within the DAS85 program shell. Calibration blocks were used to move the plunger to three independent predetermined displacements. Recording the signals processed by the Neff for the three displacements, DAS85 calculated the appropriate calibration factor for the potentiometer. The calibration factors were verified through a similar process of moving the potentiometer plunger to a predetermined displacement and by comparing the known displacement value to the value read by the data acquisition system.

The axial load was applied through two high-strength rods, located on the east and west sides of the column, attached to a spreader beam spanning across the column top. Each rod was connected in series to a loading jack, a load cell, and a clevis attached to the laboratory floor. The axial load was reacted into the concrete strong floor via steel post-tension rods anchored through the floor. Each loading jack was controlled by a pneumatic pump that was operated manually during testing. The load cells were used to monitor the applied axial load during testing.

The simulated earthquake loading was applied through a horizontal actuator connected to the column top. The lateral force was applied under displacement control in a reversed, cyclic manner. The applied lateral load was reacted against a steel reaction frame connected to the laboratory strong floor. A load cell was placed in series with the actuator to monitor the applied load during testing.

A schematic representation of the laboratory test set up is shown in Figure 2.7. The columns were tested in the upright position. The horizontal load was applied to the free end of the column, and the top of the column was free to translate and rotate. The anchor block was secured to the laboratory floor with post-tensioning rods. The rods were placed on the north and south sides of the column at a distance of 3 feet from the column center.

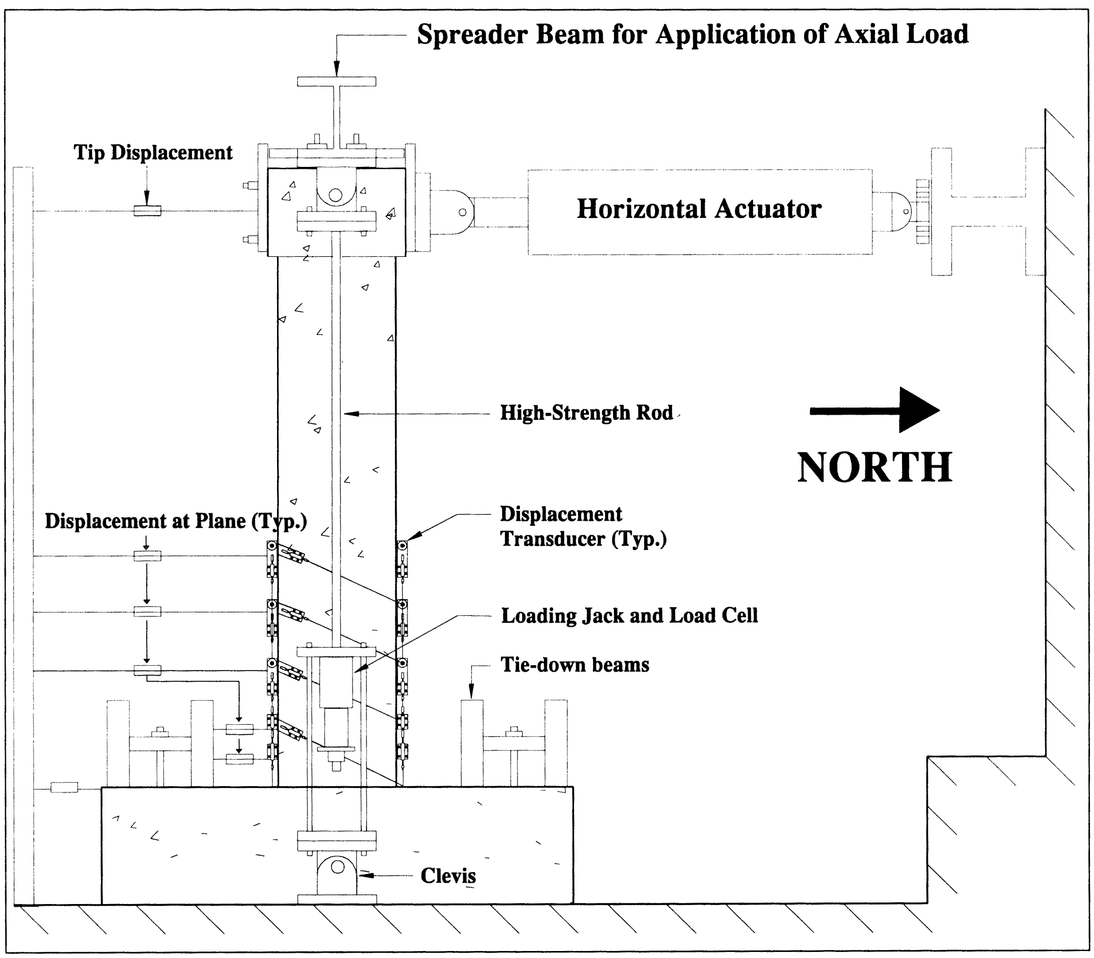

Figure 2.7: Test Set-Up Configuration

2.8 TEST PROCEDURE

The testing program commenced with setting all instrumentation to a zero value using DAS85. The axial load was then applied, simulating the gravity load on the column. The applied axial load was maintained at a constant level throughout the test.

Reversed lateral loading was applied at the column top by a hydraulic actuator. The actuator load was applied pseudo-statically to facilitate observations of the column behavior, such as cracking, spalling, bar buckling, and bar fracture. By applying the load in a pseudo-static manner, cracks and damage were allowed to propagate in a more accentuated manner than would be likely to occur under dynamic loading.

Data were recorded by the data acquisition system, which required manual control, throughout the application of the axial and lateral loads. The lateral load and column tip displacement were recorded continuously using an X-Y plotter. Once the maximum displacement was reached for each cycle, the lateral load was allowed to drop slightly and the displacement was held constant, while cracks were marked and photographs of the test specimen were taken. In general, a test was concluded when the column strength deteriorated to less than 60 percent of its maximum strength. For Column 828, the test was concluded when the travel limits of the horizontal actuator were reached. Upon completion of a test, the column was displaced to a position of zero lateral load, and the axial load on the column was released.

2.9 LOADING DESCRIPTION

The displacement history for each column was predetermined based on a cross-sectional analysis of the column. The test specimen was cycled three times at each displacement level. A single cycle consisted of pulling the actuator north and pushing the actuator south (Figure 2.7) to the prescribed displacement level. In addition, a small cycle equal to one third of the preceding displacement level was applied following the “inelastic” cycles. The “elastic” displacement cycles imposed include cycles at cracking, two cycles between cracking and yield, and cycles at the estimated yield displacement. The inelastic displacement cycles were imposed at approximately 1.5, 2, 3, 5, and 7 times the yield displacement.

The anticipated cracking and yield displacements for Columns 328 and 328T were determined from analysis to be approximately 0.05 inches and 0.40 inches, respectively. The two cycles between cracking and yield were imposed at global displacements of 0.10 inches and 0.20 inches, respectively. Subsequent inelastic displacement cycles were imposed at displacement ductilities of 1.5, 2, 3, 5, 7, 10, and 13.

The displacement histories imposed on Columns 828 and 1028 during testing were the same as those for Columns 815 and 1015 [Lehman, 1998]. The purpose for using the same displacement histories for the two test series was to facilitate comparison of the behavior and response of slender columns with identical aspect ratios.

3 Experimental Results

3.1 INTRODUCTION

This chapter presents the experimental data along with visual observations performed during testing of each column. Visual observations include the initiation and progression of cracking and spalling throughout the column height. Measured observations are primarily focused on the component deformations of flexure, shear, and slip that contribute to the total column displacement. Strain profiles as measured by the external potentiometers and internal strain gages are also explored to gain insight into the strain demands imposed along the column height. A table is provided for each column that summarizes the data obtained at the peak displacements.

3.2 VISUAL OBSERVATIONS

3.2.1 Cracking

Before the experimental testing of each column, shrinkage cracks were observed and marked on the column faces. Columns 828 and 1028 exhibited more shrinkage cracking than Columns 328 and 328T. It is possible that the difficulty in placing and vibrating the concrete at the base of Columns 828 and 1028 contributed to the increasing number of shrinkage cracks in both columns.

New cracks that were observed on the column faces after the first peaks (north and south) of each displacement cycle were indicated with marking pens. The propagation of these cracks was monitored throughout the testing program. In addition, crack widths at various elevations on the north and south column faces were measured and recorded after the first peak of each displacement cycle and at the end of each displacement cycle at zero displacement. Drawings showing the column cracking and measured crack widths at each displacement cycle are presented in Appendix A. In general, the existing cracks became wider and new cracks appeared with each successive increase in lateral displacement of the column.

3.2.2 Concrete Spalling

Initial spalling, or separation between the cover concrete and core concrete, occurred at a displacement ductility between 3.25 and 3.75. The spalling height increased progressively with increasing lateral displacement of the column. Tables 3.1 through 3.4 show the spalling history of each column in the experimental program.

Table 3.1: Spalling History for Column 328

Spalling State	Displacement Cycle	Height of Spalling	
		North Face	South Face
Initial spalling	1.2 inches	7.5 inches	5 inches
Moderate spalling	2.0 inches	15 inches	7 inches
Stable spalling	2.8 inches	15 inches	15.5 inches

Table 3.2: Spalling History for Column 328T

Spalling State	Displacement Cycle	Height of Spalling	
		North Face	South Face
Initial spalling	1.2 inches	4.5 inches	6 inches
Moderate spalling	2.0 inches	8 inches	7 inches
	2.8 inches	11 inches	13.5 inches
Stable spalling	4.0 inches	14 inches	16 inches

Table 3.3: Spalling History for Column 828

Spalling State	Displacement Cycle	Height of Spalling	
		North Face	South Face
Initial spalling	7.0 inches	5 inches	5 inches
Moderate spalling	10.5 inches	22 inches	33 inches
Stable spalling	17.5 inches	38 inches	34 inches

Table 3.4: Spalling History for Column 1028

Spalling State	Displacement Cycle	Height of Spalling	
		North Face	South Face
Initial spalling	10.0 inches	22 inches	22 inches
Moderate spalling	15.0 inches	27.5 inches	36 inches
	25.0 inches	46 inches	46 inches
Stable spalling	35.0 inches	53 inches	46 inches

3.3 MEASURED OBSERVATIONS

As previously mentioned, each column was instrumented with linear potentiometers, wire potentiometers, and strain gages to record the deformations of the column during testing. The recorded data were resolved into component deformations to provide insight into the load-displacement behavior of the column. Specifically, the global deformation of each column was resolved into component deformations resulting from flexure, shear, and slip (strain penetration of the longitudinal steel into the anchor block). The strains of the longitudinal and spiral reinforcement were measured to provide an indication of the strains imposed during testing and to assist in interpreting the data obtained from the external instrumentation. The data reduction subroutines used to analyze the data were originally written by Lehman [1998] and were modified slightly to analyze the columns in this experimental program. The procedures are described below.

3.3.1 Flexural Displacement Component

The flexural displacement component was determined from the displacements measured by the four vertical potentiometers at each instrumentation level (Figures 2.4 and 2.5). First, the measured displacements on both the north side and south side of the column were averaged. The difference in the magnitudes of the resulting displacements was divided by the horizontal distance between the north and south potentiometers to obtain the rotation of the column at the subject instrumentation level. The flexural displacement component at each instrumentation level was obtained by multiplying one half of the calculated rotation by the vertical distance between instrumentation levels. Cumulative rotations and flexural displacements of lower levels were accounted for in the flexural displacement calculations as the analysis proceeded up the column height. Above the uppermost instrumentation level, the flexural displacement component was assumed to vary linearly and was calculated as the sine of the rotation angle measured at the uppermost instrumentation level multiplied by the differential column elevation above that level.

3.3.2 Shear Displacement Component

The shear displacement component was determined from the deformations measured by the diagonal potentiometers at each instrumentation level (Figures 2.4 and 2.5). The deformation measured by the diagonal potentiometers contained components due to flexural rotation of the column cross section and shear deformations. The diagonal deformation component due to flexural rotation of the column was subtracted from the overall displacement of the diagonal potentiometer to obtain the diagonal deformation resulting from shear alone. This shear deformation was then added to the original undeformed diagonal length to obtain the total deformed length of the diagonal due to shear. Given this total deformed length, as well as the original height and width of the diagonal, the change in horizontal displacement of the column due to shear was calculated. A purely translational change in displacement of the column cross section was assumed, without a change in vertical deformation. In addition, the vertical potentiometers were assumed to remain vertical, without any lateral offset between instrumentation levels. Shear deformation contributions above the uppermost instrumentation level were believed to be minimal and were ignored.

3.3.3 Slip Displacement Component

The displacement component due to slip was based on the deformations recorded by the vertical potentiometers located at the bottom instrumentation level of the column. The instruments at this level were placed at a height of approximately 6 inches above the column interface with the concrete anchor block (Figures 2.4 and 2.4). Although the deformations measured by these instruments include the change in flexural rotation within the first 6 inches of the column, it was presumed that the deformation recorded by the potentiometers at this bottom level was primarily the result of strain penetration of the longitudinal steel into the anchor block.

The method used to obtain the slip displacement component is similar to that used for obtaining the flexural displacement component, as described above. First, the two measured displacements on both the north side and south side of the column were averaged. The magnitudes of the two resulting displacements were then summed together and subsequently divided by the horizontal distance between the north and south potentiometers to obtain the rotation of the column due to slip. Assuming that the column rotated about its midpoint, the horizontal displacement component due to slip was obtained by multiplying the calculated rotation by the column elevation.

3.3.4 Global Loads and Displacements

As noted previously, the global tip displacement was measured using an LVDT or DCDT in the small displacements range and a wire potentiometer in the large displacements range. The lateral load was measured using a load cell placed in series with the horizontal actuator.

Each of the four specimens exhibited a displacement ductility greater than 8. The yield displacement of each column was defined to be the displacement corresponding to the first yield of the most extreme longitudinal bar in tension, as measured by the longitudinal strain gages. The yield strain of the longitudinal bar was determined to be 0.0024. Table 3.5 lists the yield displacement, ultimate displacement, and displacement ductility of each column.

Load-displacement relations are presented in subsequent sections.

Table 3.5: Displacement Ductility for Experimental Columns

Column No.	Yield Displacement (in.)	Ultimate Displacement (in.)	Displacement Ducility
328	0.57	5.2	9
328T	0.51	5.2	10
828	2.38	18.5+	8+
1028	3.87	35	9

3.3.5 Measured Strain Profiles

Plots of strain profiles showing nominal compressive strains in the concrete for each column are presented in Figures A.4 through A.7 of Appendix A. The plots show the strains measured along the column height at the first north and south peak of each displacement level. The concrete compressive strains shown are average strains obtained from the external potentiometer displacements, which were linearly interpolated back to the center of the spiral reinforcement. Note that the deformation measurements provided by the potentiometers at the bottom instrumentation level include contributions due to flexural rotations as well as tensile slip from the foundations and compressive indentation of the foundations. The nominal compressive strains provided in Tables 3.6 through 3.9 are from the bottom instrumentation level; it was assumed that the foundation was rigid and that compressive strain occurs only in the column.

Plots of strain profiles showing tensile strains in the transverse steel, Figures A.8 through A.11, and in the longitudinal steel, Figures A.12 through A.15, for each column are shown in Appendix A. The measured readings from the strain gages are plotted at the strain gage location and connected by straight lines. The plots show the strains measured along the column height at the first north and south peak of each displacement level.

3.4 COLUMN 328 — EXPERIMENTAL RESULTS

Column 328 exhibited ductile behavior and relatively full and stable hysteresis loops until failure. The column achieved a displacement ductility of 9. Its load-displacement response is shown in Figure 3.1.

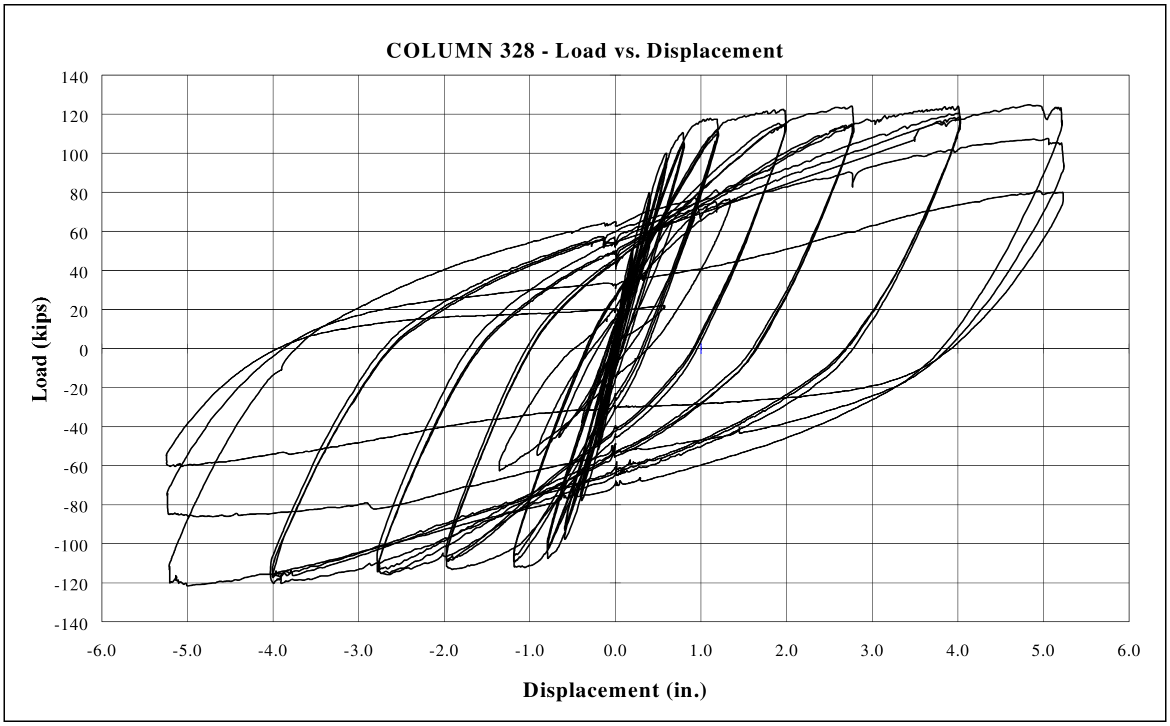

Figure 3.1: Hysteretic Response of Column 328

Figure 3.2 shows the displacement components represented as a percentage of the total displacement at each displacement cycle. In general, the slip component is significantly greater than the flexural component. In addition, as much as 15 to 20 percent of the total displacement consists of shear deformations. A significant amount of error, 30 percent, exists at the lowest displacement levels. This error is primarily due to the sensitivity of the vertical potentiometers, which are not capable of measuring the minute deformations during these low-level cycles. Also, note that the sum of the component deformations at the larger displacement cycles exceeds the total column deformation. This error is likely due to the cumulative affect of instrument errors and errors in the simplified models and procedures used to resolve the measured behavior into component deformations.

Flexural cracking in Column 328 was first observed during the 0.20-inch displacement cycle, approximately one third of the yield displacement and 0.28 percent drift. The average crack spacing was observed to be approximately 5.5 inches. The cracks propagated further around the column and became progressively closer in spacing with increasing tip displacement. By the 0.80-inch displacement cycle, the crack spacing was observed to be approximately 4.5

inches (Figure 3.3). The cracking became somewhat stable following this displacement level, with relatively few new cracks forming.

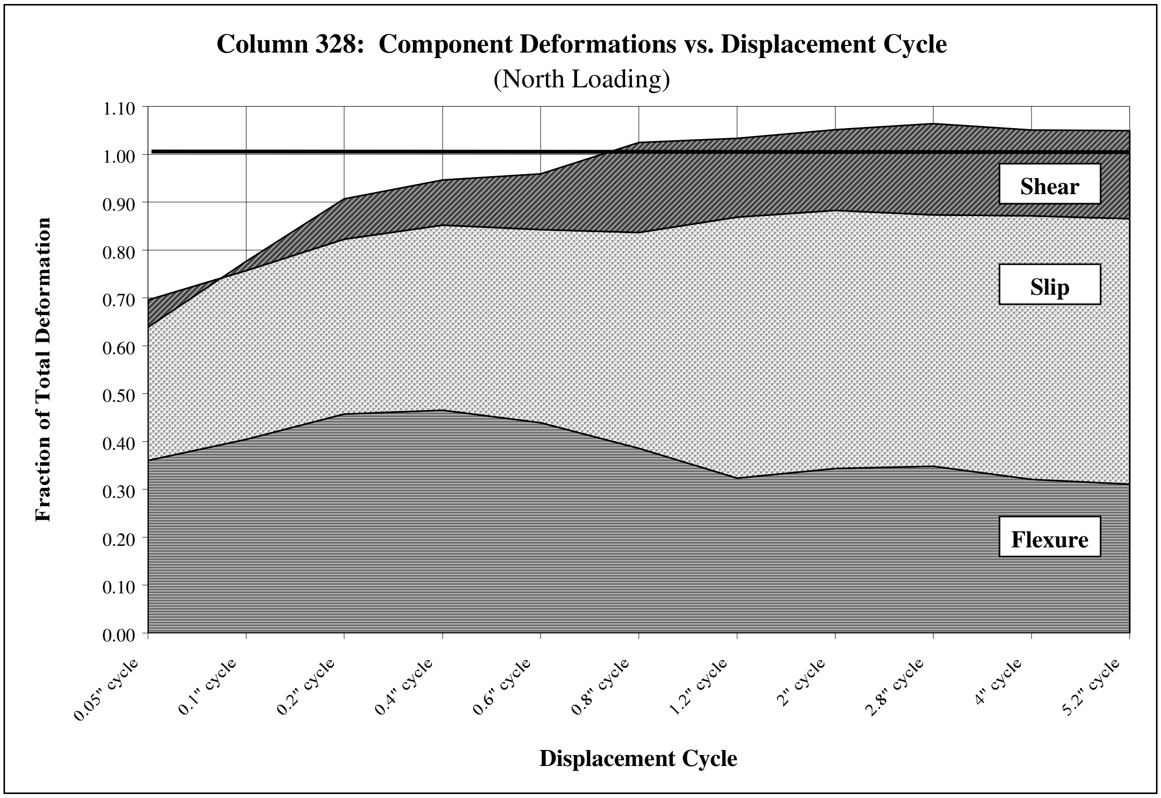

Figure 3.2: Column 328 Component Deformations

Initial concrete spalling of Column 328 occurred at a north displacement of 1.2 inches and up to a height of 7.5 inches above the column base. The height of spalling progressively increased with increasing displacement (Figure 3.4). Spalling was observed to stabilize at a displacement of 2.8 inches. The maximum spalling height was 15.5 inches above the column base (Figure 3.5). The spalled concrete cover on the north face of the column was measured to be approximately 1-inch thick.

The first yield of the south face longitudinal steel was observed at a north tip displacement of 0.57 inches. Bar buckling of the longitudinal steel was observed during the first north cycle of the 5.2-inch displacement cycle. At the north peak of this cycle, the spiral reinforcement was observed to fracture at a height of 4 inches above the column base. In addition, large diagonal cracks were visible on the west face of the column. Six longitudinal bars were observed to buckle during the second north peak of the 5.2-inch displacement cycle (Figure 3.6). Two longitudinal bars on the north side were observed to fracture and six longitudinal bars on the south side were observed to buckle as the column was displaced towards the second south peak. At the third north peak of the 5.2-inch displacement cycle, the column had lost more than one third of its original strength. The final damaged condition of Column 328 is shown in Figure 3.7.

Table 3.6 summarizes the data obtained at the first north peak of the last seven displacement cycles, including displacement and rotation ductilities, displacement components, compressive and tensile strains, spalling height, and crack widths. The yield displacement and rotations are based on values measured at the first yield of the longitudinal steel, as described in Section 3.1.

Table 3.6: Column 328 Performance History

Displacement Cycle North	0.60"	0.80"	1.20"	2.00"	2.80"	4.00"	5.20"
Displacement Ductility	1.1	1.4	2.1	3.5	4.9	7.0	9.1
Flexural Displacement (in.)	0.3	0.3	0.4	0.7	1.0	1.3	1.6
Slip Displacement (in.)	0.2	0.4	0.7	1.1	1.5	2.2	2.9
Shear Displacement (in.)	0.1	0.2	0.2	0.3	0.5	0.7	1.0
Rotation Ductility @ 6" el.	1.0	1.6	2.8	4.7	6.4	9.6	12.5
Rotation Ductility @ 24" el.	1.0	1.2	1.5	2.0	4.1	5.9	7.1
Nominal Compressive Strain[1]	-0.0062	-0.0088	-0.0138	-0.0241	-0.0345	-0.0527	-0.0688
Longitudinal Steel Tensile Strain[2]	0.0037	0.0169	0.0195	0.0239	0.0331	N/A	N/A
Transverse Steel Strain[3]	0.0002	0.0004	0.0007	0.0013	0.0020	0.0032	N/A
Spalled Height (in.)	N/A	N/A	7.5	15	15	15	15
Max. Crack Width @ 11.6" (in.)	0.007	0.013	0.02	0.03	0.04	0.06	0.05

[1]Nominal compressive strain determined by vertical potentiometer data, linearly interpolated back to center of spiral hoop; obtained at a height of 6 inches.

[2]Longitudinal steel strain read by gage at base of column on south face.

[3]Transverse steel strains shown are from the first north peak of each respective displacement cycle at a height of 6 inches above the column base.

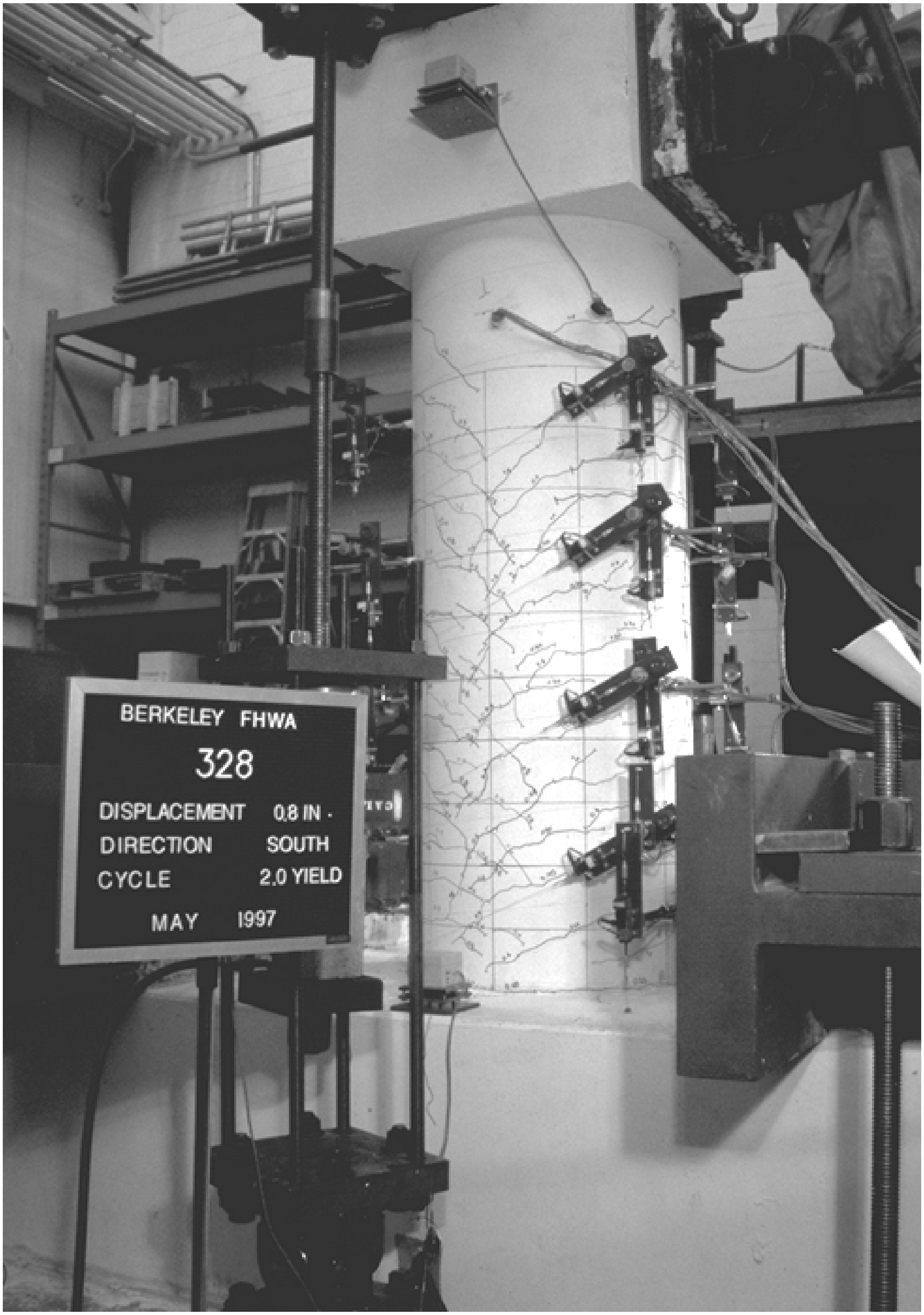

Figure 3.3: Column 328 at a South Displacement of 0.8 inches

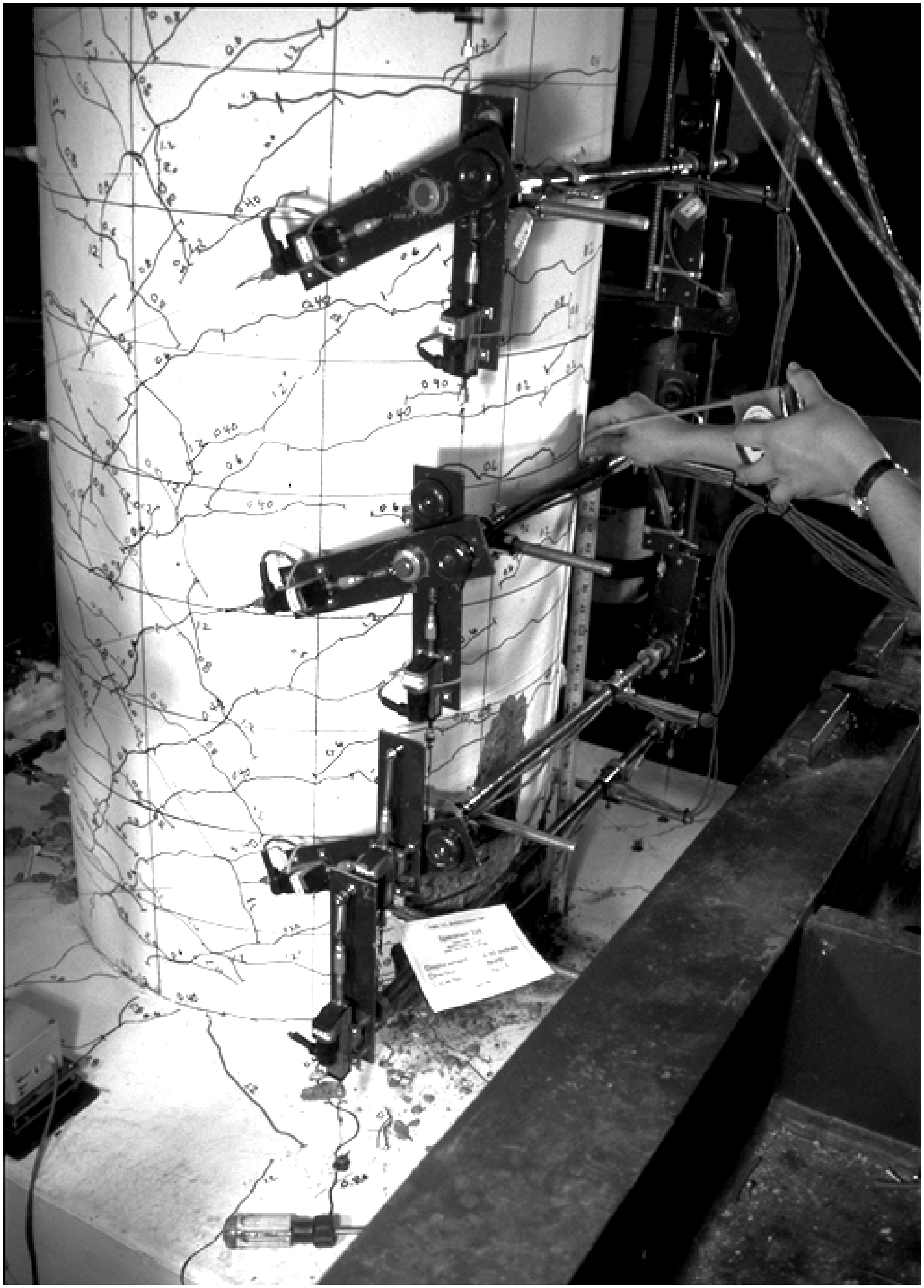

Figure 3.4: North Face of Column 328 at a North Displacement of 2.0 Inches

Figure 3.5: South Face of Column 328 at a North Displacement of 5.2 Inches

Figure 3.6: Buckled Longitudinal Steel of Column 328 at a North Displacement of 5.2 Inches, Second Cycle

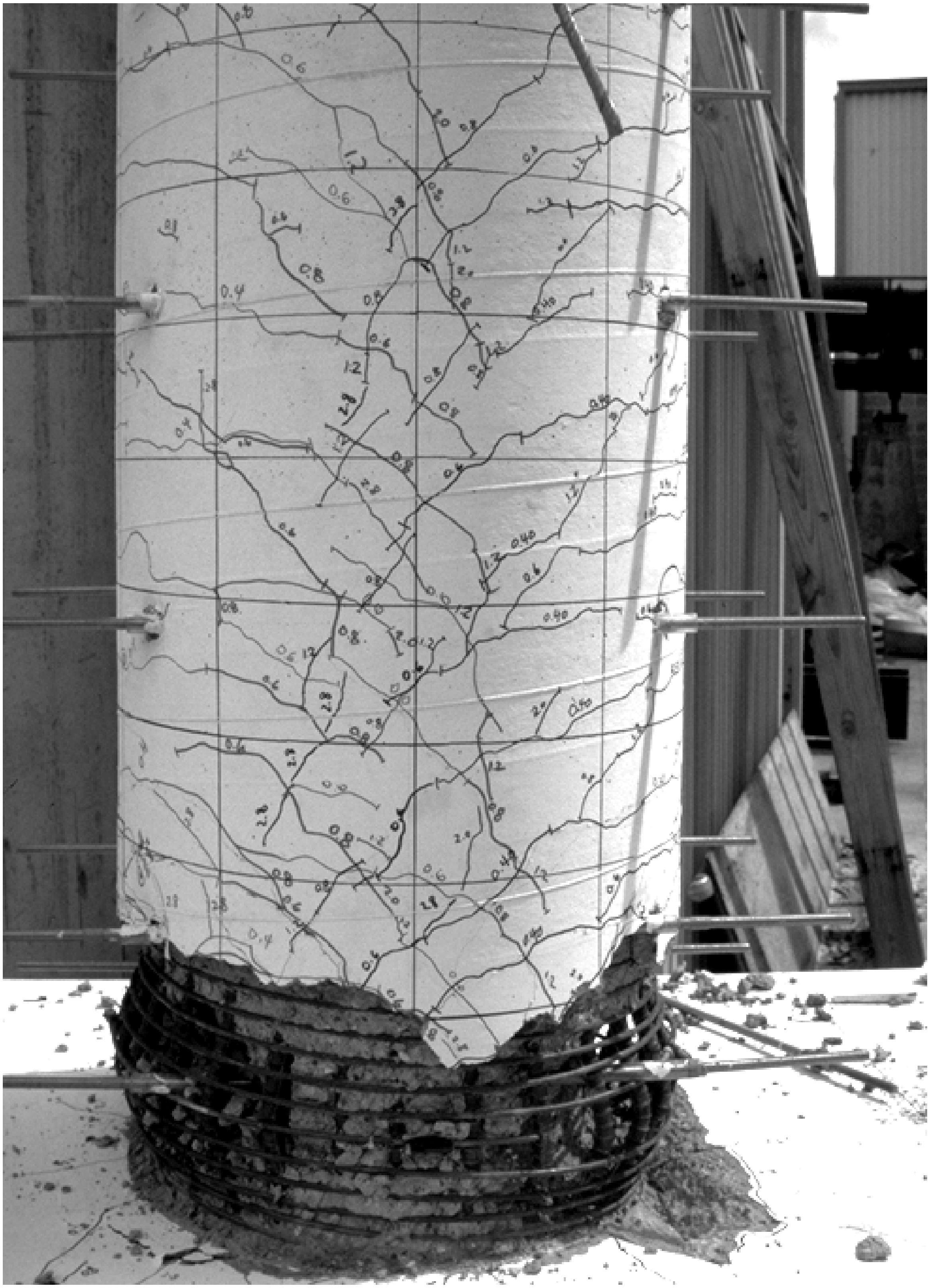

Figure 3.7: Final Damaged Condition of Column 328

3.5 COLUMN 328T — EXPERIMENTAL RESULTS

Although Column 328T was designed to be shear critical, it displayed overall load-displacement behavior that was similar to Column 328. The column achieved a displacement ductility of 10. The load-displacement history for Column 328T is shown in Figure 3.8.

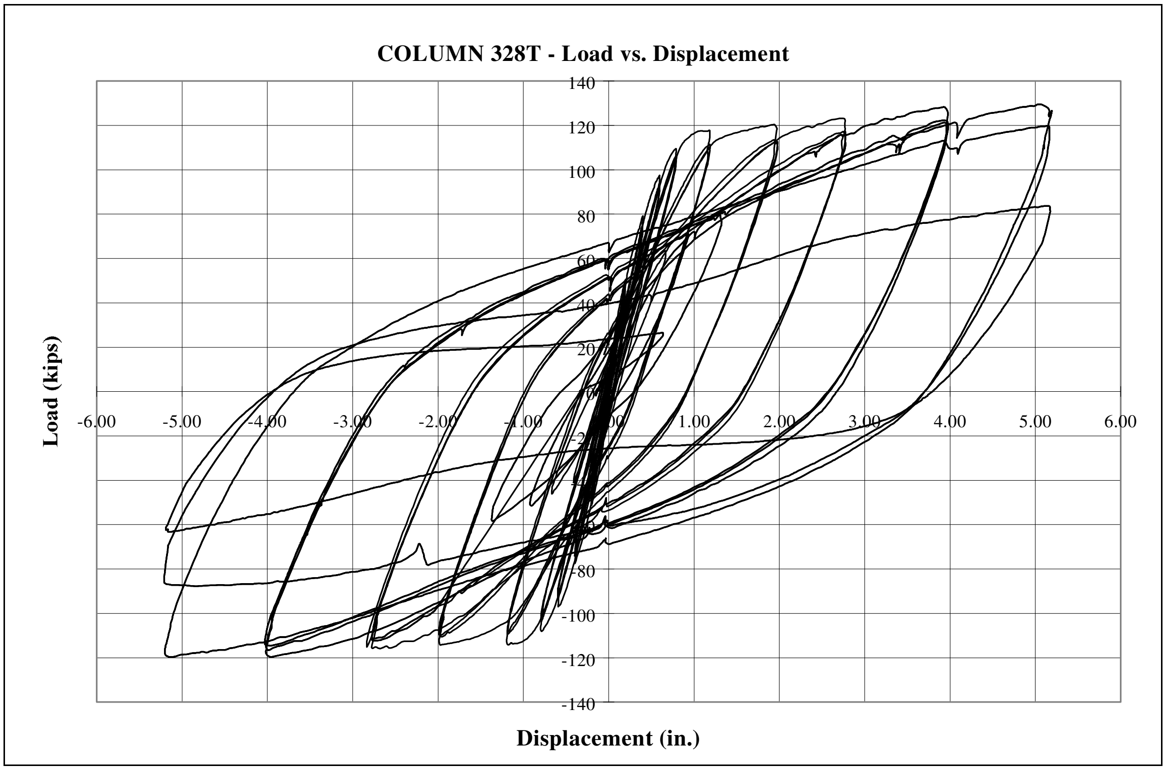

Figure 3.8: Hysteretic Response of Column 328T

Figure 3.9 shows the displacement components at each displacement cycle as a percentage of the total displacement for Column 328T. The slip component is significantly greater than the flexural contribution. In addition, as much as 15 to 20 percent of the total displacement consists of shear deformations. The general trend of the displacement component percentages is similar to that of Column 328. A significant amount of error, 28 percent, exists at the lowest displacement levels. Also, note that the sum of the component deformations at the larger displacement cycles exceeds the total column deformation. Possible sources of these errors were discussed previously.

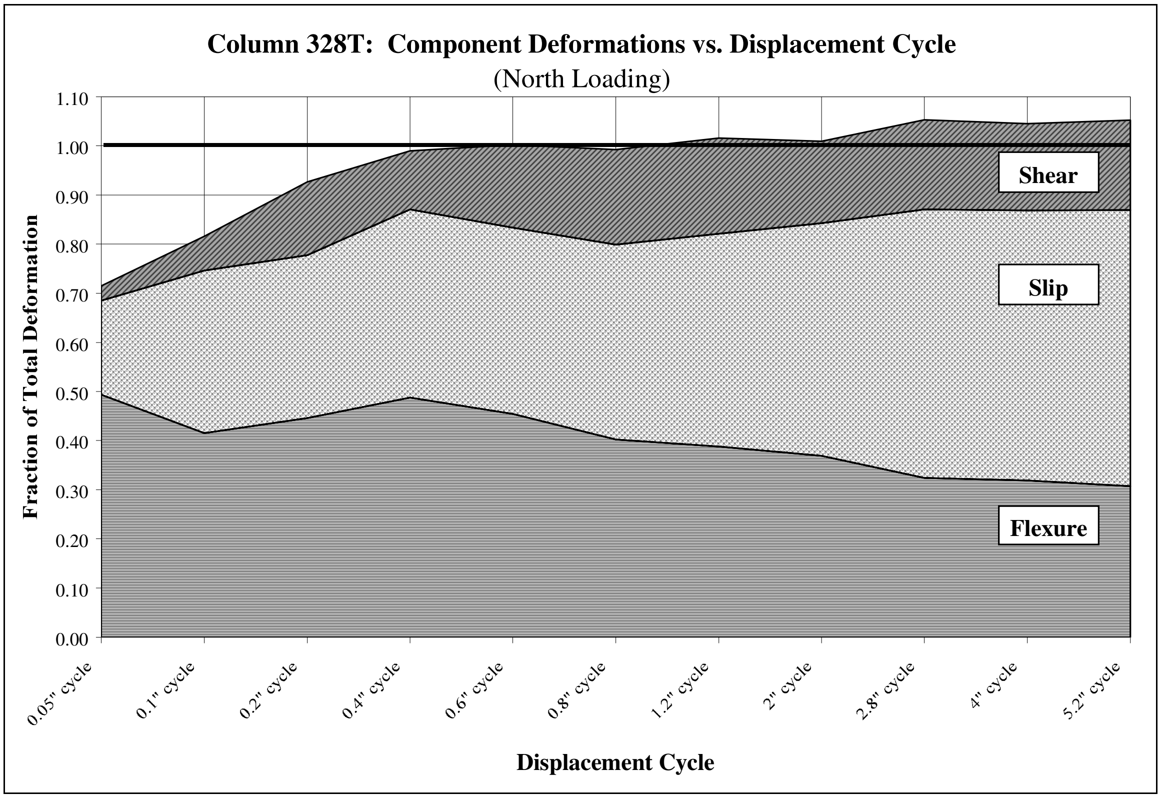

Figure 3.9: Column 328T Component Deformations

Flexural cracking in Column 328T was first observed during the 0.20-inch displacement cycle, approximately 40 percent of the yield displacement and 0.28 percent drift. The average crack spacing was observed to be approximately 5 inches. In general, the cracks propagated further around the column and became closer in spacing with increasing tip displacement. By the 0.80-inch displacement cycle, the crack spacing was observed to be approximately 4 inches. The cracking became somewhat stable following this displacement level, with relatively few new cracks forming.

Initial concrete spalling of Column 328T occurred at a north displacement of 1.2 inches and at a height of 6 inches above the column base. The height of spalling progressively increased with increasing displacement. Spalling was observed to stabilize at a displacement of 4 inches (Figure 3.12). The maximum spalling height ranged between 14 and 16 inches above the column base.

At displacement levels exceeding the 1.2-inch cycle, large diagonal cracks were observed outside the heavily confined zone of Column 328T (Figure 3.11). These diagonal cracks were wider than those observed in Column 328. The diagonal crack widths were measured to vary from 0.025 inches at a column elevation of 12 inches to 0.03 inches at a column elevation of 48 inches. In general, the crack width became wider as it crossed the transition zone of the transverse steel. In addition, the diagonal cracks were observed to be offset vertically along the east-west column centerline (Figure 3.10). This offset was measured to be 0.01 inches at zero displacement and 0.03 inches at a displacement of 1.2 inches. This offset appeared to become larger with increasing displacement of the column.

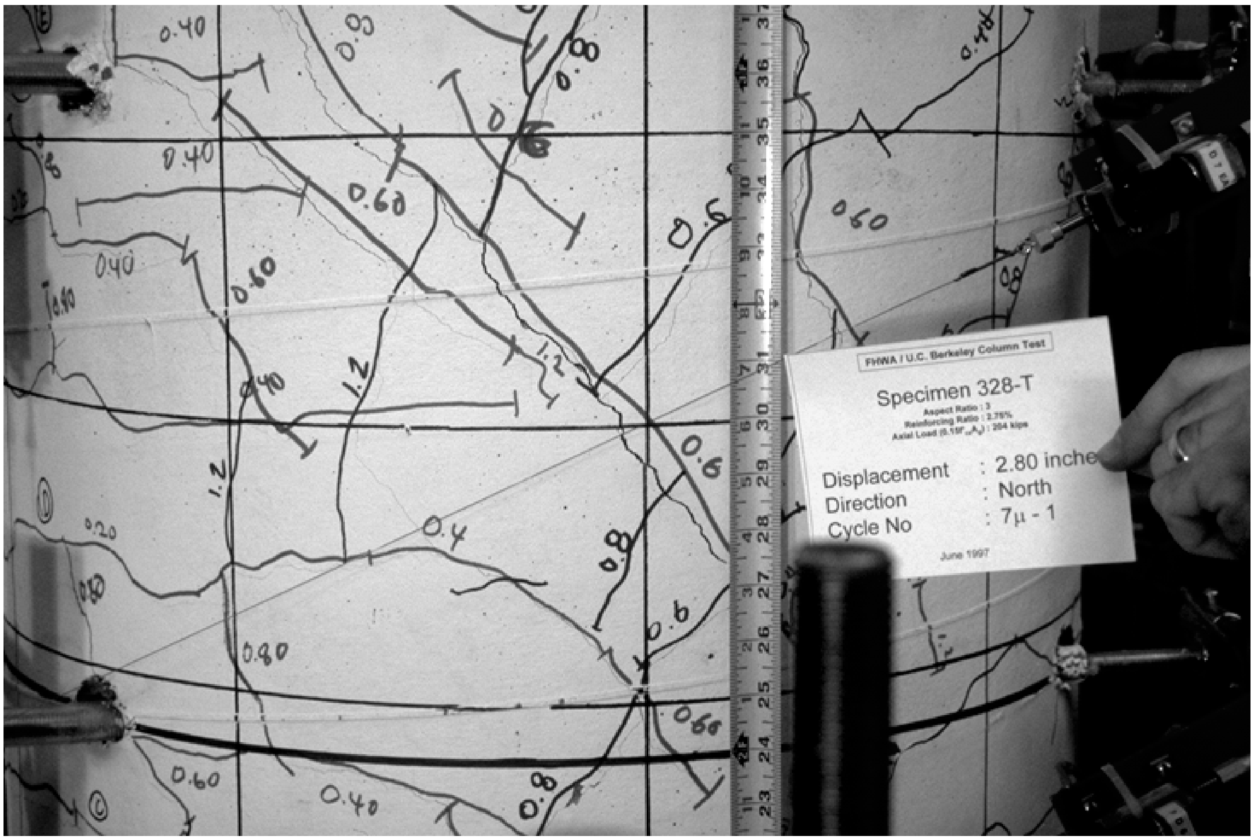

Figure 3.10: Column 328T Shear Cracking and Vertical Offset at a Displacement of 2.8 Inches

The first yield of the south face longitudinal steel was observed at a north tip displacement of 0.51 inches. Slight bowing of the transverse spiral and bar buckling of the longitudinal steel was observed during the first north peak of the 5.2-inch displacement cycle. At the second north peak of this displacement cycle, the spiral reinforcement was observed to fracture at a height of 3 inches above the column base. Five longitudinal bars were observed to buckle during this second north displacement step. Two longitudinal bars on the north side were observed to fracture and nine longitudinal bars on the south side were observed to buckle during the second south displacement step (Figure 3.13). At the third north peak of the 5.2-inch displacment cycle, the column had lost approximately one third of its original strength. Columns 328 and 328T are shown side-by-side in their final damaged state in Figure 3.14.

Table 3.7 summarizes the data, including displacement and rotation ductilities, displacement components, compressive and tensile strains, spalling height, and crack widths, obtained at the first north peak of the last seven displacement cycles. The yield displacement and rotations are based on values measured at the first yield of the longitudinal steel, as described in Section 3.1.

Table 3.7: Column 328T Performance Summary

Displacement Cycle North	0.60"	0.80"	1.20"	2.00"	2.80"	4.00"	5.20"
Displacement Ductility	1.2	1.6	2.4	3.9	5.5	7.8	10.2
Flexural Displacement (in.)	0.3	0.3	0.5	0.7	0.9	1.3	1.6
Slip Displacement (in.)	0.2	0.3	0.5	0.9	1.5	2.2	2.9
Shear Displacement (in.)	0.1	0.2	0.2	0.3	0.5	0.7	1.0
Rotation Ductility @ 6" el.	1.1	1.6	2.6	4.7	7.6	10.9	14.5
Rotation Ductility @ 24" el.	1.1	1.3	1.4	1.9	3.3	4.8	5.9
Nominal Compressive Strain[1]	-0.0062	-0.0081	-0.0129	-0.0185	-0.0365	-0.0502	-0.0637
Longitudinal Steel Tensile Strain[2]	0.0037	0.0155	0.0224	0.0274	N/A	N/A	N/A
Transverse Steel Strain[3]	0.0002	0.0003	0.0005	0.0009	0.0015	0.0024	0.0027
Spalled Height (in.)	N/A	N/A	4.5	8	11	14	14
Max. Crack Width @ 7"	0.009	0.013	0.04	0.06	0.04	0.05	0.02

[1]Nominal compressive strain determined by vertical potentiometer data, linearly interpolated back to center of spiral hoop; obtained at a height of 6 inches.

[2]Longitudinal steel strain read by gage at base of column on south face.

[3]Transverse steel strains shown are from the first north peak of each respective displacement cycle at a height of 6 inches above the column base.

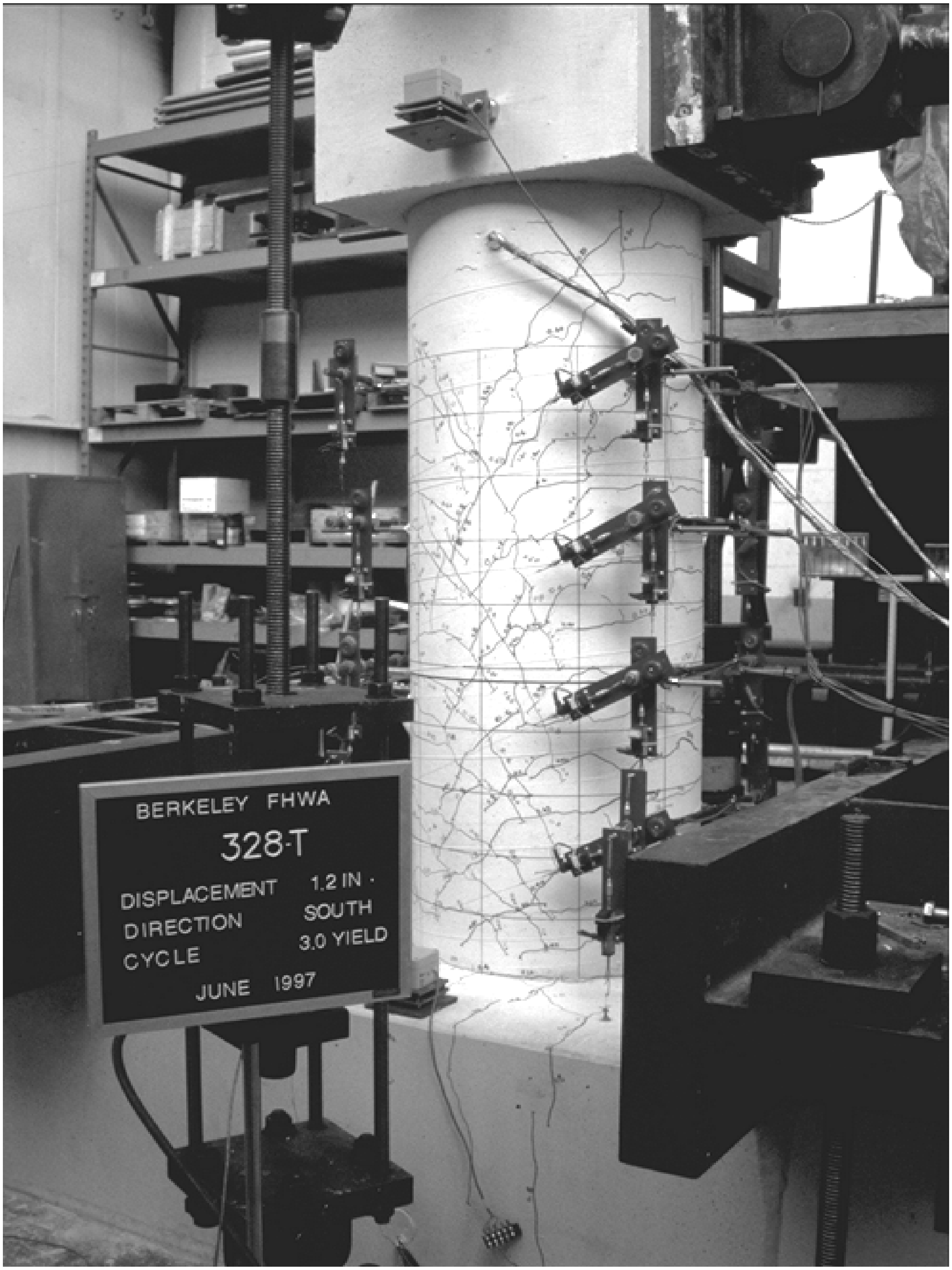

Figure 3.11: Column 328T at a South Displacement of 1.2 Inches

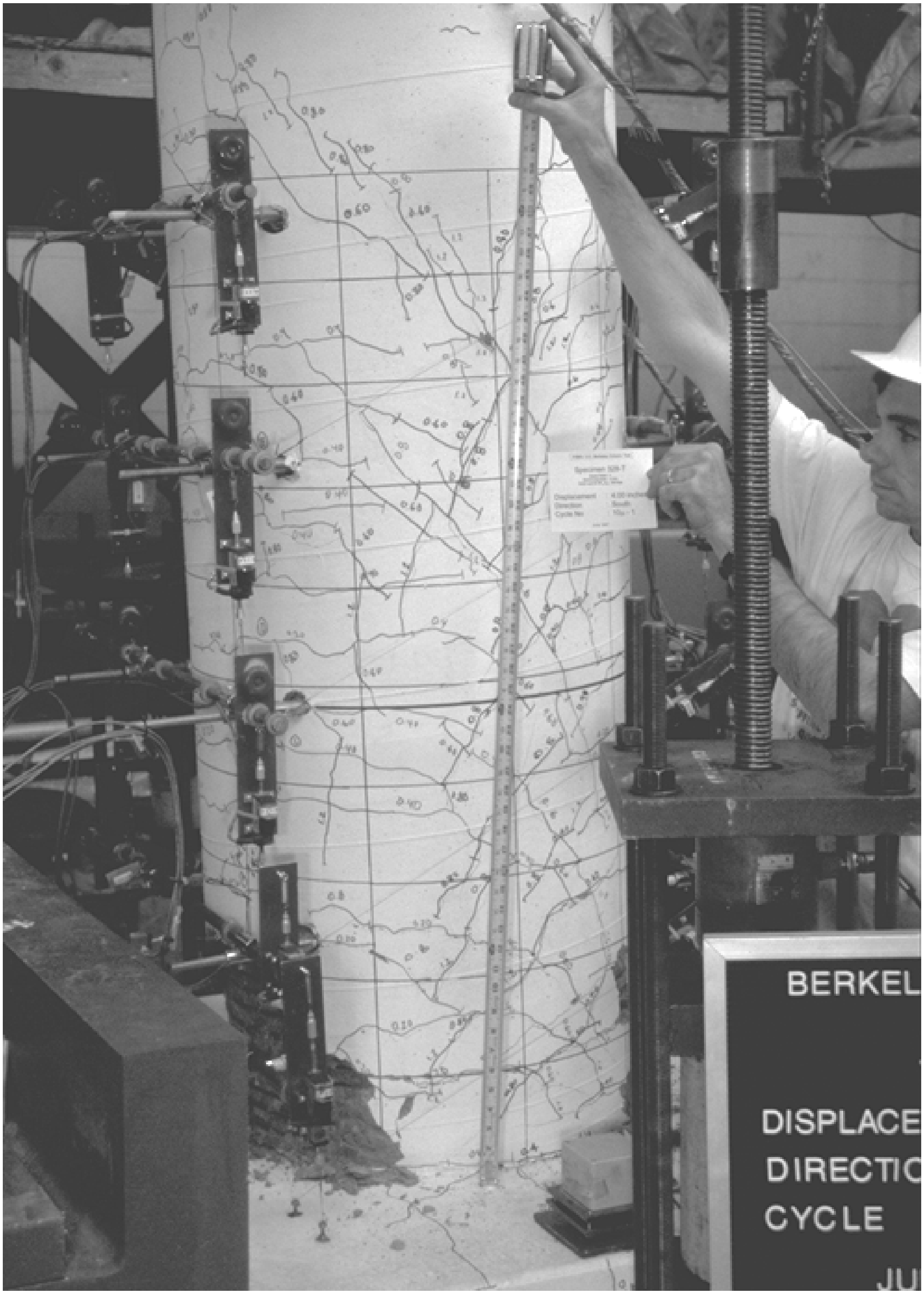

Figure 3.12: Column 328T at a South Displacement of 4.0 Inches

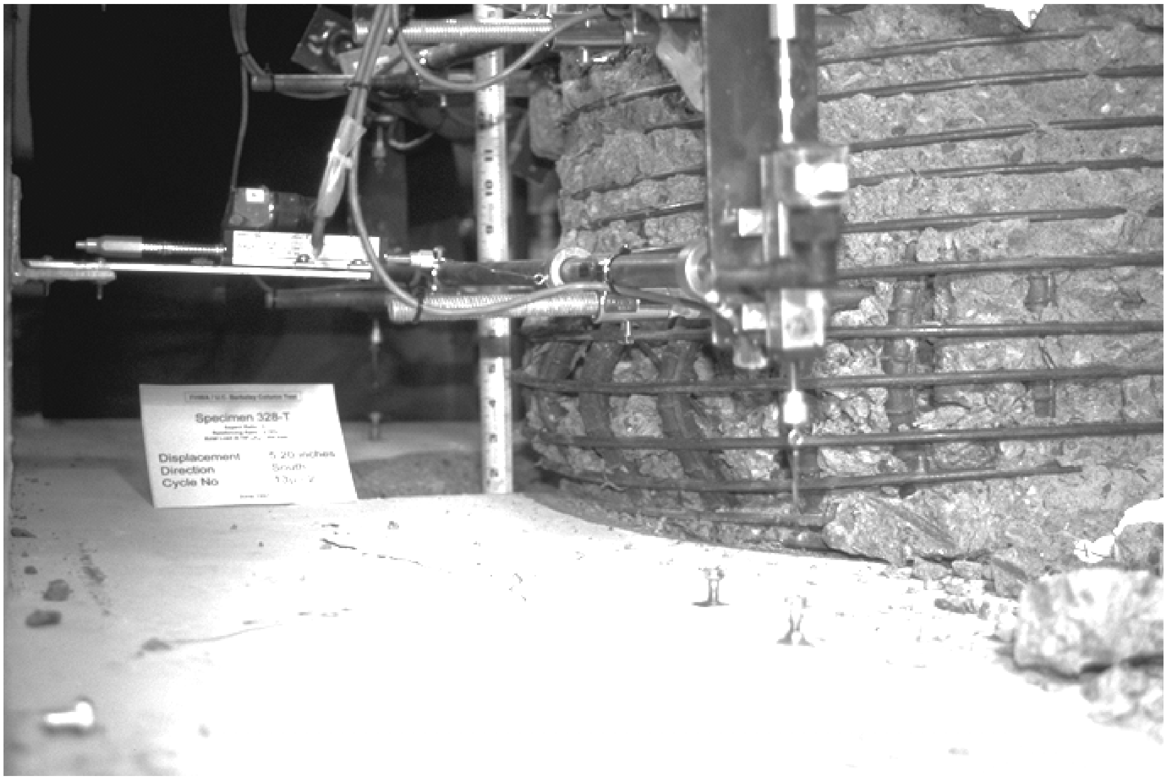

Figure 3.13: Buckling of Longitudinal Steel in Column 328T at a South Displacement of 5.2 Inches, Second Cycle

Figure 3.14: Final Damaged Condition of Column 328T (left) and Column 328 (right)

3.6 COLUMN 828 — EXPERIMENTAL RESULTS

Column 828, designed in accordance with the provisions of ATC-32 [1996], also showed ductile response with relatively full hysteresis loops until the end of testing. However, the load-displacement loops were slightly more pinched at large displacement amplitudes than those of Columns 328 and 328T. The column achieved a displacement ductility of at least 8. The load-displacement history for this column is shown in Figure 3.15.

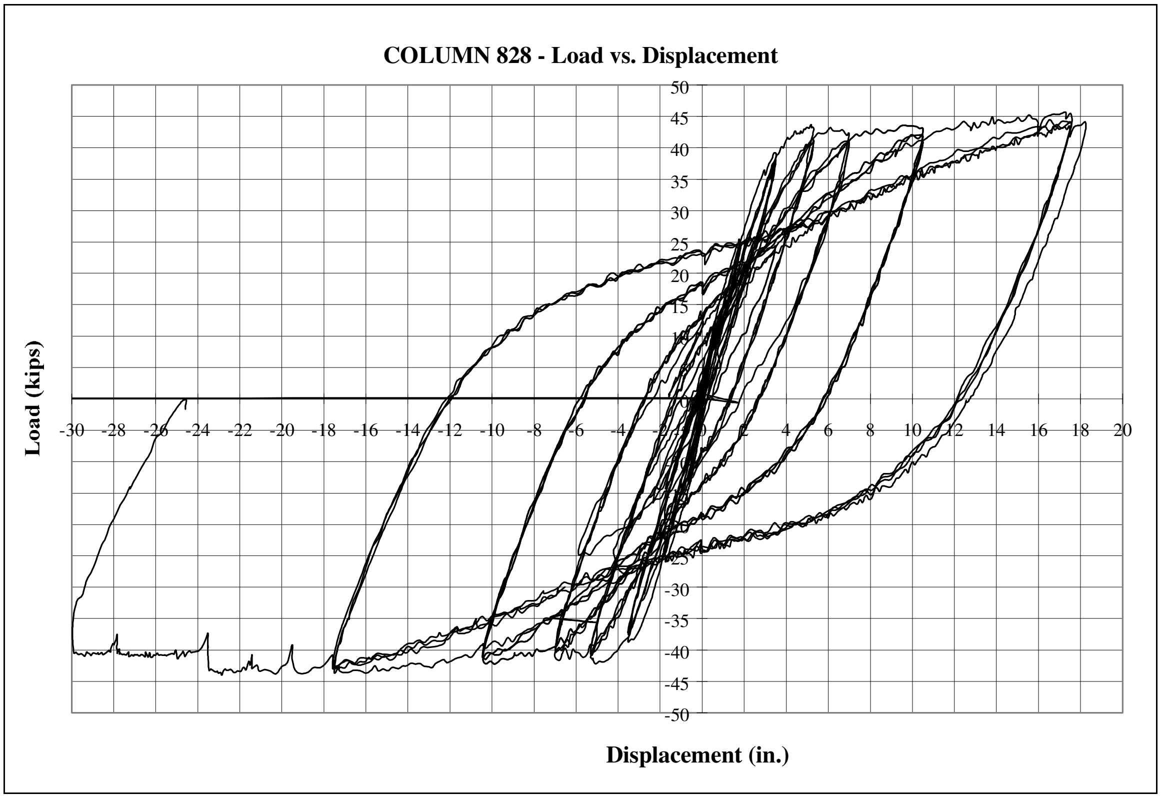

Figure 3.15: Hysteretic Response of Column 828

Figures 3.16 and 3.17 show the north and south displacement components, respectively, expressed as a percentage of the total displacement at each displacement cycle for Column 828. In general, the flexural component deformation was the predominant contributor to the total column displacement. Nevertheless, as much as 20 to 30 percent of the total displacement consists of slip. A significant amount of error, 37 percent, exists at the lowest displacement levels for reasons described previously. Note that the shear deformations contributed little to the total column displacement.

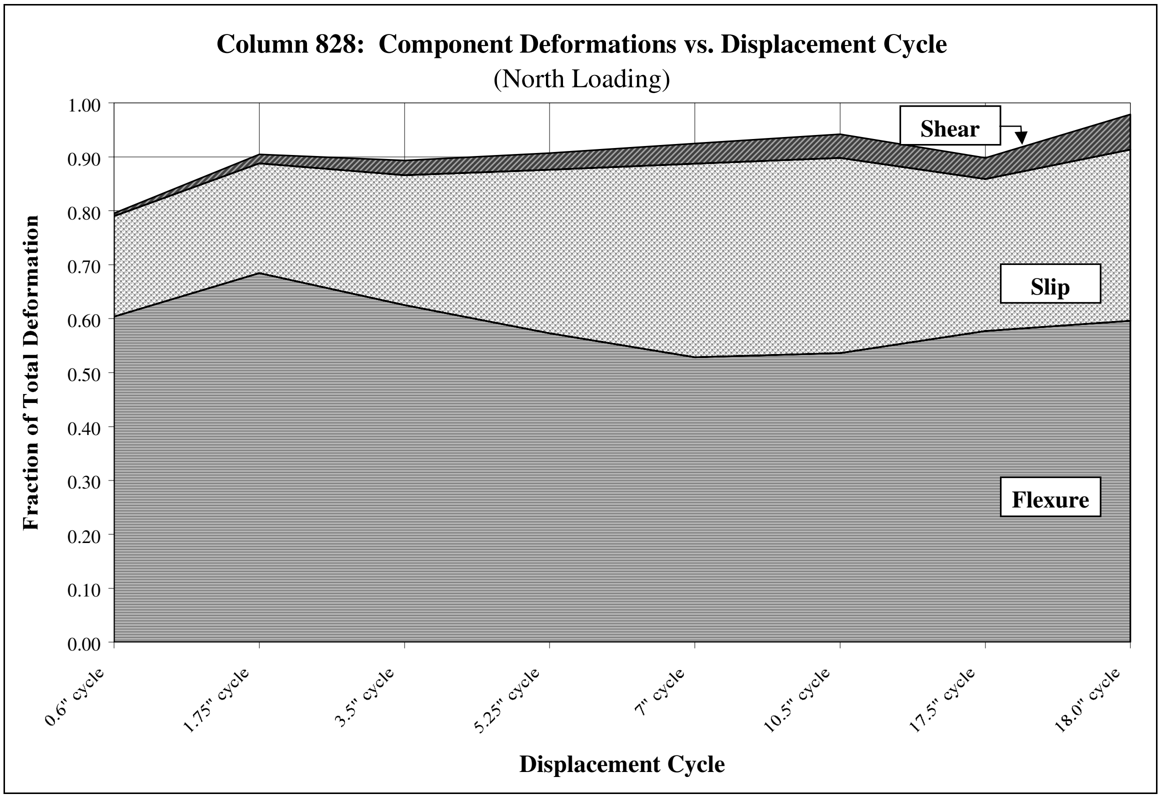

Figure 3.16: Column 828 North Component Deformations

For Specimen 828, the first flexural cracks were observed at a displacement of 0.60 inches, approximately 25 percent of the yield displacement and 0.3 percent drift. The average spacing between cracks in Column 828 was observed to be approximately 5 inches. Crack widths above the transition zone in the transverse reinforcement were observed to be slightly wider than those below the transition zone. The crack width at the interface of the column and anchor block of Column 828 ranged from 0.01 inches at a displacement of 1.75 inches to 0.24 inches at a displacement of 17.5 inches. First yield of the south face longitudinal steel was observed at a north tip displacement of 2.38 inches. The condition of Column 828 at a south displacement of 3.5 inches is shown in Figure 3.18.

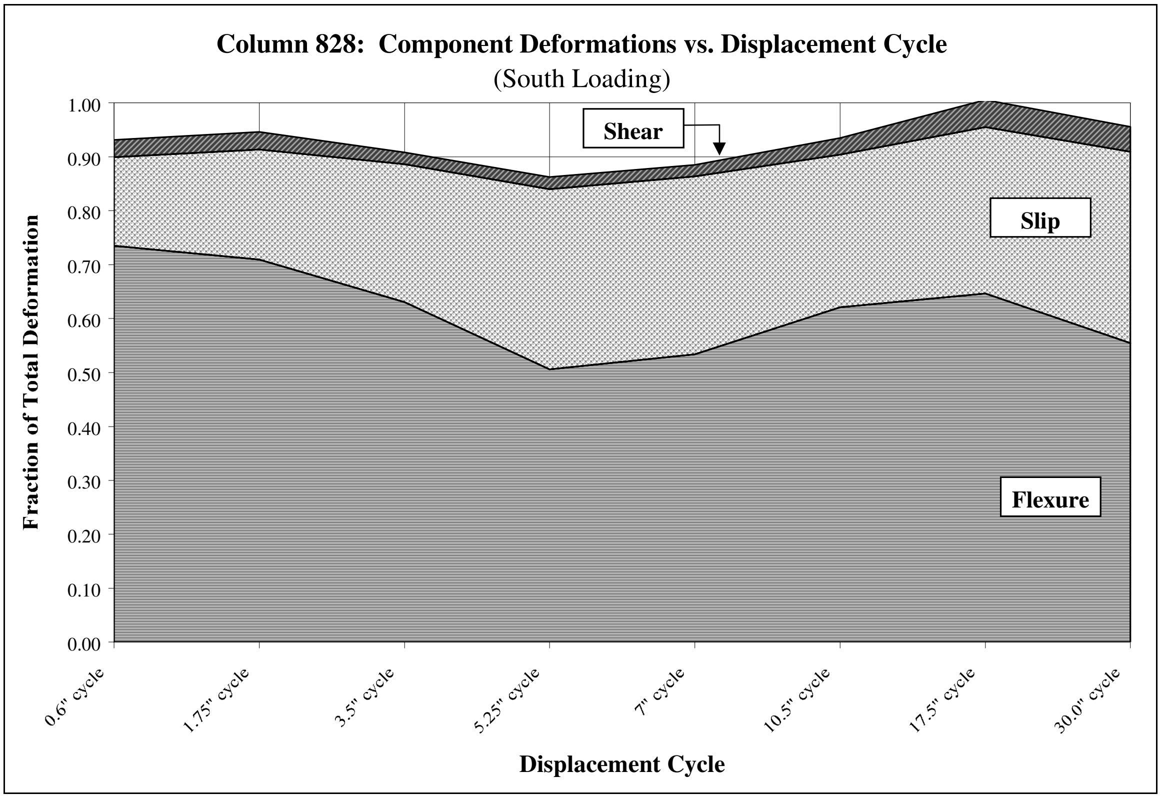

Figure 3.17: Column 828 South Component Deformations

Concrete spalling for Column 828 was initiated during the 5.25-inch displacement cycle and progressed significantly throughout the 7-inch displacement cycle. The height of spalling increased with increasing displacement. At a displacement of 10.5 inches, first north cycle, the spalled height on the south face was observed to be approximately 12 inches above the column base (Figure 3.19). At the completion of the third 10.5-inch displacement cycle, the spalled height on the south column face was observed to progress as high as 32 inches above the column base. The spalling stabilized at a displacement of 17.5 inches, with the maximum spalling height ranging from 34 inches to 37 inches above the interface between the column and anchor block (Figures 3.20 and 3.21).

The available stroke of the horizontal actuators used to displace the column tip was expended following the completion of the 17.5-inch displacement cycle. At this stage, the residual strength remaining in the column exceeded 95 percent of its maximum strength. No fracturing of transverse or longitudinal steel reinforcement was observed, and the concrete core appeared to be intact (Figure 3.20). At this juncture, it was decided to push the column as far as possible. After pulling the column north to a displacement of 18 inches, the column was pushed in the south direction to a displacement of 30 inches (Figure 3.21). To achieve this, the horizontal actuators were detached from the column and withdrawn, spacers were inserted between the actuators and the column to increase the stroke limit of the actuators, and the actuators were then reattached to the assembly.

During this 30-inch displacement step, the center longitudinal bar on the north face of the column fractured at a south displacement of 23.5 inches; the fracture occurred at an approximate height of 6 inches above the interface of the column and anchor block. At 30 inches, the spiral reinforcement was observed to fracture at a height of 3 inches above the column base. In addition, the center bar was observed to buckle over a spacing of between 6 and 7 inches. At a displacement of 30 inches, the residual strength in the column exceeded 90 percent of its maximum strength, although it is possible that significant strength degradation would have been achieved under additional cycles since spiral fracture and bar buckling had begun to occur.

Tables 3.8 and 3.9 summarize the data, including displacement and rotation ductilities, displacement components, compressive and tensile strains, spalling height, and crack widths, obtained at the first north peak of the last seven displacement cycles. The yield displacement and rotations provided are based on values measured at the first yield of the longitudinal steel.

Table 3.8: Column 828 North Cycle Performance Summary

Displacement Cycle North	0.60"	1.75"	3.50"	5.25"	7.00"	10.50"	17.50"	18.00"
Displacement Ductility	0.3	0.7	1.5	2.2	2.9	4.4	7.4	7.6
Flexural Displacement (in.)	0.4	1.2	2.3	3.1	3.8	5.7	10.2	10.7
Slip Displacement (in.)	0.1	0.4	0.8	1.6	2.5	3.8	4.9	5.7
Shear Displacement (in.)	0.0	0.0	0.1	0.2	0.3	0.5	0.7	1.2
Rotation Ductility @ 6" el.	0.2	0.8	1.8	3.4	5.5	8.2	10.7	10.7
Rotation Ductility @ 24" el.	0.3	0.9	1.5	2.2	3.6	8.4	8.3	8.3
Nominal Compressive Strain[1]	-0.0013	-0.0034	-0.0058	-0.0097	-0.0156	-0.0318	-0.0240	-0.0369
Steel Tensile Strain[2]	0.0005	0.0018	0.0244	0.0259	0.0288	0.0388	0.0594	0.0621
Transverse Steel Strain[3]	0.0000	0.0001	0.0002	0.0006	0.0010	0.0016	N/A	N/A
Spalled Height (in.)	N/A	N/A	N/A	N/A	5	22	38	38
Max. Crack Width @ 14"	N/A	0.007	0.016	0.04	0.10	0.06	0.10	0.10

[1]Nominal compressive strain determined by vertical potentiometer data, linearly interpolated back to center of spiral hoop; obtained at a height of 6 inches.

[2]Longitudinal steel strain read by gage at base of column on south face.

[3]Transverse steel strains shown are from the first north peak of each respective displacement cycle at a height of 6 inches above the column base.

Table 3.9: Column 828 South Cycle Performance History

Displacement Cycle South	0.60"	1.75"	3.50"	5.25"	7.00"	10.50"	17.50"	30.00"
Displacement Ductility	0.3	0.7	1.5	2.2	2.9	4.4	7.3	12.5
Flexural Displacement (in.)	0.4	1.2	2.2	2.7	3.7	6.5	11.3	16.6
Slip Displacement (in.)	0.1	0.4	0.9	1.8	2.3	3.0	5.4	10.6
Shear Displacement (in.)	0.0	0.1	0.1	0.1	0.1	0.3	0.9	1.4
Rotation Ductility @ 6" el.	0.2	0.7	1.8	3.5	4.6	5.9	10.8	10.8
Rotation Ductility @ 24" el.	0.2	0.7	1.6	2.4	3.6	7.7	13.4	13.4
Nominal Compressive Strain[1]	-0.0011	-0.0026	-0.0057	-0.0092	-0.0134	-0.0097	-0.0313	-0.0682
Steel Tensile Strain[2]	0.0005	0.0019	0.0260	0.0294	0.0345	N/A	N/A	N/A
Transverse Steel Strain[3]	0.0000	0.0001	0.0001	0.0003	0.008	0.0016	0.0025	N/A
Spalled Height (in.)	N/A	N/A	N/A	N/A	5	22	38	38
Max. Crack Width @ 14"	N/A	0.007	0.016	0.04	0.10	0.06	0.10	N/A

[1]Nominal compressive strain determined by vertical potentiometer data, linearly interpolated back to center of spiral hoop; obtained at a height of 6 inches.

[2]Longitudinal steel strain read by gage at base of column on south face.

[3]Transverse steel strains shown are from the first north peak of each respective displacement cycle at a height of 6 inches above the column base.

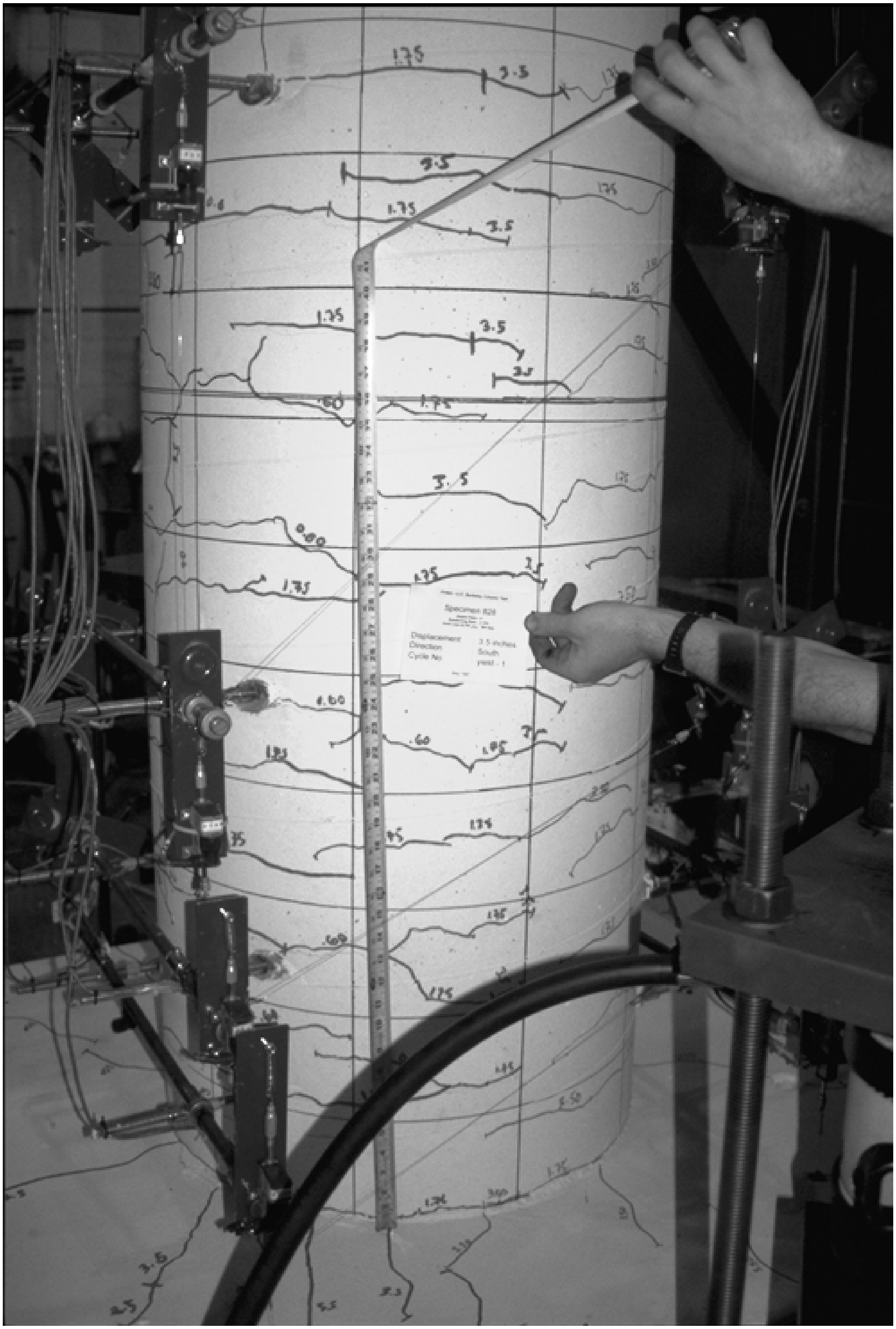

Figure 3.18: Column 828 at a South Displacement of 3.5 Inches

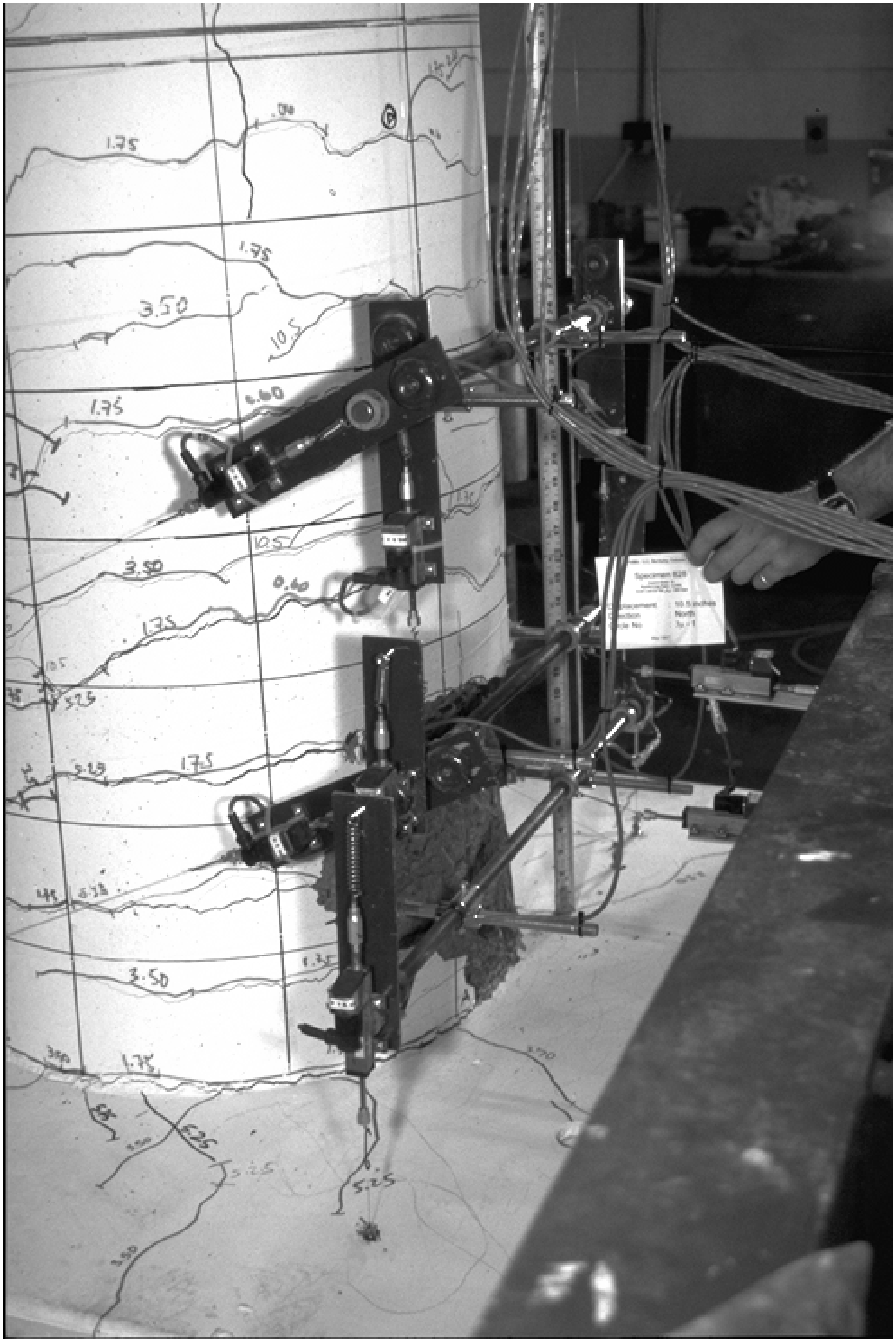

Figure 3.19: Column 828 at a North Displacement of 10.5 Inches

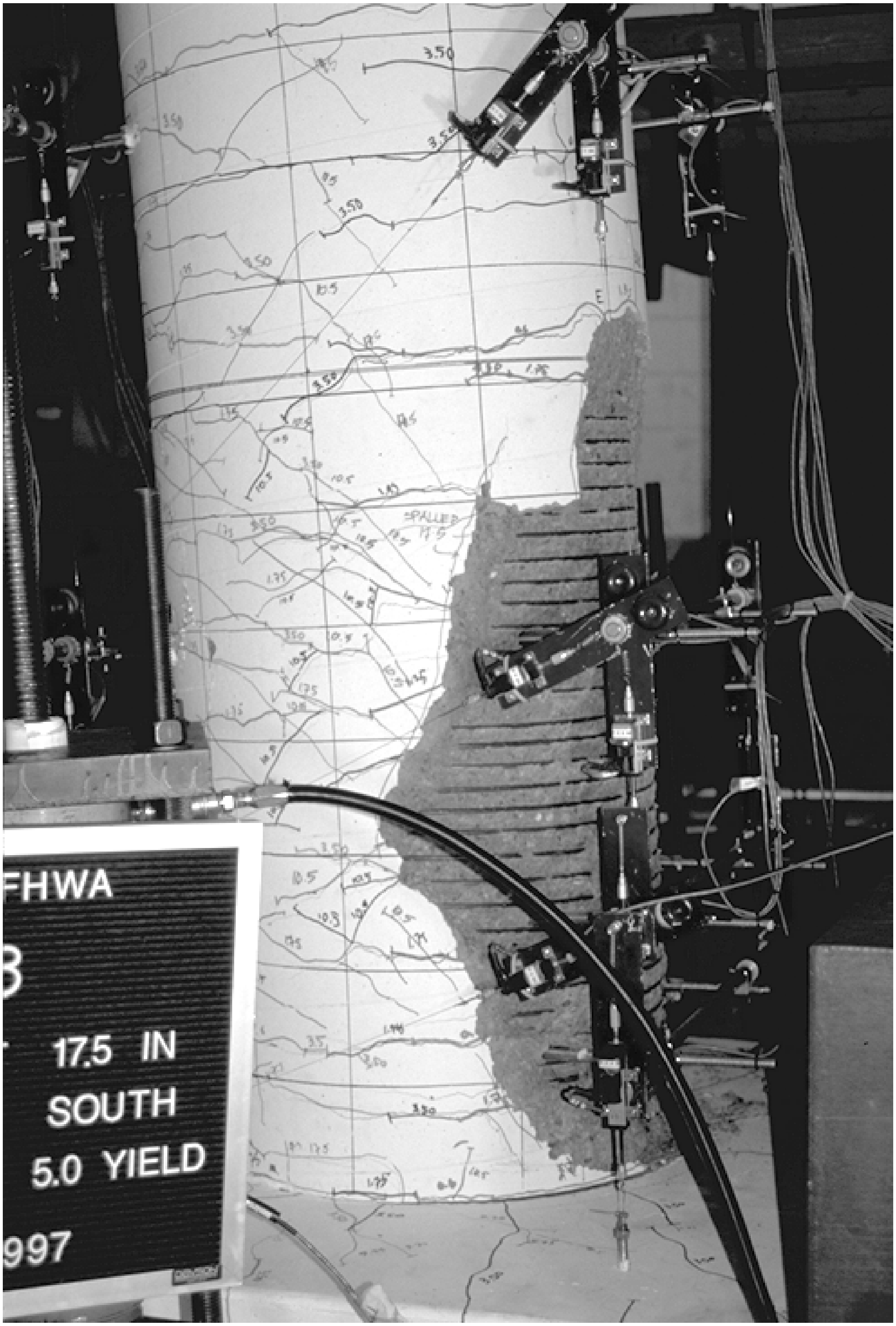

Figure 3.20: Column 828 at a South Displacement of 17.5 Inches

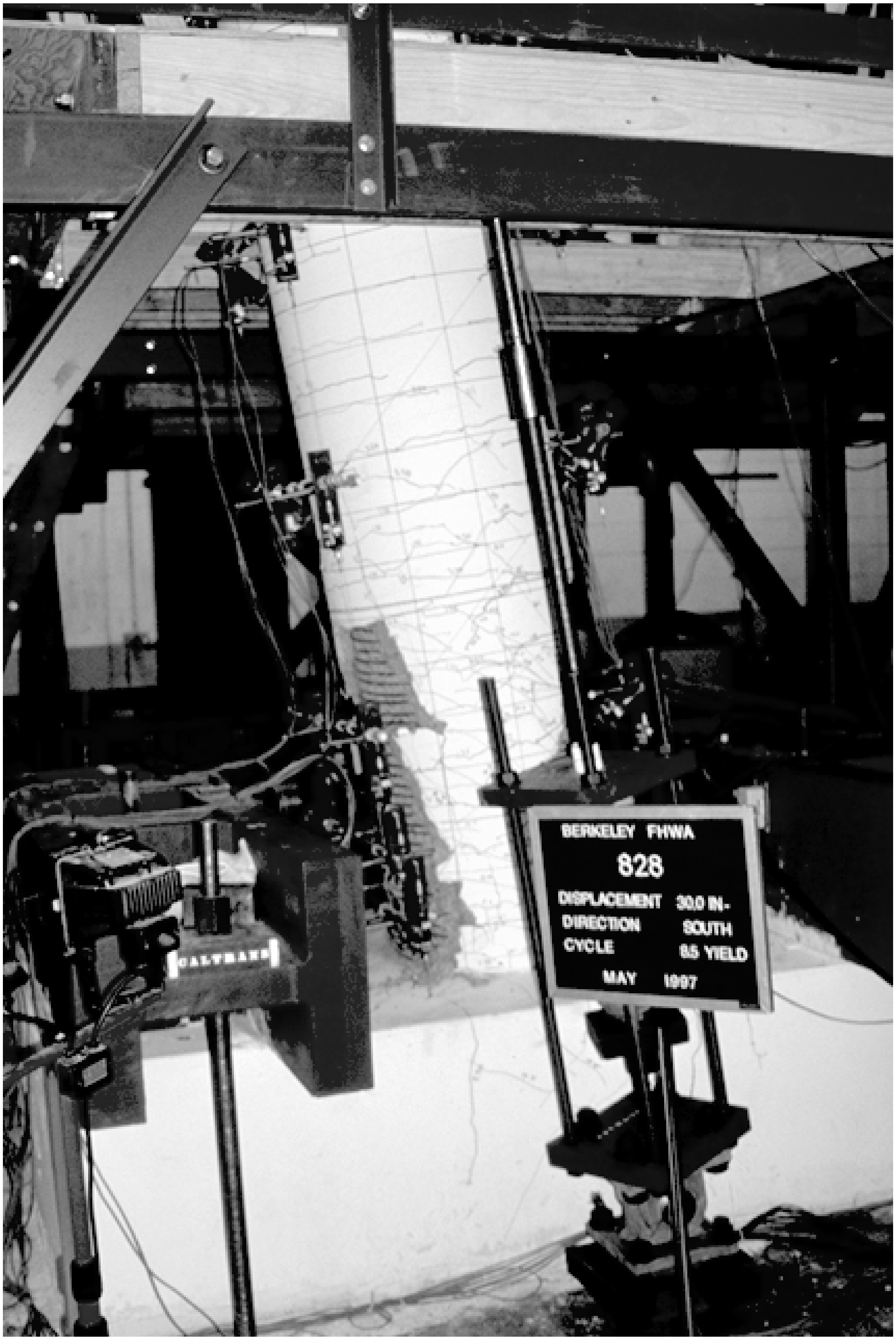

Figure 3.21: Column 828 at a South Displacement of 30.0 inches

3.7 COLUMN 1028 — EXPERIMENTAL RESULTS

Column 1028, designed in accordance with the provisions of ATC-32 [1996], achieved a displacement ductility of 9 and showed ductile response similar to that of Column 828. The load-displacement history for this column is shown in Figure 3.22.

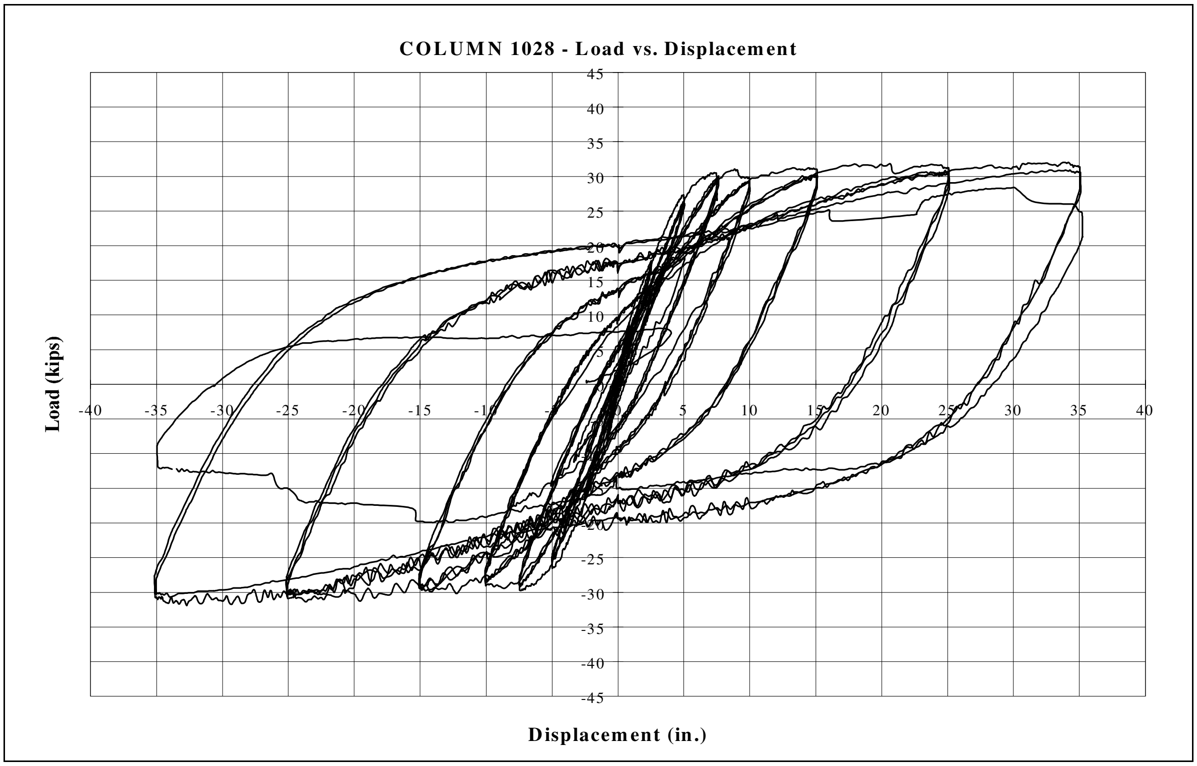

Figure 3.22: Hysteretic Response of Column 1028

Figure 3.23 shows the displacement components at each displacement cycle as a percentage of the total displacement for Column 1028. For this slender column, the flexural component deformation contributed approximately 65 to 70 percent of the total column displacement. Slip accounted for as much as 20 to 25 percent of the total displacement. Less than 5 percent of the total displacement was attributable to shear deformations. An error of approximately 15 percent exists at the lowest displacement levels for reasons described previously.

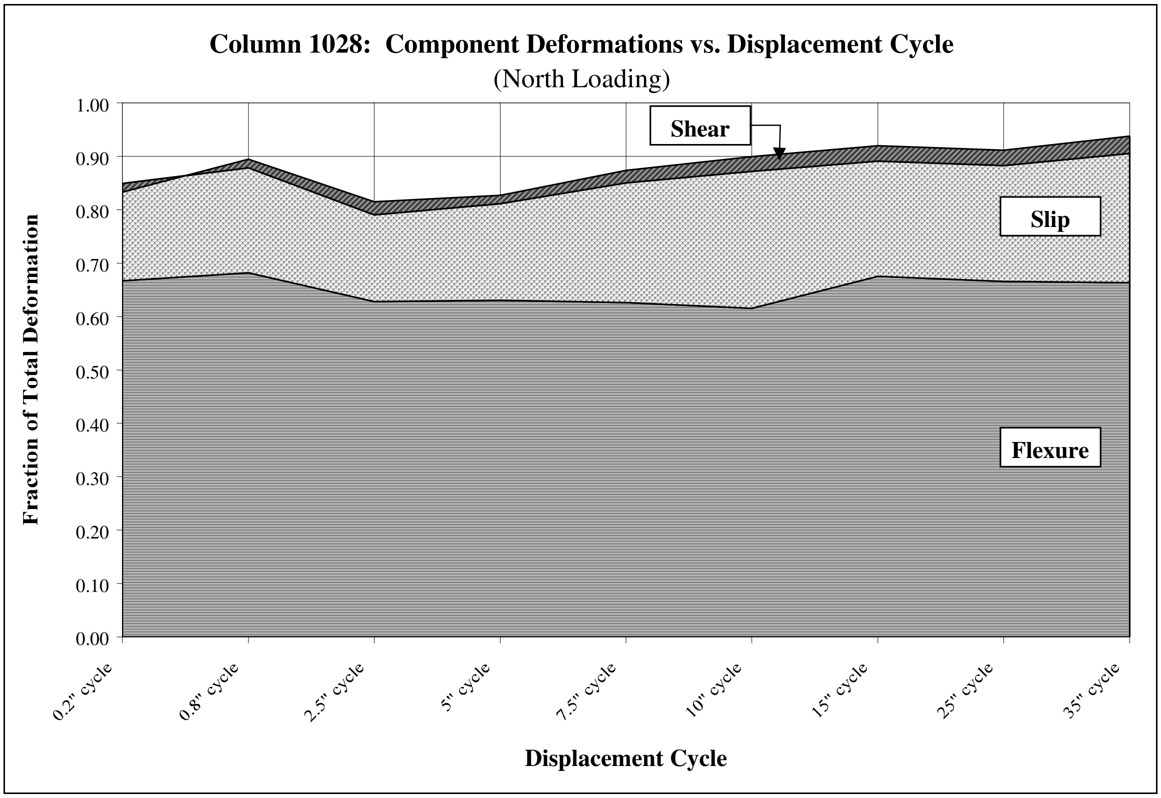

Figure 3.23: Column 1028 Component Deformations

For Specimens 1028, the first flexural cracks were observed at a displacement of 0.80 inches, approximately 20 percent of the yield displacement and 0.33 percent drift. Flexural cracking within Column 1028 occurred at closer intervals than in Column 828. The spacing between cracks on the face of Column 1028 ranged between 4 and 5 inches, while flexural cracking within Column 828 typically occurred at spacings slightly greater than 5 inches. The crack width at the interface of the column and anchor block of Column 1028 ranged from 0.03 inches at a displacement of 5 inches to 3/16 inches at a displacement of 35 inches. Diagonal cracks were observed to form in the vicinity of the transition zone of the transverse steel during the first south displacement step of the 35-inch displacement cycle.

Initial concrete spalling for Column 1028 was observed at a displacement of 10 inches. The spalled height at this displacement level reached 22 inches above the column base (Figure 3.24). The height of spalling increased with increasing displacement. Spalling stabilized at a displacement between 25 and 35 inches, progressing to a height of 46 to 53 inches above the interface between the column and anchor block (Figures 3.25 and 3.26). The concrete cover thickness was measured to range between 1.12 and 1.25 inches.

First yield of the south face longitudinal steel occurred at a displacement of 3.87 inches. During the second displacement step to 35 inches north, plastic deformation of the spiral was observed on the north face at a height of approximately 9.5 inches above the interface between the column and anchor block. In addition, buckling of the extreme longitudinal bars was observed. The center longitudinal bar appeared to be buckling over a length between 13.5 inches and 17.5 inches above the column base. During the third cycle to 35 inches north, buckling of the longitudinal bars and fracture of the spiral reinforcement was observed at displacements of 15.5 inches and 16.4 inches, respectively (Figure 3.27). Column 1028 at its final damaged state is shown in Figure 3.28.

Table 3.10 summarizes the data obtained at the first north peak of the last seven displacement cycles, including displacement and rotation ductilities, displacement components, compressive and tensile strains, spalling height, and crack widths. The yield displacement and rotations provided are based on values measured at the first yield of the longitudinal steel, as described in Section 3.1.

Table 3.10: Column 1028 Performance History

Displacement Cycle North	2.50"	5.00"	7.50"	10.00"	15.00"	25.00"	35.00"
Displacement Ductility	0.6	1.3	1.9	2.6	3.9	6.5	9.0
Flexural Displacement (in.)	1.6	3.2	4.7	6.2	10.1	16.6	23.2
Slip Displacement (in.)	0.4	0.9	1.7	2.6	3.2	5.4	8.5
Shear Displacement (in.)	0.1	0.1	0.2	0.3	0.4	0.7	1.1
Rotation Ductility @ 6" el.	0.6	1.4	2.6	4.0	5.0	8.4	13.1
Rotation Ductility @ 24" el.	0.7	1.3	2.3	3.6	7.2	12.4	16.0
Nominal Compressive Strain[1]	-0.0012	-0.0022	-0.0044	-0.0085	-0.0255	-0.0381	-0.0320
Longitudinal Steel Tensile Strain[2]	0.0015	0.0086	0.0234	0.0216	0.0302	0.0262	0.0108
Transverse Steel Strain[3]	0.0000	0.0001	0.0004	0.0009	0.0017	0.0024	0.0026
Spalled Height (in.)	N/A	N/A	N/A	22	27.5	46	53
Max. Crack Width @ 12" (in.)	N/A	0.016	0.04	0.06	0.04	0.03	0.03

[1]Nominal compressive strain determined by vertical potentiometer data, linearly interpolated back to center of spiral hoop; obtained at a height of 6 inches.

[2]Longitudinal steel strain read by gage at base of column on south face.

[3]Transverse steel strains shown are from the first north peak of each respective displacement cycle at a height of 6 inches above the column base.

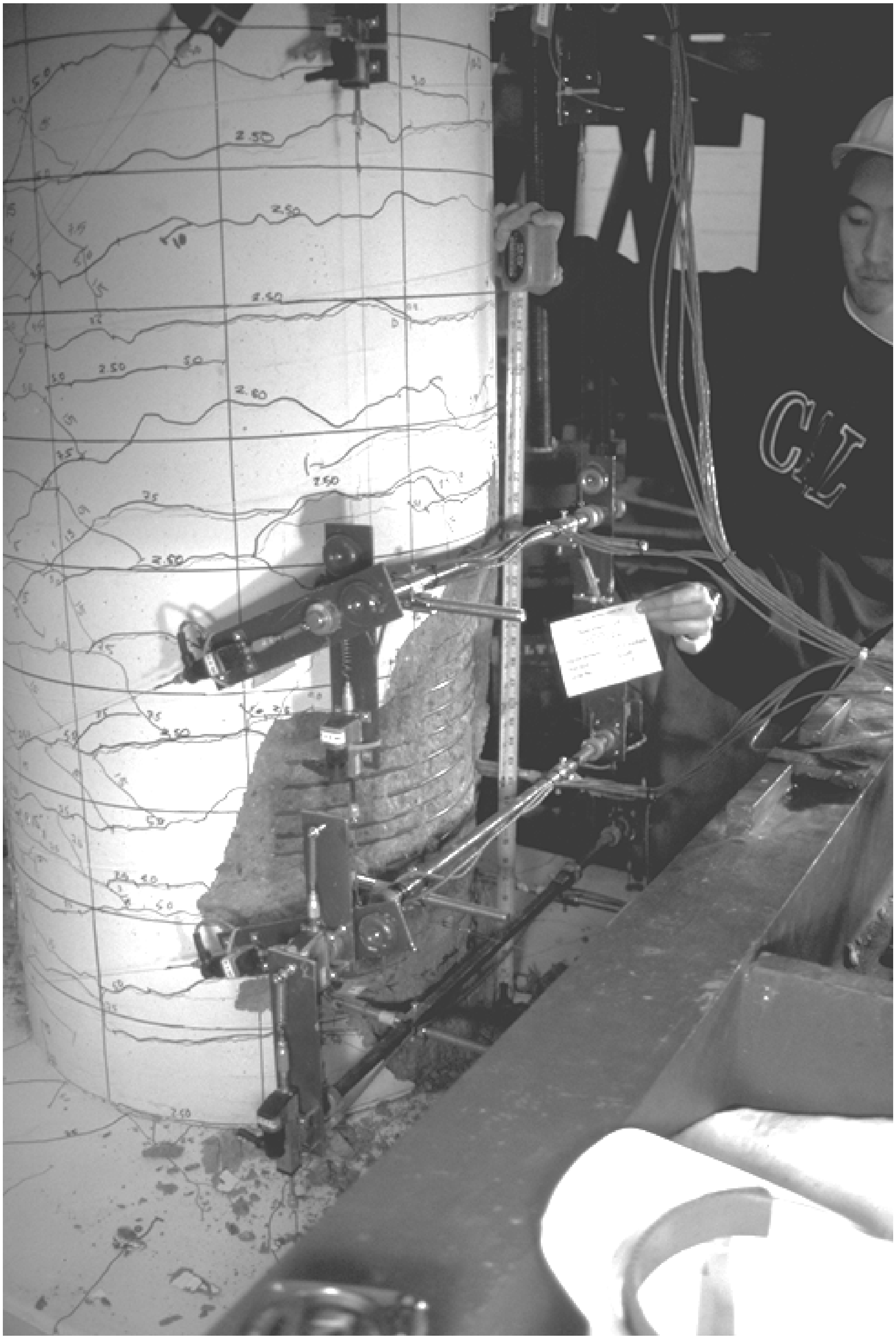

Figure 3.24: Column 1028 at a South Displacement of 10.0 Inches

Figure 3.25: Column 1028 at a South Displacement of 25.0 Inches

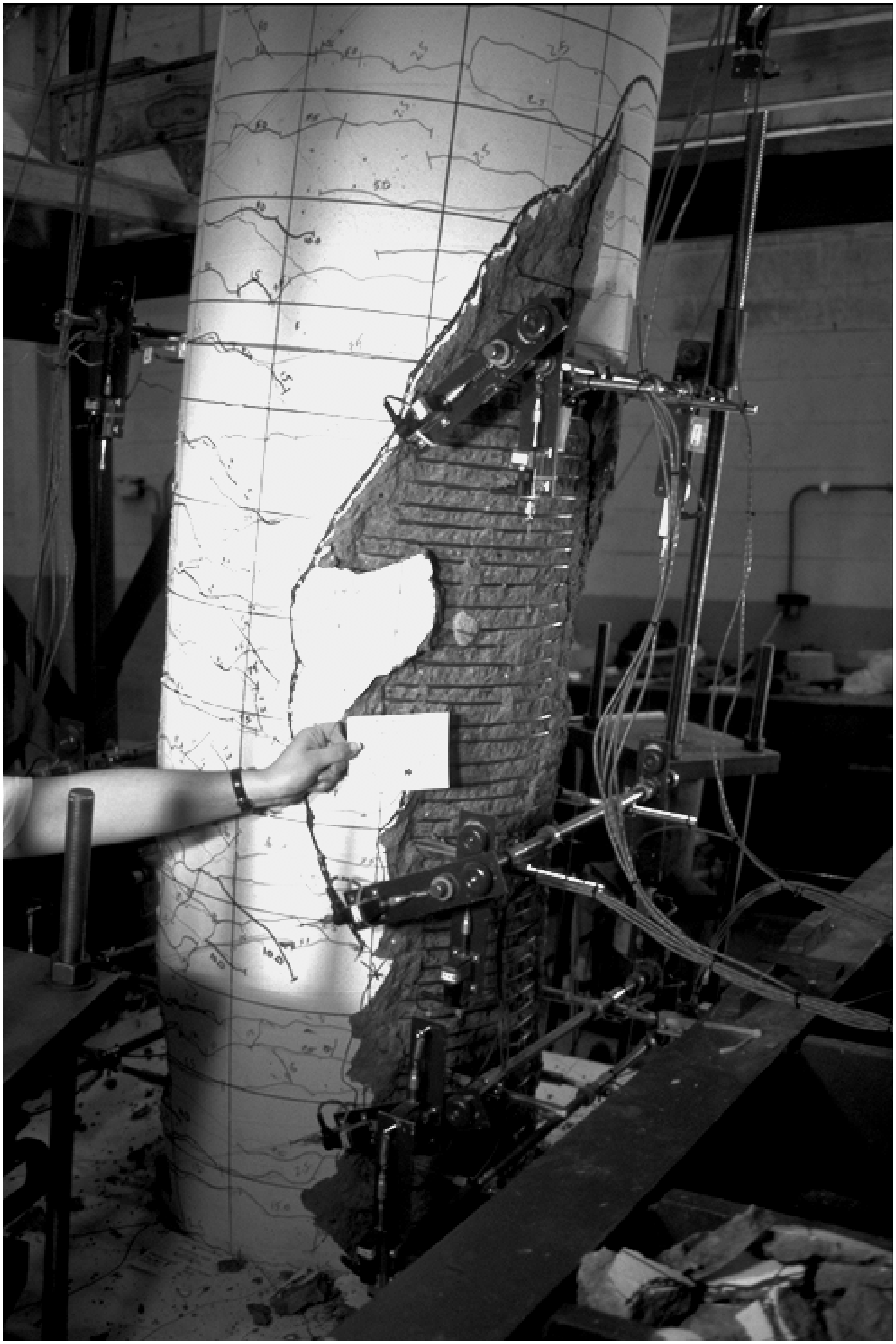

Figure 3.26: Column 1028 at a North Displacement of 35.0 Inches

Figure 3.27: Buckling of Longitudinal Steel in Column 1028 at a North Displacement of 35.0 Inches, Third Cycle

Figure 3.28: Final Damaged State of Column 1028 at a South Displacement of 35.0 Inches

4 Evaluation of Experimental Data

4.1 INTRODUCTION

This chapter explores analytical models for determining the load-displacement behavior and the shear strength of reinforced concrete columns. Comparisons are drawn between calculated results and the actual behavior observed during testing. Confinement length requirements proposed by ATC-32 [1996], the Standards Assocation of New Zealand (NZS) [1982], and Watson et al. [1989] are compared with the spalling observed during testing. Finally, damage progression as a function of loading is discussed.

In general, the ultimate moment strength of each test specimen was lower than the strength calculated in the design analysis; thus, the maximum shear demands were less than anticipated. One explanation for the lower ultimate moment capacity is that the column longitudinal steel exhibited less strain hardening and a lower ultimate strength, during monotonic material testing, than was assumed during the design phase. Figure 4.1 shows a comparison between the stress-strain relationships of the longitudinal steel used in the design analysis and that obtained from material testing.

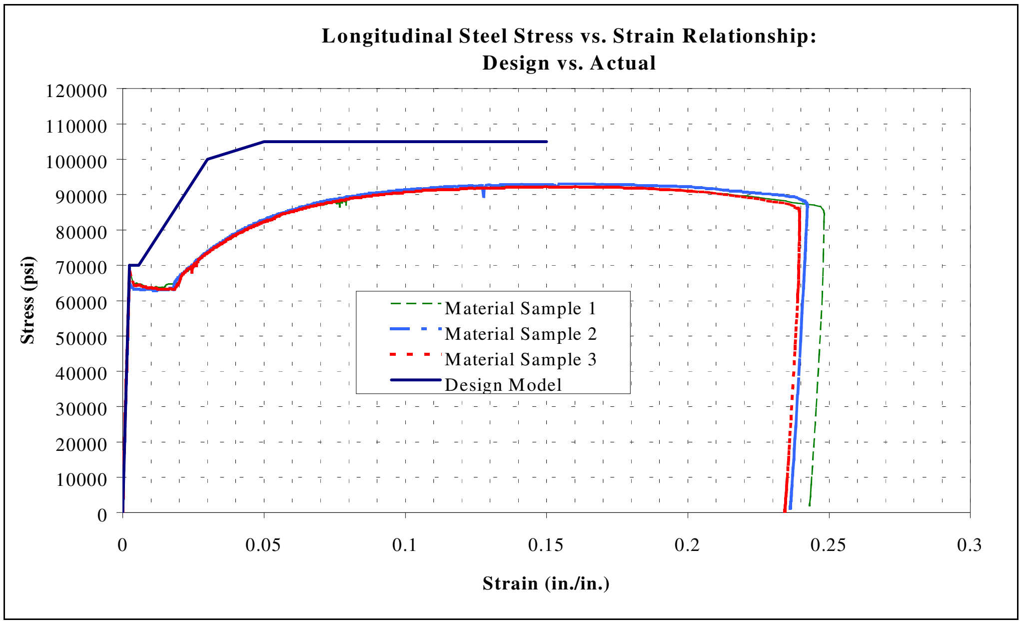

Figure 4.1: Longitudinal Steel Stress vs. Strain Relationship

This over-estimation of strength in the design model had the most significant effect on the design objectives of Specimen 328T. Although the quantity of transverse steel outside the zone of plastic hinging was designed to achieve minimal overstrength capacity in shear, the amount of transverse steel provided was more than sufficient to resist the shear demands imposed during testing.

4.2 FORCE-DISPLACEMENT RESPONSE

The ability to predict the force-displacement response of a reinforced concrete column from a section analysis is a valuable design tool. Ideally, the model should account for ineleastic phenomena such as cracking, yielding, and slip of the longitudinal reinforcement. The following sections summarize a method for calculating the force-displacement response as proposed by Lehman [1998]. The force and curvature demands used in the model are based on a cross-sectional analysis of the test specimens using stress-strain relationships obtained from material testing of the longitudinal steel. The stress-strain relationships for the confined and unconfined concrete are based on models proposed by Mander [1988] and Todeschini [1964], respectively, using averaged compressive strengths obtained from material testing. Results using the Lehman model as applied to the columns in this experimental program are summarized in the following sections. Results also are compared with results obtained from the ATC-32 [1996] recommendations.

4.2.1 Response at Cracking

The response up to cracking is assumed to be linearly-elastic and can be computed for a cantilever column with a point load at the free end as follows:

$$\Delta_{cr} = \frac{\phi_{cr} L^2}{3} \qquad \text{(Eq. 4-1)}$$

$$F_{cr} = \frac{M_{cr}}{L} \qquad \text{(Eq. 4-2)}$$

where Δ_{cr} is the column tip displacement at cracking, ϕ_{cr} is the curvature at cracking, L is the column length, and F_{cr} and M_{cr} are the cracking force demand and moment demand, respectively. Based on a cross-sectional analysis of the columns in the test series, ϕ_{cr} and M_{cr} were determined to be $1.10 \cdot 10^{-5}$ inches^{-1} and 635 kip-inch, respectively. The calculated cracking responses for the columns in the experimental program are shown in Table 4.1. Note that cracking was first observed in the concrete at displacements significantly exceeding the calculated values.

Table 4.1: Calculated Cracking Response

Column	Δ_{cr}	F_{cr}
328	0.019 in.	8.8 kips
328T	0.019 in.	8.8 kips
828	0.14 in.	3.3 kips
1028	0.21 in.	2.6 kips

4.2.2 Response at Section Yield

The yielding of a circular-cross-section reinforced concrete column is progressive. Thus, models that estimate the yield displacement of a column based on first yield of the longitudinal reinforcement, while perhaps appropriate for rectangular columns, generally underestimate the change in stiffness associated with section yielding of a circular-cross-section column. Lehman computes the effective yield displacement as the sum of contributing component displacements, including flexure (Δ'_{fy}), slip (Δ'_{sy}), and shear (Δ'_{vy}), expressed as follows:

$$\Delta'_y = \Delta'_{fy} + \Delta'_{sy} + \Delta'_{vy} \qquad \text{(Eq. 4-3)}$$

where

$$\Delta'_{fy} = \frac{L^2}{3}\phi'_y \qquad \text{(Eq. 4-4)}$$

$$\Delta'_{sy} = L \cdot \phi'_y \cdot \frac{1}{2} \cdot \frac{d_b f_y}{4u} \qquad \text{(Eq. 4-5)}$$

$$\Delta'_{vy} = \frac{V_n \cdot L}{0.4E_c \cdot 0.8(A_g)} \qquad \text{(Eq. 4-6)}$$

$$\phi' = \frac{M_n}{M_y} \cdot \phi_y \qquad \text{(Eq. 4-7)}$$

L is the column length, ϕ'_y is the effective yield curvature, ϕ_y is the calculated curvature corresponding to the first yield of the longitudinal steel, M_n is the calculated moment strength corresponding to a compressive strain of 0.003, M_y is the calculated moment corresponding to the first yield of the longitudinal steel, d_b is the diameter of the longitudinal bar, f_y is the yield strength of the longitudinal steel, f'_c is the nominal compressive strength of the concrete, V_n is the shear demand corresponding to reaching the moment M_n, E_c is the elastic modulus of the concrete, and A_g is the gross cross-sectional area of the column.

Equation 4-4 defines the yield displacement due to curvature, which is assumed to have a maximum value of ϕ'_y at the column base and varies linearly to zero at the free end. Equation 4-5 defines the displacement due to slip of the longitudinal steel within its anchorage. The equation is based on the assumptions of a uniform bond stress of $12\sqrt{f'_c}$ (psi) and that the slip rotation occurs about the neutral axis of the column cross section. Equation 4-6 defines the displacement due to shear deformations, assuming uniform shear distortion over the column height. The term $0.4E_c$ represents the effective shear modulus, G_c, and the term $0.8A_g$ represents an effective shear area.

M_n and M_y for the columns are 8220 kip-inch and 6000 kip-inch, respectively. The values for ϕ_y and ϕ'_y are 0.00018 in.$^{-1}$ and 0.00025 in.$^{-1}$, respectively. Table 4.2 lists the effective yield displacement components as calculated by the preceding method.

Table 4.2: Calculated Effective Yield Displacement of Test Columns

Column	Δ'_{fy}	Δ'_{sy}	Δ'_{vy}	Δ'_{y}
328	0.43 in.	0.13 in.	0.014 in.	0.57 in.
328T	0.43 in.	0.13 in.	0.014 in.	0.57 in.
828	3.07 in.	0.35 in.	0.014 in.	3.43 in.
1028	4.80 in.	0.44 in.	0.014 in.	5.25 in.

4.2.3 Estimated Maximum Response

The ultimate displacement of a reinforced concrete column can be computed as follows:

$$\Delta_u = \Delta'_y + (\phi_u - \phi'_y) \cdot l_p \cdot (L - 0.5 \cdot l_p) \qquad \text{(Eq. 4-8)}$$

where ϕ_u is the curvature capacity of the column, l_p is the plastic hinge length, and all other terms are as defined previously. The model proposed by Lehman is based on the premise that the plastic displacement of the column is the sum of the bending and slip displacement components. The plastic displacement is represented as follows:

$$\Delta_p = \Delta_u - \Delta'_y = \Delta_{fp} + \Delta_{sp} \qquad \text{(Eq. 4-9)}$$

where

$$\Delta_{fp} = \frac{1}{2}(\phi_u - \phi'_y) \cdot l_y \cdot (L - \frac{l_y}{3}) \quad \text{with} \quad l_y = \frac{M_u - M_n}{M_n} \cdot L \qquad \text{(Eq. 4-10)}$$

$$\Delta_{sp} = \frac{1}{2}(\phi_u - \phi'_y) \cdot (f_u - f_y) \cdot \frac{d_b}{4u} \cdot \mathrm{L} \qquad \text{(Eq. 4-11)}$$

Δ_p is the plastic displacement, Δ_u is the ultimate displacement, Δ_{fp} is the plastic flexural displacement, Δ_{sp} is the plastic slip displacement, ϕ_u is the ultimate curvature capacity, f_u and f_y are the ultimate and yield strengths of the longitudinal reinforcement, respectively, and u is an assumed average uniform bond stress taken equal to $6\sqrt{f'_c}$ (psi). All other terms are as defined previously. Rewriting the proposed model for determining the plastic displacement, the plastic hinge length may be expressed as follows:

$$l_p = \frac{l_y}{2} + \frac{1.2(f_u - f_y) \cdot d_b}{(48\sqrt{f'_c})} \text{(psi)} \qquad \text{(Eq. 4-12)}$$

The values for M_u, f_u, and f_y used in the calculations are 9730 kip-inch, 93,000 psi, and 67,000 psi, respectively.

Table 4.3 shows the ultimate displacement for each column as calculated by applying Equation 4-8 using the plastic hinge length defined by Equation 4-12 and an ultimate curvature capacity of 0.0049 inches^{-1}. This ultimate curvature capacity is based on a limiting tensile strain demand of 0.075 in the longitudinal steel, which corresponds to approximately one third of the ultimate tensile strain observed in monotonic testing of the steel coupons. In turn, this limiting steel tensile strain corresponds to an ultimate compression strain in the confined concrete of 0.03. Note that this ultimate compression strain is approximately 50 percent greater than the limiting compression strain of 0.019 obtained by the Mander model.

Table 4.3: Calculated Ultimate Displacements

Column	l_y	l_p	Δ_u	$l_{p\ \mathrm{ATC\text{-}32}}$	$\Delta_{u\ \mathrm{ATC\text{-}32}}$[1]	$\Delta_{u\ \mathrm{ATC\text{-}32}}$[2]
328	13 in.	13.5 in.	4.6 in.	12.5 in.	4.5 in.	2.5 in.
328T	13 in.	13.5 in.	4.6 in.	12.5 in.	4.5 in.	2.5 in.
828	35 in.	24.5 in.	23 in.	22 in.	22 in.	13 in.
1028	44 in.	29 in.	35 in.	26 in.	33 in.	19 in.

[1]Ultimate displacement based on a limiting tensile strain demand of the longitudinal steel of 0.075.

[2]Ultimate displacement based on the ATC-32 limiting compressive strain demand of the confined concrete

ATC-32 [1996] has proposed a simplified approach for estimating the plastic hinge length, which is composed of two components:

$$l_p = 0.08\, l_c + 9\, d_{bl} \qquad \text{(Eq. 4-13)}$$

l_c is the distance between the section of maximum moment within the plastic hinge and the section of zero moment (i.e., the point of contraflexure). For the test columns, l_p is assumed to be the column height, and d_{bl} is the nominal diameter of the longitudinal reinforcement. The first component accounts for the spread of inelasticity as a function of the length between the critical section and the point of contraflexure. The second component accounts for the increased plastic rotation due to strain penetration of the longitudinal reinforcement into the column footing. Table 4.3 shows the calculated ultimate displacements for each column in the experimental program based on the plastic hinge length provision of ATC-32, an ultimate curvature based on a limiting tensile strain demand of 0.075 in the longitudinal steel, and the yield displacement determined from the proposed Lehman model.

The ATC-32 and Lehman models produce results that are similar for a limiting tensile strain demand (ε_s) of 0.075. Furthermore, the ultimate displacements calculated by the two models are reasonably close to the maximum column displacements observed during testing. The ATC-32 and Lehman models underestimated the ultimate displacements for Columns 328 and 328T by approximately 13 percent. The two plastic hinge length models produced roughly the same ultimate displacement capacities for Column 828 and Column 1028. The ultimate displacements calculated by the two models for Column 1028 were within 6 percent of the maximum displacement observed during testing. The ultimate displacement under cyclic loading for Column 828 could not be readily determined from the experiment since failure of the test specimen was not achieved. Nevertheless, the ultimate displacements of 22 inches and 23 inches calculated by the ATC-32 and Lehman plastic hinge length models, respectively, compare favorably with the damage states of Column 828 at its maximum displacement of 18 inches.

It is noted that ATC-32 [1996] does not use $\varepsilon_s = 0.075$ as a limiting factor in the plastic analysis of columns. ATC-32 Paragraph 8.18.2.4.1 specifies that for designs based on plastic analyses, the amount of transverse reinforcement provided in the plastic end region shall not be less than

$$\rho_s = 0.09(\varepsilon_{cu} - 0.004) \cdot \frac{f'_{cc}\,(\text{psi})}{1000} \qquad \text{(Eq. 4-14)}$$

where $f'_{cc} = 1.5 f'_{ce} = 1.5 \cdot (1.3 f'_c)$, ρ_s is the transverse reinforcement ratio provided, ε_{cu} is the ultimate compressive strain of the confined concrete, f'_{cc} is the compression strength of the confined concrete, f'_{ce} is the expected concrete compression strength, and f'_c is the nominal concrete concrete compression strength. Substituting the transverse reinforcement ratio provided in the well-confined zones of the test columns (0.0092) into Equation 4-14 and solving for ε_{cu} gives an ultimate compressive strain of 0.015 in the confined concrete. Based on a moment-curvature analysis of the column cross section, this ultimate compressive strain corresponds to a steel tensile strain demand and an ultimate curvature of 0.041 and 0.0026 inches^{-1}, respectively. Using these limits prescribed by ATC-32 results in a significant reduction in the calculated ultimate displacement. Table 4.3 shows the calculated displacements of the columns in this experimental program based on the limiting compressive strain of the confined concrete derived from ATC-32.

Based on an analysis of the column cross section and the Lehman model, a comparison of the calculated force-displacement response and the actual response of the experimental columns is shown graphically in Figures 4.2 and 4.3. The Lehman model, used in conjunction with appropriate methods for determining the column strength and curvature capacities, gives reasonable estimates of the force-displacement response of these reinforced concrete columns.

While the force-displacement results of the Lehman model compare favorably with the response of the test columns, it is of interest to compare the relative displacement components (flexure, slip, and shear) computed by the Lehman model with those observed during testing. Figures 4.4 through 4.7 show a comparison between the calculated and experimental displacement components expressed as a percentage of the total displacement. The calculated displacement components were computed at ϕ'_y, 5 ϕ'_y, $10\phi'_y$, and $15\phi'_y$.

In general, the component deformation relationships calculated by the Lehman model follow the same general trends as those obtained from the test data. The displacement components calculated using the Lehman model appear to compare more favorably with the experimental displacement components for slender columns, such as Columns 828 and 1028, than for short columns. Beyond the effective yield displacement of the column, the Lehman model neglects any additional shear deformation contributions to the total displacement. While this assumption appears to be appropriate for slender columns, such as Columns 828 and 1028 (Figures 4.6 and 4.7), the shear deformation contributions computed by the Lehman model significantly underestimate the experimental shear deformations for Columns 328 and 328T (Figures 4.4 and 4.5). For each column, the Lehman model overestimates the apparent flexural displacement contribution and underestimates the apparent slip displacement contribution. The difference between the calculated and experimental displacement components appears to decrease with increasing column aspect ratio.

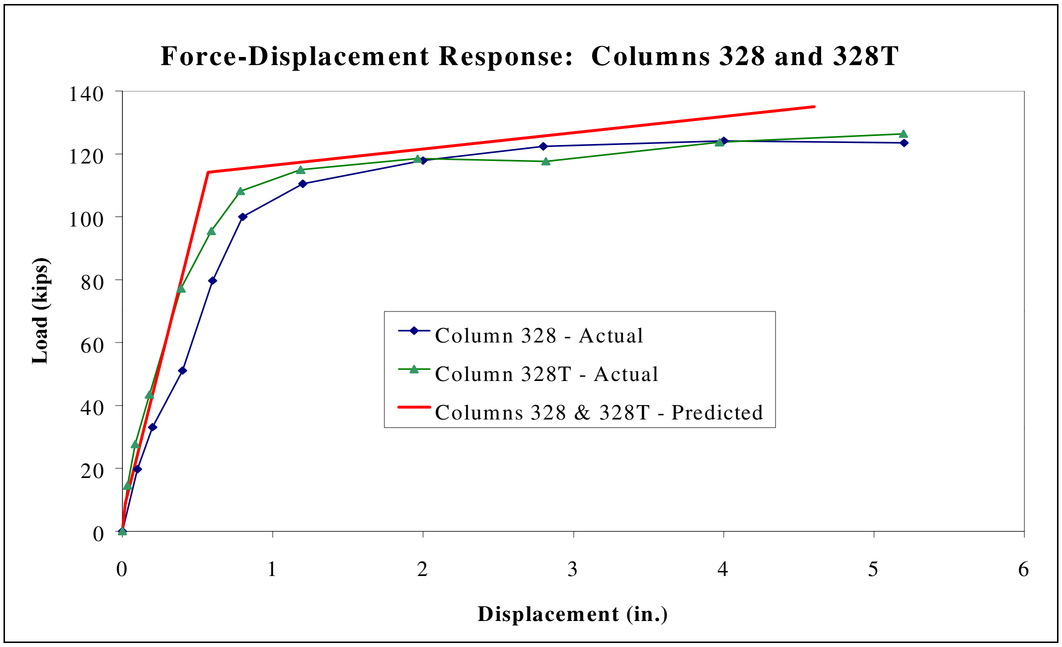

Figure 4.2: Columns 328 and 328T Force-Displacement Response

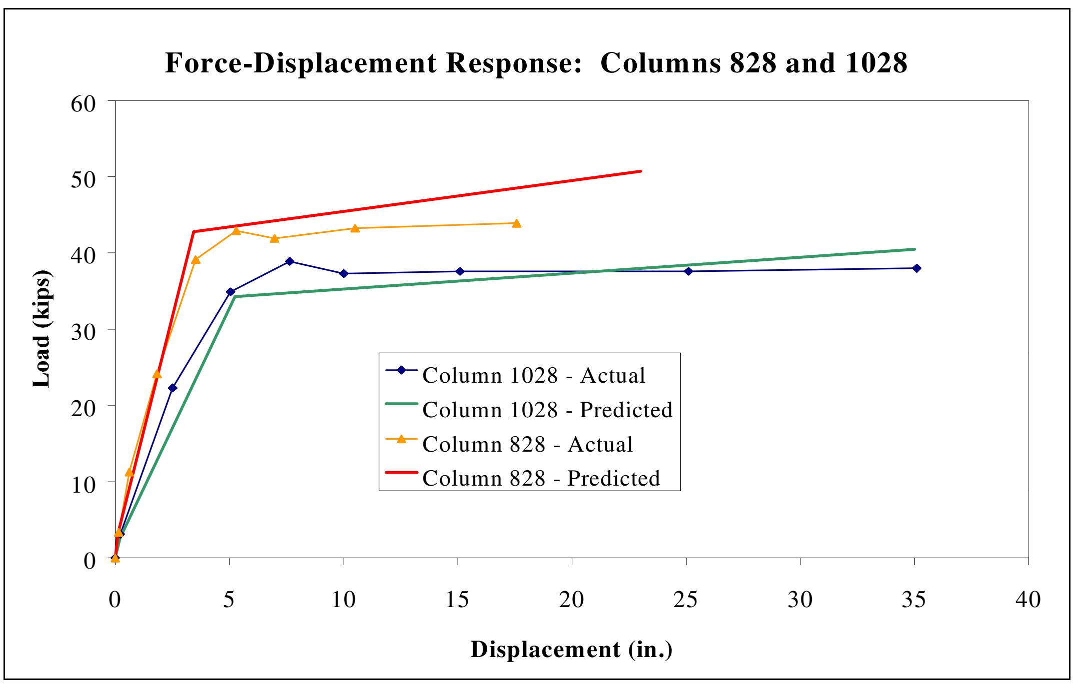

Figure 4.3: Columns 828 and 1028 Force-Displacement Response

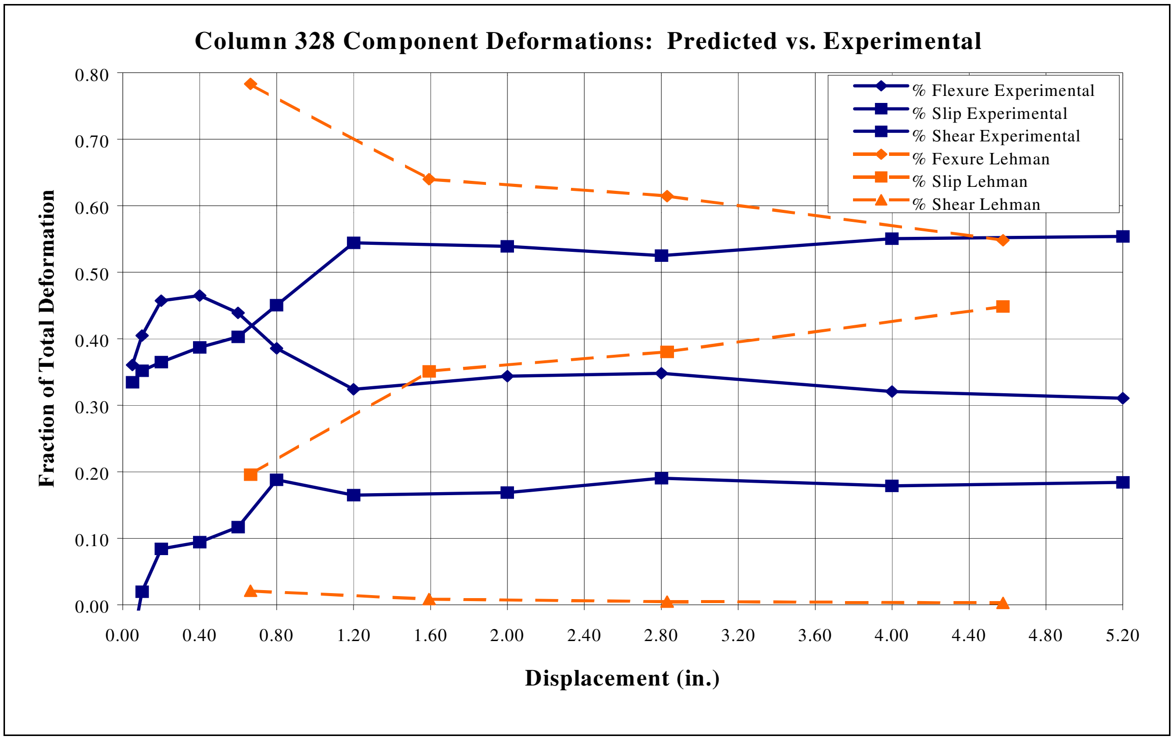

Figure 4.4: Column 328 Component Deformations (Calculated vs. Experimental)

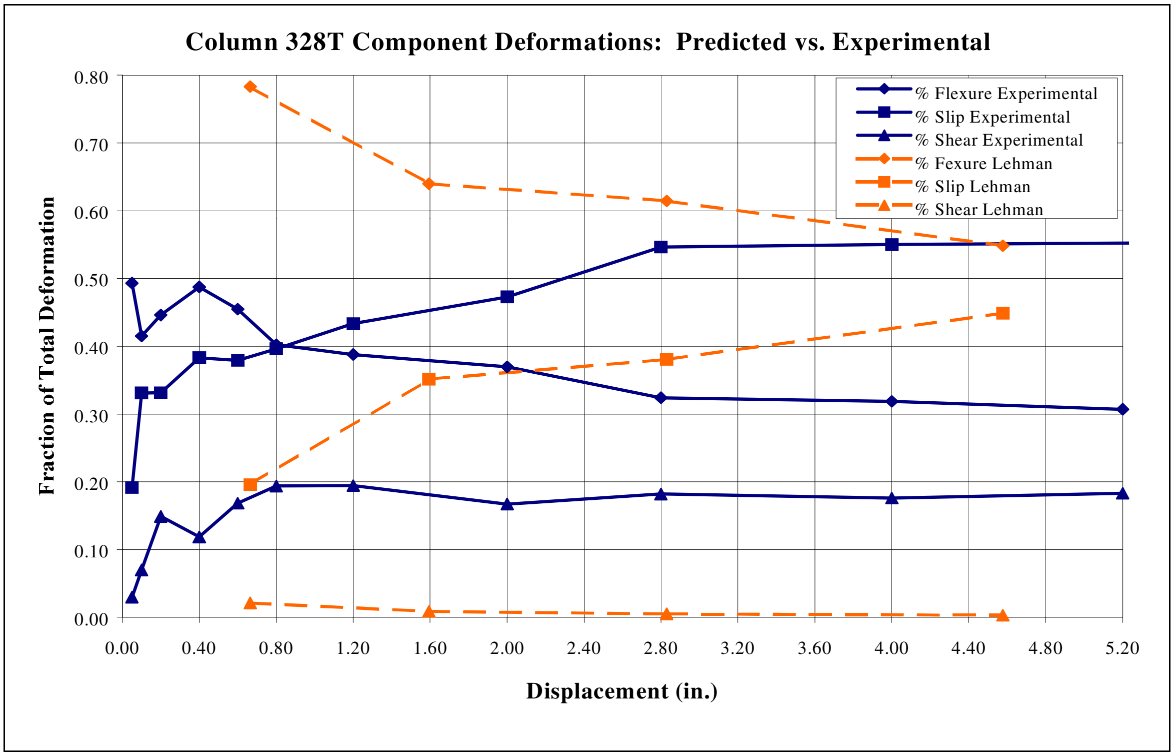

Figure 4.5: Column 328T Component Deformations (Calculated vs. Experimental)

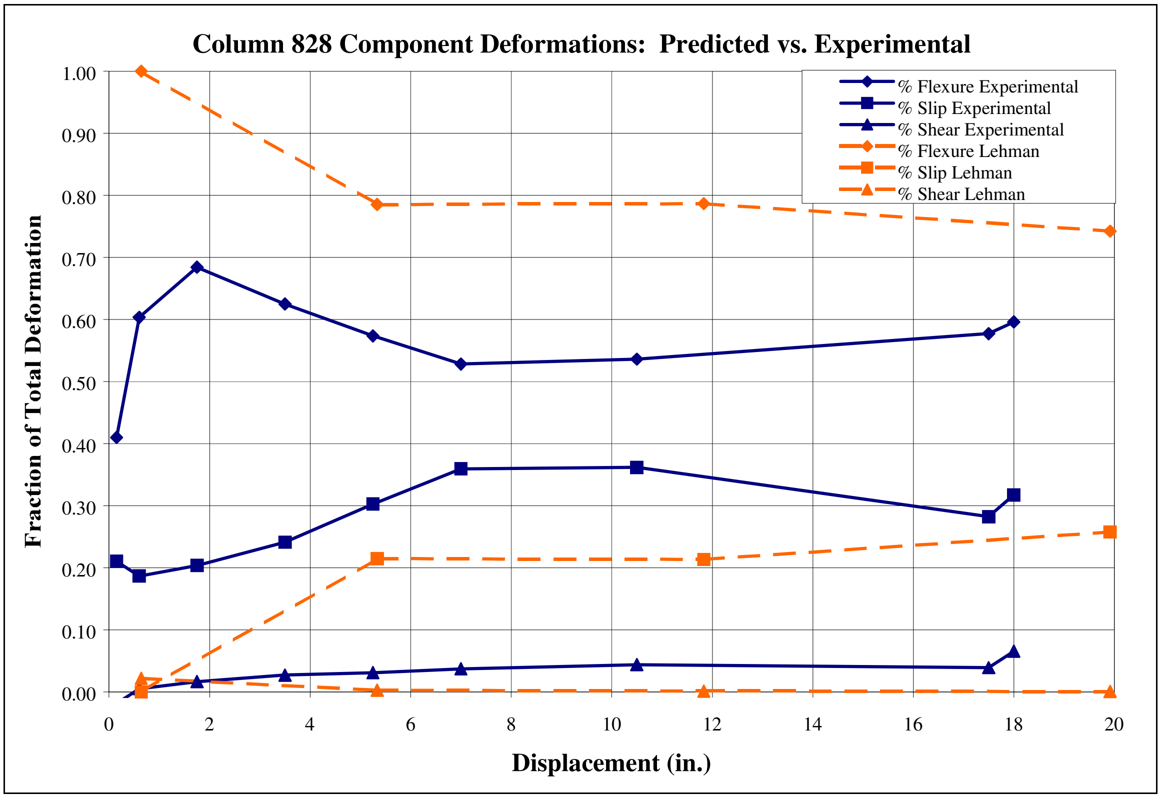

Figure 4.6: Column 828 Component Deformations (Calculated vs. Experimental)

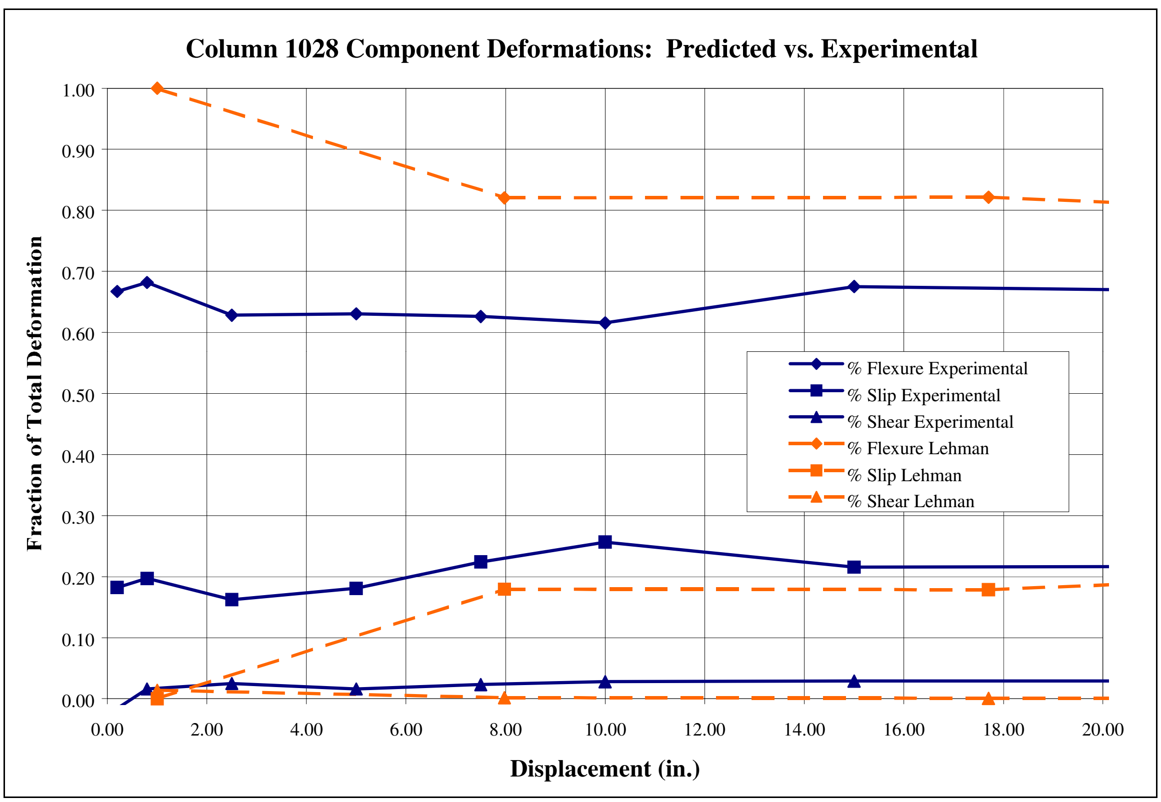

Figure 4.7: Column 1028 Component Deformations (Calculated vs. Experimental)

4.3 LENGTH OF CONFINEMENT REQUIREMENTS

In order to provide adequate ductility and energy dissipation under seismic loadings, it is necessary to provide adequate confinement within the plastic hinge region(s) of reinforced concrete columns. There has been considerable debate regarding the necessary length of this confined region to ensure that the ductility demand can be achieved. An indicator of the spread of inelasticity, or high strain demands, is the length over which spalling occurs. Thus, it may be prudent to provide confinement over the spalled length to ensure that premature failure of a column does not occur outside the confined region. ATC-32 [1996], NZS-3101 [1982], and Watson [1989] have proposed methods for determining an appropriate length of confinement. These methods are summarized below.

ATC-32:

for $P_e/f'_cA_g<0.3$,	L_c =	greater of	(a) column cross-sectional dimension in the plane of loading and (b) portion of column over which $M \geq 0.80\ M_{max}$
for $P_e/f'_cA_g \geq 0.3$,	L_c =	greater of	1.5 times the requirements listed above

NZS-3101:

for $P_e/f'_cA_g \leq 0.25$,	L_c = greater of	(a) column cross-sectional dimension in the plane of loading and (b) portion of column over which $M \geq 0.80\ M_{max}$
for $0.25<P_e/f'_cAg \leq 0.50$	L_c = greater of	(a) 2.0 times the column cross-sectional dimension in the plane of loading and (b) portion of column over which $M \geq 0.70\ M_{max}$
for $P_e/f'_cA_g>0.50$,	L_c = greater of	(a) 3.0 times the column cross-sectional dimension in the plane of loading and (b) portion of column over which $M \geq 0.70\ M_{max}$

Watson:

for all P_e/f'_cA_g,

$$L_c = D \cdot \left(1 + 2.8 \cdot \frac{P_e}{f'_c \cdot A_g}\right) \qquad \text{(Eq. 4-14)}$$

where L_c is the length of confinement, P_e is the expected axial load, f'_c is the nominal concrete compressive strength, A_g is the gross cross-sectional area of the column, M is the moment demand at the location in question, M_{max} is the maximum moment demand at the critical section of the column, and D is the gross diameter of the column.

The length of confinement requirements proposed by ATC-32 [1996], NZS-3101[1982], and Watson [1989] were compared against the spalled length observed during experimental testing of Columns 328, 328T, 828, and 1028. The results of this comparison are shown in Table 4.4. The variables L_c and L_{spall} are the length of confinement provided and length of spalling observed during testing, respectively.

Table 4.4: Length of Spalling vs. Length of Confinement Required

Column	L_c	L_{spall}	$\frac{L_{spall}}{L}$	$\frac{L_{spall}}{L_{ATC-32}}$	$\frac{L_{spall}}{L_{NZS}}$	$\frac{L_{spall}}{L_{Watson}}$
328T	24"	16"	0.22	0.67	0.67	0.53
828	36"	38"	0.20	1.05	1.05	1.26
1028	48"	53"	0.22	1.10	1.10	1.76

It is of interest to note that Watson [1989] concluded that the required length of a confined region is independent of the column aspect ratio and is primarily a function of the axial load ratio and section depth. However, it is evident from the results of this experimental program that the column aspect ratio has a significant effect on the length of spalling and the spread of plastic hinging. Based on these results, it is concluded that the confinement length equation proposed by Watson yields results that are not conservative for slender columns.

The confinement length requirements of ATC-32 [1996] and NZS-3101 [1982] are essentially the same for the four columns in this experimental program since the axial load ratio for these columns is less than 10 percent. Unlike Watson, the confinement length requirements specified by ATC-32 and NZS-3101 indirectly account for aspect ratio by requiring confinement over at least 20 percent of the column shear span, or where the moment demand exceeds 80 percent of the maximum moment demand. This requirement appears to correlate well with the spalling length observed in the test columns; however, the effect of higher axial loads on the spalled length of slender columns was not identified in this test program and may be of interest for future research.

In addition to the length of spalling, the compressive strain demands of the test columns were approximated at the peak displacements. Of particular interest was the assurance that the compressive strain demands were not excessively high outside the confined regions of Columns 828 and 1028. The approximate strain demands were determined by averaging the recorded linear potentiometer displacements at each instrumentation level along the column height and interpolating linearly back to the column face. Figures 4.8 and 4.9 show the compressive strain demands for Columns 828 and 1028 plotted at various peak displacements.

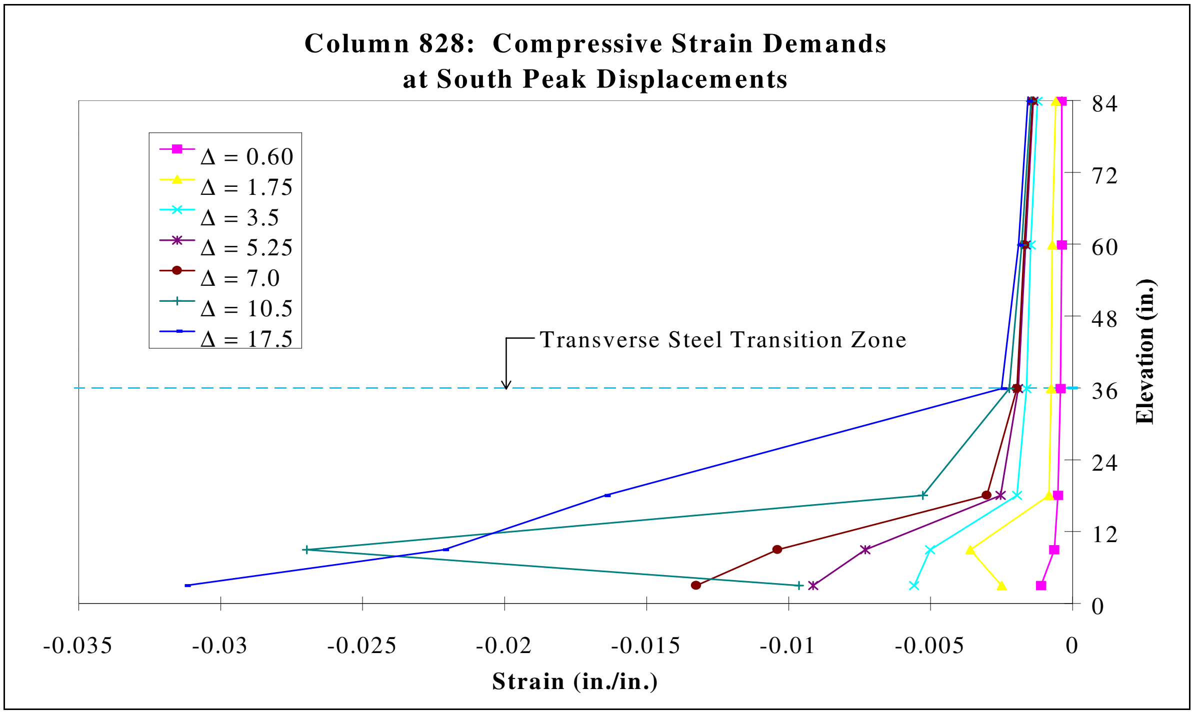

Figure 4.8: Column 828 Compressive Strain Demands

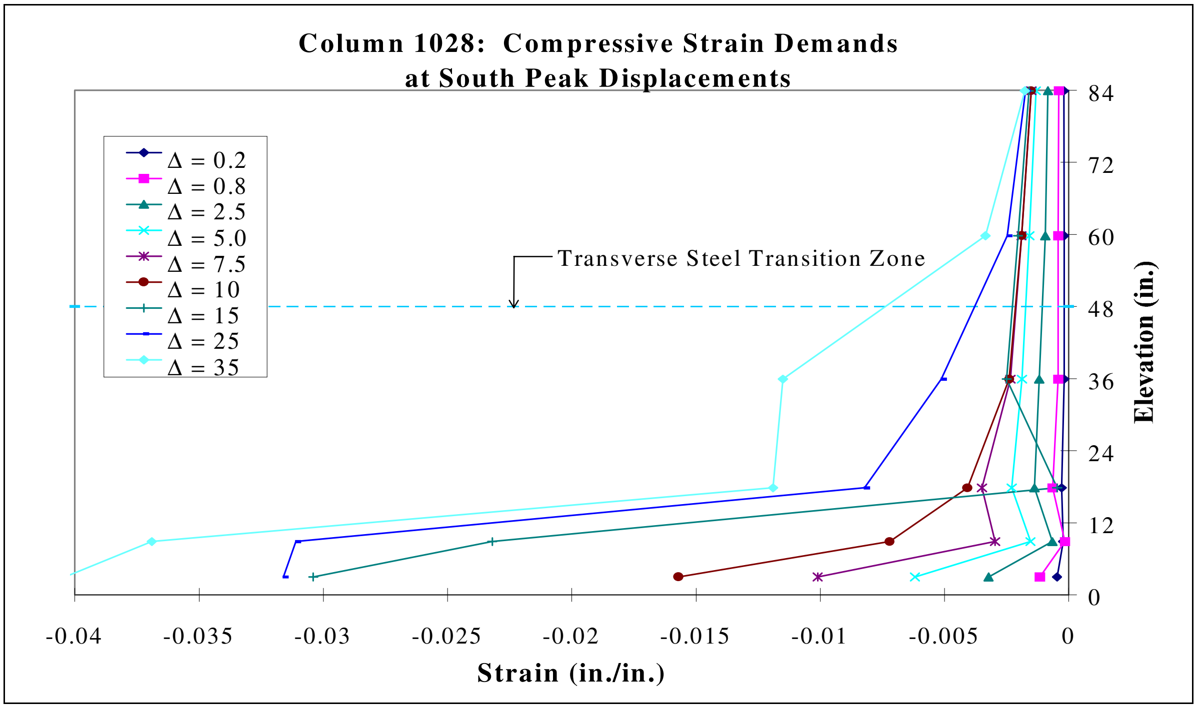

Figure 4.9: Column 1028 Compressive Strain Demands

The maximum estimated compressive strain demands at the transition zone of the transverse steel in Columns 828 and 1028 are 0.0025 and 0.0065, respectively. Because the nominal moment capacity of a column is typically regarded as the moment achieved at a peak compressive strain of 0.003, it would be reasonable in design to preclude the compressive strain demand from exceeding 0.003 outside of the well-confined region. This postulation is satisfied in Column 828. However, the peak compressive strains in Column 1028 exceed 0.003 to a height of 70 inches above the critical face. Nonetheless, this column achieved a displacement ductility of approximately 9. The ductile behavior of Column 1028 can be explained by the fact that the strain capacity provided by the transverse steel outside of the well-confined region is well above the strain demand. Using the expression $\varepsilon_{cu} = 0.004 + 0.02\rho_{sp} f_y$ [Qi and Moehle, 1991] to estimate the peak concrete compressive strain capacity, where f_y = yield strength of spiral not to exceed 60 ksi, and ρ_{sp} = volume ratio of spiral steel ($\approx$ 0.0045), ε_{cu} is calculated to be 0.009, which exceeds the measured strain at the transition. Although the transverse reinforcement ratio was relaxed by one-half at the transition, there was not an abrupt change in the geometry of the column that potentially could have led to a premature failure outside of the well-confined region.

Based on the experimental results of Columns 828 and 1028, it appears that the provisional recommendations of ATC-32 [1996] are adequate for prescribing a zone of confinement. In addition, although ATC-32 permits a reduction in the transverse reinforcement ratio along the column height, this reduction is not sufficient to cause an abrupt change in geometry, which could prohibit a column from achieving reasonably ductile behavior and energy dissipation during reversed cyclic loading.

4.4 SHEAR STRENGTH

Numerous methods have been proposed for calculating the shear strength of reinforced concrete columns. Six such methods were employed in this experimental investigation to ascertain their validity in providing reasonable estimates of the shear strength of the columns tested. Although shear was not a major contributor to the failure mechanism of the four columns tested, comparing the results of the proposed methods with the observed behavior, particularly that of Column 328T, can provide a general indication of the validity of each shear strength model. The six models investigated included the following: the American Concrete Institute (ACE-318)

[1995], the Caltrans Bridge Design Specifications [BDS, 1993], ATC-32 [1996], Aschheim et al. [1997], Ohtaki et al. [1997], and Konwinski [1996] models. While most models specify the use of nominal material strengths in the capacity calculations, actual material strengths were used for the demand/capacity comparisons in this experimental program. A summary of the demand/capacity comparisons for each model is presented in Table 4.5. Note that the nominal shear strength (actually, nominal material properties and quantities) within the heavily confined region is the same for each column, and the nominal quantities within the lightly confined region of Columns 828 and 1028 are the same.

4.4.1 ACI 318-95 and BDS

The shear strength provisions of BDS [1993] and ACI [1995] are essentially the same. The nominal shear strength prescribed by BDS and ACI is the sum of two contributions, the shear strength provided by the concrete (V_c) and the shear strength provided by the shear reinforcement (V_s).

$$V_n = V_c + V_s$$

where

$$V_c = 2\left[1 + \frac{P_e}{2000 \cdot A_g}\right]\sqrt{f_c'} \cdot b_w d \qquad \text{(Eq. 4-15)}$$

where f'_c is the nominal concrete compressive strength in psi (pounds per square inch), P_e is the expected axial load, A_g is the gross cross-sectional area of the column, b_w is taken to be the column diameter, and d is assumed to be 0.8 times the column diameter for simplicity. The steel contribution is given as follows:

$$V_s = \frac{A_v f_y d}{s} \qquad \text{(Eq. 4-16)}$$

where A_v is the area of shear reinforcement within a distance s (taken as two times the cross-sectional area of a single spiral wire), f_y is the nominal yield strength of the transverse steel, and s is the spiral pitch. For this study, d is assumed to be the core diameter of the column.

Based on the provisions of BDS and ACI using expected material strengths, the nominal shear strength within the heavily-confined region of each column was calculated to be 266 kips. Similarly, the nominal shear strengths within the lightly confined region of Column 328T and Columns 828 and 1028 were calculated to be 123 kips and 145 kips, respectively.

Based on the provisions of BDS and ACI using actual material strengths, the nominal shear strength within the heavily confined region of each column was calculated to be 286 kips. Similarly, the nominal shear strengths within the lightly confined region of Column 328T and Columns 828 and 1028 were calculated to be 149 kips and 183 kips, respectively.

4.4.2 ATC-32

Like the BDS [1993] and ACI [1995], the shear strength provisions of ATC-32 [1996] are based on the shear strength contributions of the concrete and the transverse steel.

$$V_n = V_c + V_s$$

where inside the column end region

$$V_c = 2\left[0.5 + \frac{P_e}{2000 \cdot A_g}\right]\sqrt{f_c'} \cdot 0.8 \cdot A_g \qquad \text{(Eq. 4-17)}$$

and outside the column end region

$$V_c = 2\left[1 + \frac{P_e}{2000 \cdot A_g}\right]\sqrt{f_c'} \cdot 0.8 \cdot A_g \qquad \text{(Eq. 4-18)}$$

f'_c is the nominal concrete compressive strength in psi, P_e is the expected axial load, and A_g is the gross cross-sectional area of the column. The steel contribution is given as follows:

$$V_s = \frac{\pi}{2}\frac{A_{sp} f_y D'}{s} \qquad \text{(Eq. 4-19)}$$

where A_{sp} is the cross-sectional area of the spiral wire, f_y is the nominal yield strength of the transverse steel, D' is the core diameter of the column, and s is the spiral pitch.

Based on the provisions of ATC-32 using expected material strengths, the nominal shear strength within the heavily confined region of each column was calculated to be 182 kips. Similarly, the nominal shear strengths within the lightly confined regions of Column 328T and Columns 828 and 1028 were calculated to be 111 kips and 135 kips, respectively.

Based on the provisions of ATC-32 [1996] using actual material strengths, the nominal shear strength within the heavily confined region of each column was calculated to be 199 kips. Similarly, the nominal shear strengths within the lightly confined region of Column 328T and Columns 828 and 1028 were calculated to be 117 kips and 144 kips, respectively.

4.4.3 *Aschheim Model*

The shear strength model proposed by Aschheim [1997] is also composed of the contributions of the nominal shear strength provided by the concrete and the nominal shear strength provided by the shear reinforcement.

$$V_c = 3.5\left[k + \frac{P_e}{2000 \cdot A_g}\right]\sqrt{f_c'} \cdot 0.8 \cdot A_g \qquad \text{(Eq. 4-20)}$$

where f'_c is the nominal concrete compressive strength in psi, P_e is the expected axial load, A_g is the gross cross-sectional area of the column, and k is a factor based on the displacement ductility of the column as shown in Figure 4.10.

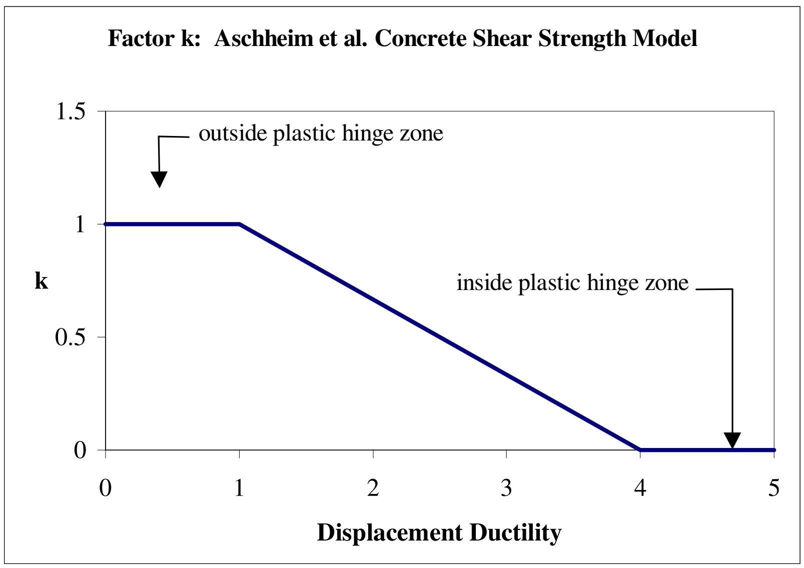

Figure 4.10: Aschheim Model—k factor

The shear strength contribution due to the transverse steel reinforcement is given by the following relationship:

$$V_s = \frac{\pi}{2}\frac{A_{sp} f_y D'}{s \cdot \tan\theta} \qquad \text{(Eq. 4-21)}$$

where A_{sp} is the cross-sectional area of the spiral, f_y is the nominal yield strength of the transverse steel, D' is the core diameter of the column, s is the spiral pitch, and θ is the angle between the diagonal compression strut of the truss mechanism and the longitudinal axis of the column. For assessment purposes, θ is typically assumed to be 30 degrees.

Based on the model proposed by Aschheim [1997] and using expected material strengths, the nominal shear strength within the heavily confined region (k=0) of each column was calculated to be 272 kips. Similarly, the nominal shear strengths within the lightly confined region (k=1) of Column 328T and Columns 828 and 1028 were calculated to be 194 kips and 235 kips, respectively.

Based on the model proposed by Aschheim and using actual material strengths, the nominal shear strength within the heavily confined region of each column was calculated to be 301 kips. Similarly, the nominal shear strengths within the lightly confined region of Column 328T and Columns 828 and 1028 were calculated to be 203 kips and 250 kips, respectively.

4.4.4 Ohtaki Model

In the Ohtaki model, the nominal shear strength is composed of three contributions: the resistance of the transverse reinforcement resulting from the truss mechanism, the concrete shear resistance, and the axial load contribution. Based on this model, the nominal shear strength of a reinforced concrete column is expressed as follows:

$$V_n = V_s + V_c + V_p \qquad \text{(Eq. 4-22)}$$

where

$$V_s = \frac{\pi}{2} A_{sp} f_y \frac{D' - c}{s} \cot\theta \qquad \text{(Eq. 4-23)}$$

A_{sp} is the cross-sectional area of the spiral, f_y is the expected yield strength of the transverse steel, D' is the core diameter of the column, s is the spiral pitch, c is the depth of the compression zone, and θ is the angle between the diagonal compression strut of the truss mechanism and the longitudinal axis of the column. For assessment purposes, θ is typically assumed to be 30 degrees. The concrete contribution is given as follows:

$$V_c = \alpha\beta K \sqrt{f'_c} \cdot 0.8 \cdot A_g \qquad \text{(Eq. 4-24)}$$

where f'_c is the concrete compressive strength in psi and A_g is the gross cross-sectional area of the column. The factors α, β, and K are dependent upon the column aspect ratio, the longitudinal reinforcement ratio, and the section curvature ductility, respectively. The relationships for determining the values of these three factors are shown below and in Figure 4.11.

$$1 \le \alpha \le \left(2 - \frac{M}{VD}\right) + 1 \le 1.5 \qquad \text{(Eq. 4-25)}$$

$$\beta = 0.5 + 20\rho_l \le 1 \qquad \text{(Eq. 4-26)}$$

where M and V are the expected moment and shear demands, D is the column diameter, and ρ_l is the longitudinal reinforcement ratio. The axial load component is expressed as follows:

$$V_p = P \tan \theta = P \frac{D - c - \operatorname{cov}er}{2a} \qquad \text{(Eq. 4-27)}$$

where P is the column axial load, a is the shear span, and D and c are as previously defined.

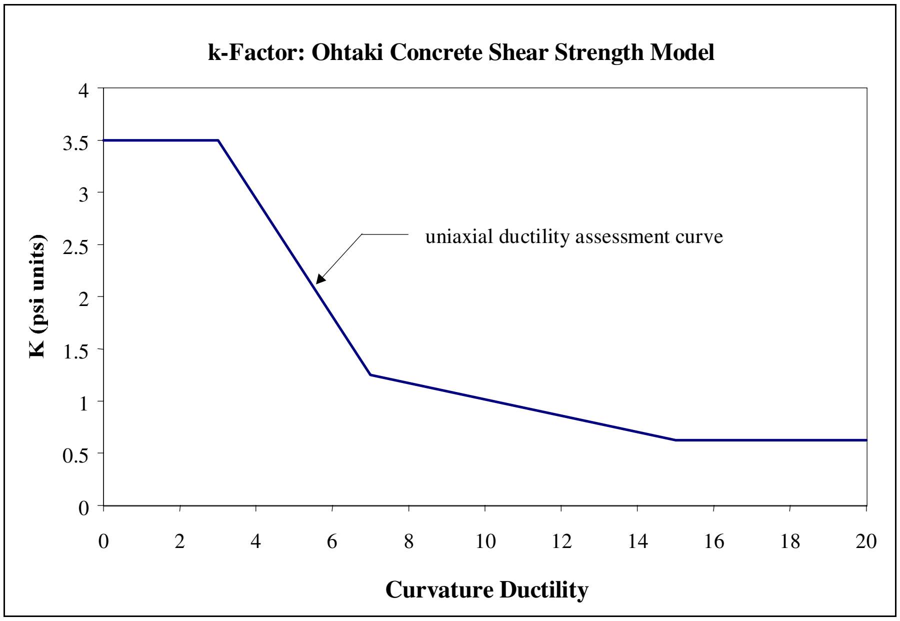

Figure 4.11: Ohtaki Model—k factor

Based on the Ohtaki model using expected material strengths, the nominal shear strength within the heavily confined region of each column was calculated to be 266 kips. Similarly, the nominal shear strengths within the lightly confined region of Column 328T and Columns 828 and 1028 were calculated to be 188 kips and 216 kips, respectively.

Based on the Ohtaki model and using actual material strengths, the nominal shear strength within the heavily confined region of each column was calculated to be 286 kips. Similarly, the nominal shear strengths within the lightly confined region of Column 328T and Columns 828 and 1028 were calculated to be 195 kips and 225 kips, respectively.

4.4.5 Konwinski Model

The shear strength model proposed by Konwinski consists of two components, the shear strength attributable to the transverse steel reinforcement and the shear strength of the concrete. The unit shear strength model proposed by Konwinski is expressed as $v_n = v_s + v_c$, where

$$v_s = r \cdot f_y \qquad \text{and} \qquad r = \frac{A_v}{D \cdot s} \tag{Eq. 4-28}$$

$$v_c = \alpha \cdot \sqrt{f_c'} \cdot \sqrt{1 + \frac{\sigma}{12 \cdot \sqrt{f'_c}}} \qquad \alpha = \frac{6 \cdot D}{a} \qquad \sigma = \frac{P}{A_g} \tag{Eq. 4-29}$$

v_n is the unit shear strength of the reinforced concrete column (psi), v_s is the unit shear strength attributable to the transverse reinforcement (psi), f_y is the yield strength of the transverse steel reinforcement, A_v is the total area of the transverse reinforcement within a distance s, s is the spiral pitch, D is the column diameter, v_c is the unit shear strength of the concrete (psi), f'_c is the concrete compressive strength (psi), a is the shear span, and σ is the expected axial stress (psi). Note that the factor α accounts for the column aspect ratio. The limits on α are as follows: $2 \leq \alpha \leq 4$. The column shear strength may then be expressed as follows:

$$V_n = v_n \, 0.85 \, A_g \tag{Eq. 4-30}$$

where A_g is the gross cross-sectional area of the column.

Based on the Konwinski model using expected material strengths, the nominal shear strength within the heavily confined region of each column was calculated to be 218 kips. Similarly, the nominal shear strengths within the lightly confined region of Column 328T and Columns 828 and 1028 were calculated to be 117 kips and 142 kips, respectively.

Based on the Konwinski model and using actual material strengths, the nominal shear strength within the heavily confined region of each column was calculated to be 235 kips. Similarly, the nominal shear strengths within the lightly confined region of Column 328T and Columns 828 and 1028 were calculated to be 123 kips and 151 kips, respectively.

4.5 DISCUSSION OF SHEAR DEMAND/CAPACITY RESULTS

Table 4.5 summarizes the shear demand-capacity ratios for the four columns in the experimental program based on the aforementioned shear strength models using actual material strengths. The shear strength within the well-confined zone of each column and within the lightly confined zone of Columns 828 and 1028 are well above the shear demand imposed during experimental testing. However, based on the results using ATC-32 [1996] and Konwinski [1996], the shear demand exceeds the shear capacity within the lightly confined zone of Column 328T. Although significant shear cracking was visible in the lightly confined region of Column 328T, shear was not a primary contributor to the ultimate failure of the column. It appears that although the ATC-

32 and Konwinski models are overly conservative for assessing the shear strength of a reinforced concrete column, they may be suitable for design purposes since they appear to yield conservative results.

Furthermore, the Konwinski model for determining the unit shear strength of the concrete is independent of location along the column height. Thus, the concrete shear strength is the same inside and outside the plastic regions of the column.

Note that the concrete shear strength inside and outside the plastic end region is prescribed to be the same value by ACI [1995] and BDS [1993]. This is the case since the axial load ratio, P_e/A_{core}, exceeds 0.1 f'_c. If this were not the case, the concrete shear strength would have been reduced inside the plastic hinge region in accordance with Paragraph 8.16.6.11.4.a of BDS and Paragraph 21.4.5.2 of ACI.

The Ohtaki and Aschheim models for assessing the shear strength in the lightly confined region of Column 328T appear to be overly optimistic. Based on visual observation of the shearing distortion across the cracks on the east and west column faces, as well as the increasing crack widths above the transition zone in the transverse steel, it appears that the column might have been close to achieving a balanced shear/flexure failure mechanism. The design strengths given by ACI and BDS appear to be more consistent with the degree of damage observed for Column 328T.

Table 4.5: Shear Demand/Capacity Ratios for Test Specimens

All Columns	Heavily Confined Region					
Shear Strength Model	V_s	V_c	V_p	V_{328}/V_n	V_{828}/V_n	V_{1028}/V_n
ACI 318-95	206	80	---	0.45	0.17	0.13
Caltrans BDS	206	80	---	0.45	0.17	0.13
ATC-32	162	37	---	0.64	0.24	0.19
Aschheim et al.	281	20	---	0.43	0.16	0.13
Ohtaki et al.	184	58	44	0.45	0.17	0.13
Konwinski	168	67	---	0.54	0.20	0.16

Column 328T	Lightly Confined Region			
Shear Strength Model	V_s	V_c	V_p	V_{328T}/V_n
ACI 318-95	69	80	---	0.86
Caltrans BDS	69	80	---	0.86
ATC-32	54	63	---	1.09
Aschheim et al.	93	110	---	0.63
Ohtaki et al.	61	90	44	0.66
Konwinski	56	67	---	1.04

Columns 828 & 1028	Lightly Confined Region				
Shear Strength Model	V_s	V_c	V_p	V_{828}/V_n	V_{1028}/V_n
ACI 318-95	103	80	---	0.26	0.21
Caltrans BDS	103	80	---	0.26	0.21
ATC-32	81	63	---	0.33	0.26
Aschheim et al.	140	110	---	0.19	0.15
Ohtaki et al.	91	90	44	0.21	0.17
Konwinski	84	67	---	0.32	0.25

V_c = shear strength contribution of the concrete (kips)
V_s = shear strength contribution of the transverse reinforcement (kips)
V_p = shear strength contribution based on the axial load (kips)
V_{328} and V_{328T} = 128 kips (actual shear demand on Columns 328 and 328T)
V_{828} = 48 kips (actual shear demand on Column 828)
V_{1028} = 38 kips (actual shear demand on Column 1028)

4.6 PROGRESSION OF DAMAGE

Appendix A contains data on crack widths and visual damage patterns (Tables A.1-A.4). These data can be used qualitatively to assess performance levels of the columns as a function of loading history. Such comparison can be useful in developing performance-based design methodologies in which visual appearance and required repair may be qualitative performance descriptors. Of course, the indications from the test columns are limited to the specific loading conditions and configurations used in this test program.

Crack width in a reinforced concrete section is related to several parameters, including the reinforcement spacing, concrete cover, section curvature, and reinforcement tensile strain. For the test columns, the main variable is the reinforcement tensile strain, which increases progressively during a test. Tensile strain was measured for the test columns using strain gages. This measurement can be unreliable at small deformations because cracks may occur away from gage locations, and may be unreliable at large deformations because of gage failure. For these reasons, rotation ductility measured in the lower 6 inches of the specimen was used as a substitute for strain.

Figures 4.12 through 4.15 plot maximum crack widths as a function of rotation ductility. Widths are plotted at each of three elevations along the column height (identified by A, B, and C). Widths measured at the peak of a displacement cycle are plotted with a continuous line, and widths measured after the column was returned to zero tip displacement are plotted with a discontinuous line.

Assuming that a column returns to an essentially plumb position following an earthquake, which may be a prerequisite for a structure to provide continued function, the residual crack widths corresponding to zero tip displacement probably are the more relevant for gaging serviceability. In a full-scale structure, a residual crack width of approximately 0.04 inches is acceptable without repair. Assuming that crack spacing and width scale in proportion with the scale of the test specimens, this corresponds to a crack width of approximately 0.02 inches in the half-scale test columns. Residual crack widths reached this value at rotational ductilities of approximately 5 for Columns 328 and 328T, and rotational ductilities of approximately 3 for Columns 828 and 1028.

Peak tensile steel strains measured by strain gages ranged from approximately 0.022 to 0.029 for the rotational ductilities cited in the previous paragraph. These are localized strains, and probably exceed values that would be calculated for a rotational ductility of 3 to 5 using a plastic hinge length model. Instead, for rotational ductilities of 3 to 5 one should anticipate calculated strains on the order of 0.007 to 0.01 (that is, 3 to 5 times the yield strain).

The occurrence of spalling also signals the need for special repairs, and significant spalling that exposes the core of the confined concrete may signal need for core concrete and reinforcement repairs. As described in Chapter 3, spalling initiated during the 1.2, 1.2, 7.0, and 10.0-inch displacement cycles for Columns 328, 328T, 828, and 1028, respectively. Corresponding concrete compression strains inferred at the centroid of the hoop reinforcement were 0.0138, 0.0129, 0.0134, and 0.0085, respectively.

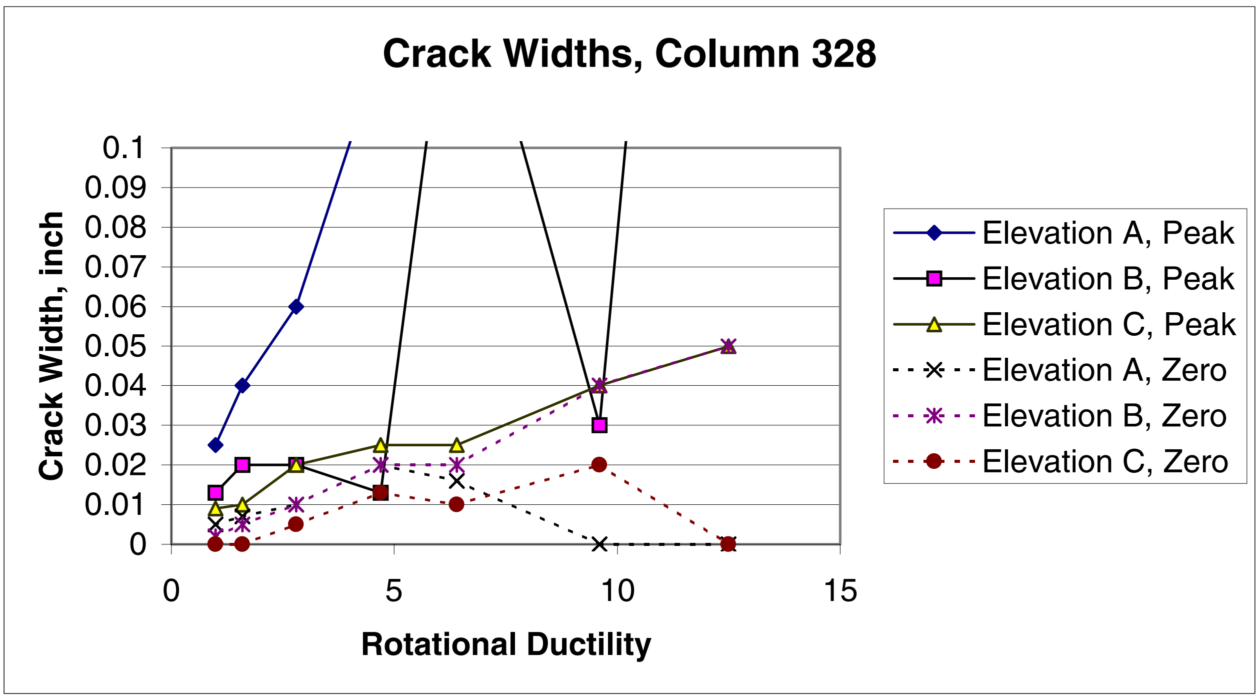

Figure 4.12: Crack Widths Measured in Column 328, North Face (elevations A, B, and C are 0, 5, and 10.25 inches, respectively, above the top of the foundation block)

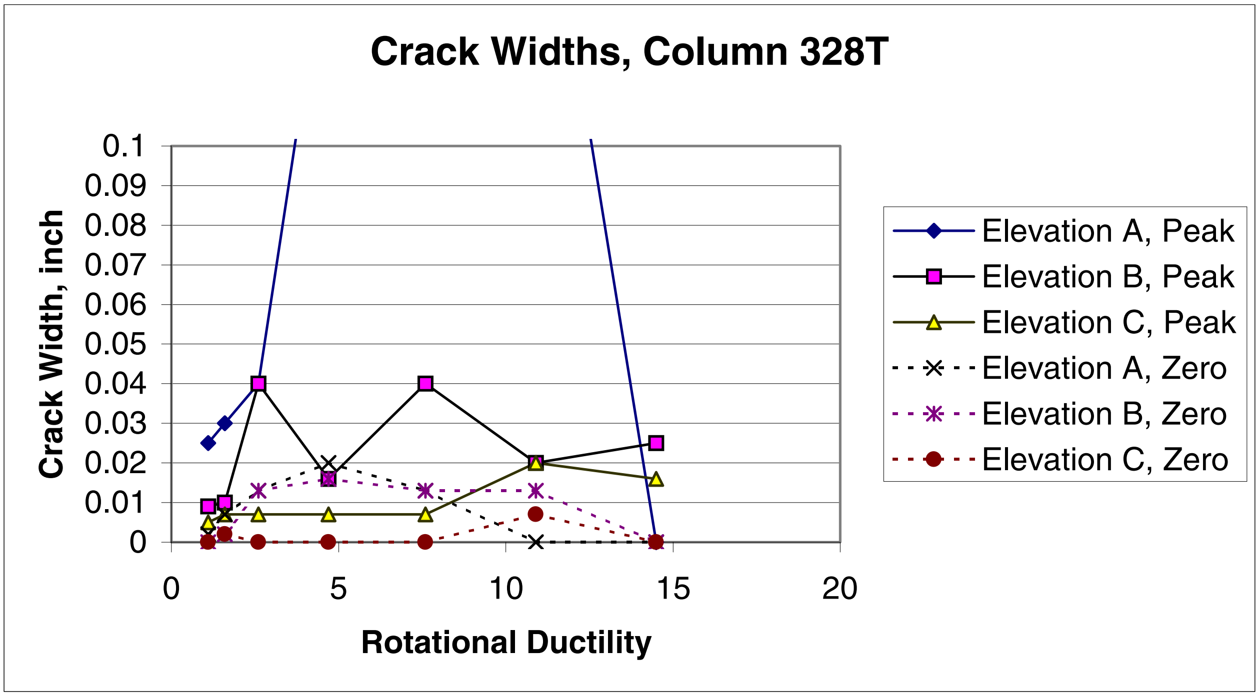

Figure 4.13: Crack Widths Measured in Column 328T, North Face (elevations A, B, and C are 0, 7, and 21 inches, respectively, above the top of the foundation block)

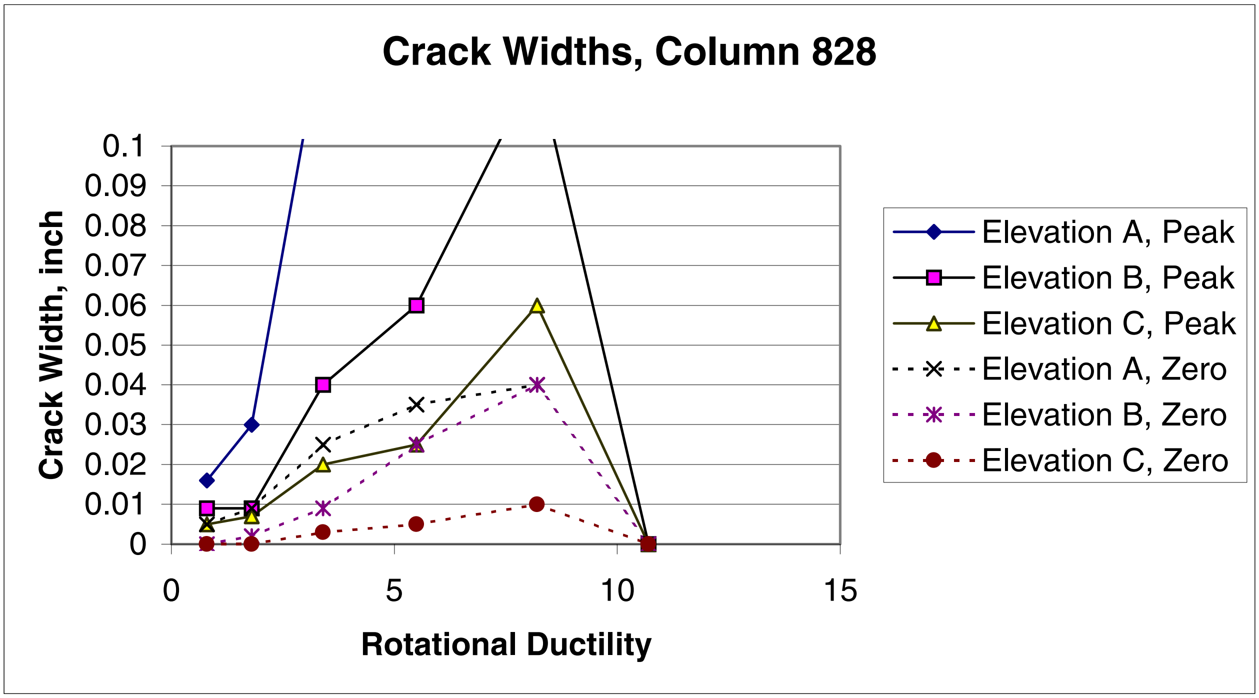

Figure 4.14: Crack Widths Measured in Column 828, North Face (elevations A, B, and C are 0, 12, and 25.5 inches, respectively, above the top of the foundation block)

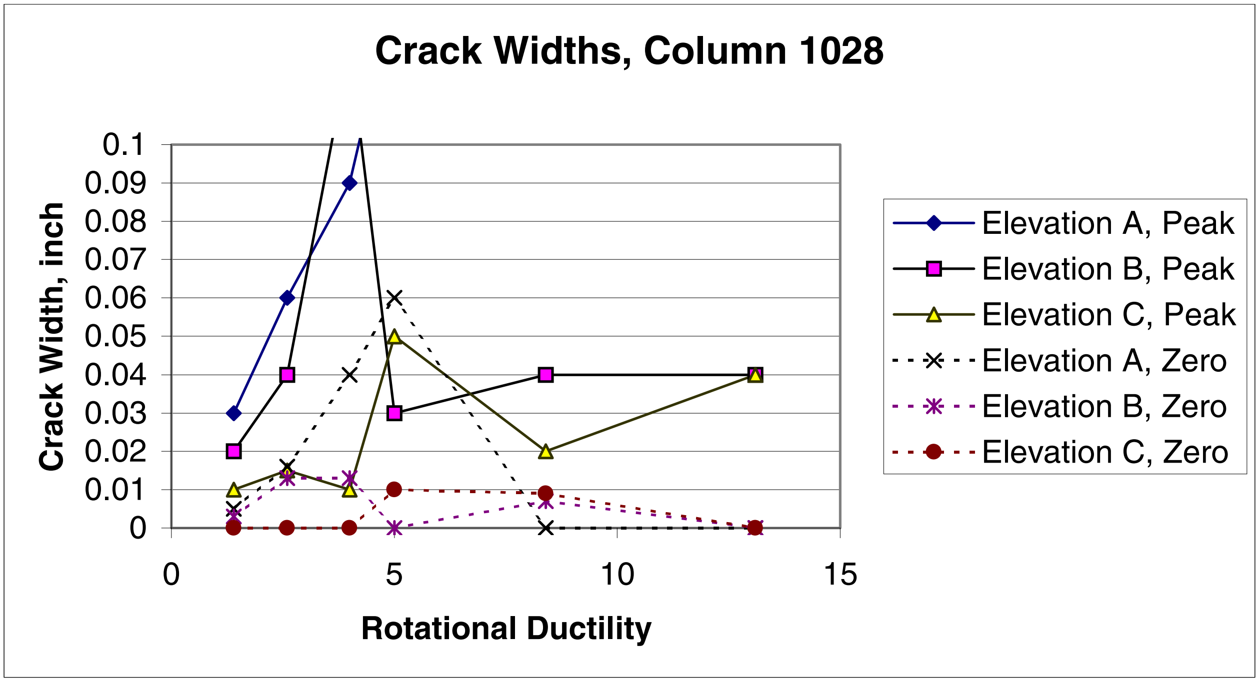

Figure 4.15: Crack Widths Measured in Column 1028, North Face (elevations A, B, and C are 0, 12.75, and 23.5 inches, respectively, above the top of the foundation block)

5 Summary and Conclusions

5.1 SUMMARY

Four columns were studied experimentally and analytically. The columns were half-scale models of circular-cross-section, spirally reinforced, concrete bridge columns. The cantilever columns were fixed at the base to large reinforced concrete anchor blocks. Two of the columns had an aspect ratio (height/diameter) of 3.0, one had an aspect ratio of 8.0, and the other had an aspect ratio of 10.0. Column diameter was 2 feet for all columns.

The columns were constructed of normal-weight aggregate concrete having compressive strength at the time of testing equal to approximately 4800 psi. Column longitudinal reinforcement was No. 6 Grade 60 deformed bar conforming to A706 and having measured yield strength of approximately 64,000 psi. Transverse reinforcement was No. 2 plain bar conforming to A82. The longitudinal reinforcement ratio was 0.027. Spiral reinforcement was provided at variable pitch. One of the objectives of the test program was to examine the effect of reducing the spiral reinforcement ratio to just outside the defined flexural plastic hinge zone. Longitudinal and transverse reinforcement was provided without splices. Specimens were cast in a vertical position.

The test specimens were tested under constant axial load and reversed cyclic lateral forces in a single horizontal direction. The axial load corresponded to 0.092 $A_g f'_c$, where A_g = gross cross-sectional area of the column, and f'_c is the nominal concrete compressive strength of 4000 psi. Lateral loads were applied near the free end of the cantilevered columns. The load history consisted of sets of deformation cycles at progressively increasing displacement amplitude. Each set of deformation cycles consisted of three cycles at constant displacement amplitude followed by an additional cycle at a reduced amplitude. For each cycle, a test column was displaced equally in both positive and negative directions. Tests continued until (or, in the case of one column, near) failure. Data were recorded continuously throughout a test.

Test results for the four test columns are reported and discussed in relation to one another and in relation to various analytical models. On the basis of the test results and their analyses, several conclusions and recommendations can be made.

5.2 CONCLUSIONS

5.2.1 Column Behavior

Each column exhibited ductile behavior, with displacement ductility greater than 8, where displacement ductility is defined as the ultimate displacement capacity divided by the displacement at first yield. An alternate definition of the yield displacement was obtained by establishing a secant through the displacement at first yield and extending that secant to a moment equal to the nominal moment capacity of the cross section. Using this definition, the displacement ductilities of the columns were reduced by approximately 30 percent. Up to this ductility level, the load-displacement hysteresis loops were relatively full and stable.

The primary failure mechanism of each column was the buckling of the longitudinal reinforcement and the subsequent fracturing of that steel upon lateral load reversal. It is possible that using transverse reinforcement of lower strength would have reduced the confinement strength of the spiral and would have led to buckling of the longitudinal reinforcement at lower displacement levels; this hypothesis was not investigated.

Concrete cracking was predominantly horizontal, suggesting a predominance of flexural action. This was confirmed by the external instrumentation. In addition to flexure, slip of the reinforcement from the foundation block contributed significantly to the overall flexibility of the columns. Consistent with theory, the relative contribution of slip decreased with increasing aspect ratio. It is recommended that slip contributions to displacements be included where design is sensitive to calculated displacements.

Crack widths generally grew with increasing displacement cycles. As expected, residual crack widths measured at zero displacement following a peak were less than crack widths measured at the peak. A residual crack width of 0.04 inches was defined arbitrarily as the maximum acceptable crack width not requiring repair in a full-scale column. Assuming that the crack widths scaled linearly, the maximum acceptable residual crack width for the half-scale specimens was defined as 0.02 inches. This residual crack width was observed at a rotation ductility ranging between 3 and 5 for the test columns. It is recommended that design rotation ductilities not exceed these values where one of the performance objectives is to limit cracking repair. That performance objective is likely to be relevant only for events that occur frequently during the design life of the bridge.

Concrete spalling did not occur until the inferred compression strain in the concrete at the level of the spiral reinforcement exceeded 0.008. Some design practices permit use of concrete compression strains as high as 0.005 in unconfined concrete or in confined concrete where spalling is to be avoided. On the basis of these tests, the value 0.005 appears appropriately conservative.

Spalling increased in depth, around the circumference, and up the height as testing continued. In addition, the length (height) of spalling was longer for columns with larger aspect ratio.

5.2.2 Effect of Varying Spiral Reinforcement Spacing

All four columns were detailed with No. 2 spiral wire at 1-inch pitch in the region just above the footing. This quantity of transverse reinforcement satisfies the recommendations of ATC-32 [1996] and exceeds the requirement of the Caltrans Bridge Design Specifications [1993] in effect at the time of this writing. In Column 328, the transverse reinforcement extended over the full column height at the same spacing. In Column 328T, the spacing increased to 3 inches starting a distance equal to one column diameter above the top of the footing. In Columns 828 and 1028, the spiral spacing was increased to 2 inches starting at 1.5 and 2.0 column diameters, respectively, above the top of the foundation. For these latter two columns, the location of the transition was set equal to approximately 20 percent of the column length. For the test columns, ATC-32 [1996] recommends that the transition should be located not less than the larger of one column diameter and 20 percent of the column length from the top of the footing.

The test results indicate that the transition in spacing of the spiral reinforcement did not have a negative effect on behavior of the columns.

Table 5.1 below compares the height of the transition and the height to which spalling extended during testing. The increase in spalled length with increasing column height is apparent in the tabulated results. Note that the height of spalling for Column 828 is equal to 0.20 times the column length, while that for Column 1028 is equal to 0.22 times the column length.

Table 5.1: Comparison between Height of Transition and Height of Spalling

Column	Height of Transition Above the Top of the Foundation (in.)	Maximum Height of Spalling Above the Top of Foundation (in.)
328	N/A	16
328T	24	16
828	36	38
1028	48	53

Although spalling extended beyond the transition zone for Column 1028, this did not result in failure of the test column. The quantity of spiral reinforcement above the transition zone, equal to half that below the transition zone, apparently provided adequate confinement for the low strain demands above the transition.

ATC-32 [1996] recommends that the length of the confined zone should be the larger of (a) the section dimension in the direction considered and (b) the portion of the column over which the moment exceeds 80 percent of the moment at the critical section. For axial loads over $0.3f_c'A_g$, the length of confinement is to be increased by 50 percent. Although this recommendation proved adequate for the test columns, some concerns remain. One concern is that the length of spalling is known to increase with increasing axial load [Watson, 1989]. The test columns had an axial load level less than $0.1f_c'A_g$. It is possible that at higher axial loads the extent of spalling would have extended to a height where it had a negative effect on the column behavior. A second concern is that the moment diagram in actual bridge columns is not so precisely controlled as it was in the tests. Simplified design models often misrepresent locations of inflection points and may lead to erroneous definitions of required confinement length. It is recommended that the confinement transition occur at a greater distance from the foundation level than recommended by ATC-32 or not at all.

5.3 SHEAR STRENGTH

Six proposed methods for calculating the shear strength of reinforced concrete columns were investigated in this experimental program. Based on the observed behavior of the test columns, the shear strength provisions proposed by ACI 318-95 [1995] and the BDS [1993] appear to give reasonable estimates of column shear strength, particularly that of Column 328T. The ATC-32 [1996] and Konwinski [1996] models appear to underestimate the shear strength of a reinforced concrete column, while the Ohtaki [1997] and Aschheim [1997] shear strength models appear to be overly optimistic.

5.4 FORCE-DISPLACEMENT RESPONSE

The predictive force-displacement model proposed by Lehman [1998] provided reasonable results for the columns in this experimental program. The ultimate displacements predicted by the Lehman model compared favorably with the maximum column displacements observed during testing. While the component deformations predicted by the Lehman model followed the same general trends as those obtained from the experimental data, there was a considerable difference between the predicted and actual component deformations. The displacement components calculated using the Lehman model compared more favorably with the experimental displacement components for slender columns.

The ultimate displacements predicted by ATC-32 [1996] underestimated the actual column displacements by more than 50 percent. The plastic analysis limits prescribed by ATC-32 are based on a limiting compressive strain demand in the confined concrete. This limitation results in an ultimate curvature capacity significantly less than that used in the Lehman model [1998], which is based on an ultimate curvature capacity corresponding to a limiting tensile strain demand of 0.075 in the longitudinal steel. For a limiting tensile strain demand of 0.075, the ATC-32 and Lehman models produced results that were similar for predicting the ultimate displacement of the test columns. It is known that the tensile strain capacity of reinforcement is sensitive to strain history, including the number and magnitude of cycles as well as prior buckling in compression. Additional research is needed to determine a tensile strain limit that is appropriate for other displacement histories.

References

ACI Committee 318. 1995. *Building Code Requirements for Structural Concrete (ACI 318-95) and Commentary (ACI 318R-95)*. Farmington Hills, Mich.: American Concrete Institute.

Applied Technology Council. 1996. *Improved Seismic Design Criteria for California Bridges: Provisional Recommendations.* Section 8, Reinforced Concrete, ATC-32. Redwood City, Calif.: Applied Technology Council.

Aschheim, M., Moehle, J. P., and Mahin, S. A. 1997. *Design and Evaluation of Reinforced Concrete Bridges for Seismic Resistance.* Report No. UCB/EERC-97/04. Berkeley, Calif.: Earthquake Engineering Research Center, University of California.

California Department of Transportation. 1992. *Standard Specifications*. Sacramento, Calif.: State of California.

California Department of Transportation. 1993. *Bridge Design Specifications Manual.* Section 8 – Reinforced Concrete, BDS-93. Sacramento, Calif.: Dept. of Transportation, State of California.

Konwinski, C. M.. 1996. *Shear Strength of Reinforced Concrete Bridge Piers Subjected to Earthquake Loading*. Masters Thesis, West Lafayette, Ind. Dept. of Civil Engrg., Purdue University.

Lehman, D. E., Moehle, J. P., and Mahin, S. A. 1996. Design of an Experimental Study on the Influence of Aspect Ratio and Longitudinal Reinforcement Ratio on Column Response. In *Proceedings Fourth Caltrans Seismic Research Workshop*. Sacramento, Calif.: California Department of Transportation.

Lehman, D. E., Calderone, A. J., and Moehle, J. P. 1998. Behavior and Design of Slender Columns Subjected to Lateral Loading. In *Proceedings Sixth U.S. National Conference on Earthquake Engineering*. Oakland, Calif.: Earthquake Engineering Research Institute.

Mander, J. B., Priestley, M. J. N., and Park, R. 1988. Theoretical Stress-Strain Model for Confined Concrete. *J. Struc. Engrg.* 114(8): 1804–26.

Mazzoni, Silvia. 1977. *Design and Response of Lower-Level Beam-Column Joints in Ductile Reinforced-Concrete Double-Deck Bridge Frames.* Ph.D. Thesis. Berkeley, Calif.: Dept. of Civil Engrg., University of California.

Ohtaki, T., Benzoni, G., Priestley, M. J. N., and Seible, F. 1977. Seismic Performance of a Full Scale Bridge Column — as Built and as Repaired. In *Proceedings Second National Seismic Conference on Bridges and Highways,* pp. 369–79. Sacramento, Calif.: California Department of Transportation.

Qi, X., and J. P. Moehle. *Displacement Design Approach for Reinforced Concrete.* January 1991. Report No. UCB/EERC-91/02. Berkeley, Calif.: Earthquake Engineering Research Center, University of California.

Standards Association of New Zealand. 1982. *Code of Practice for the Design of Reinforced Concrete Structures.* NZS 3101: Wellington, New Zealand.

Todeschini, C. E., Bianchini, A., and Kesler, E. Behavior of Concrete Columns Reinforced with High Strength Steels. *ACI Journal* 61(6): 701–16.

Watson, S., and Park, R. *Design of Reinforced Concrete Frames of Limited Ductility*. 1989. Research Report 89/4. Christchurch, New Zealand: Dept. of Civil Engrg., University of Canterbury.

Appendix A

The following pages contain plots of various test data. See Chapters 2 and 3 for detailed descriptions.

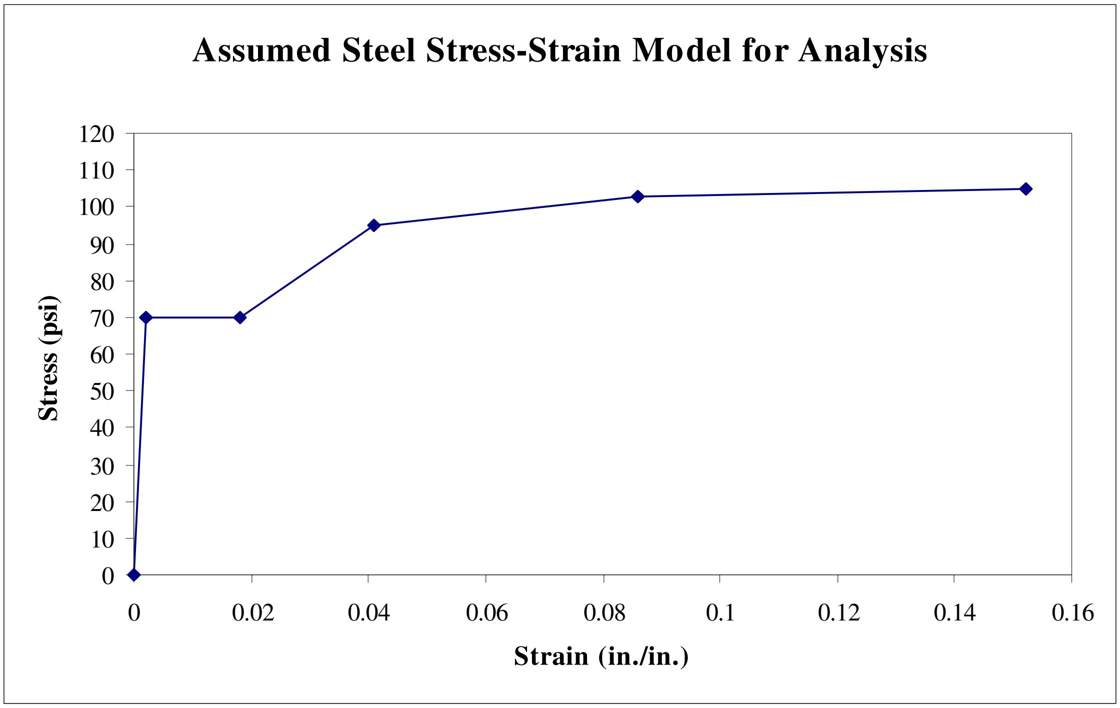

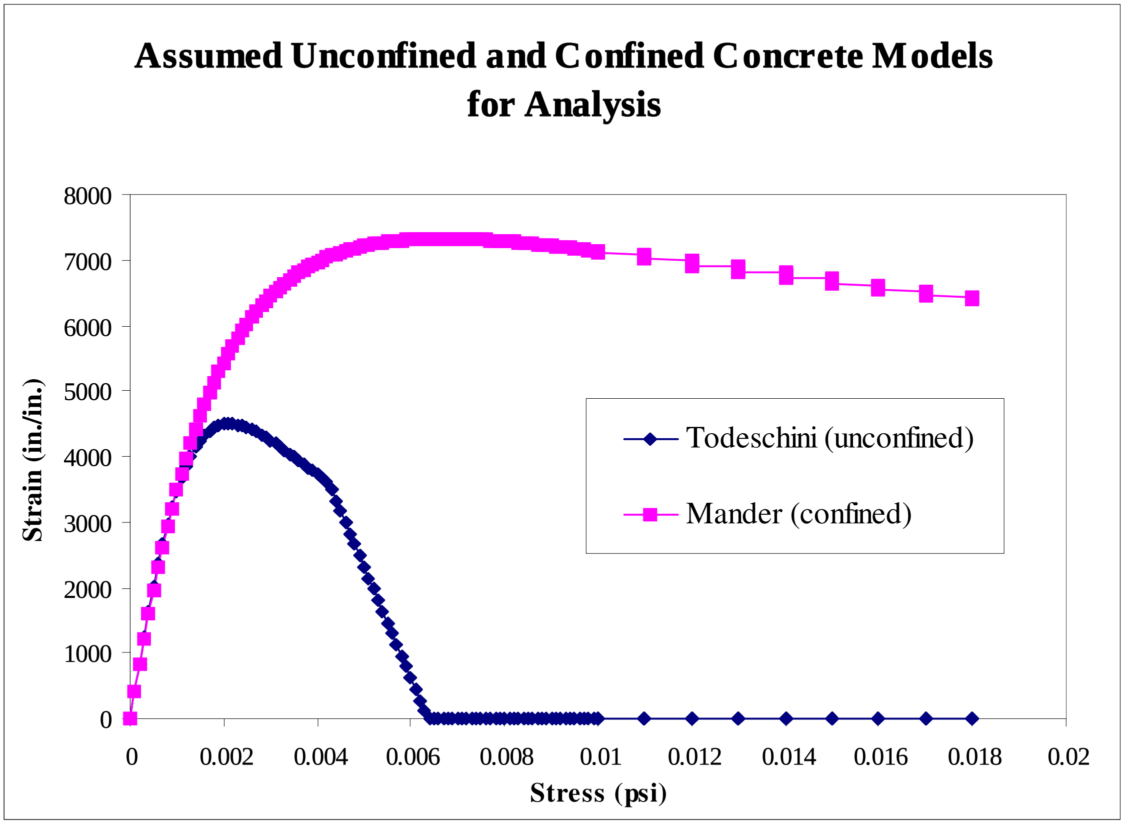

Figure A.1: Assumed Stress-Strain Relationships for Steel and Concrete Used in the Cross-Sectional Analysis of Columns 328, 328T, 828, and 1028

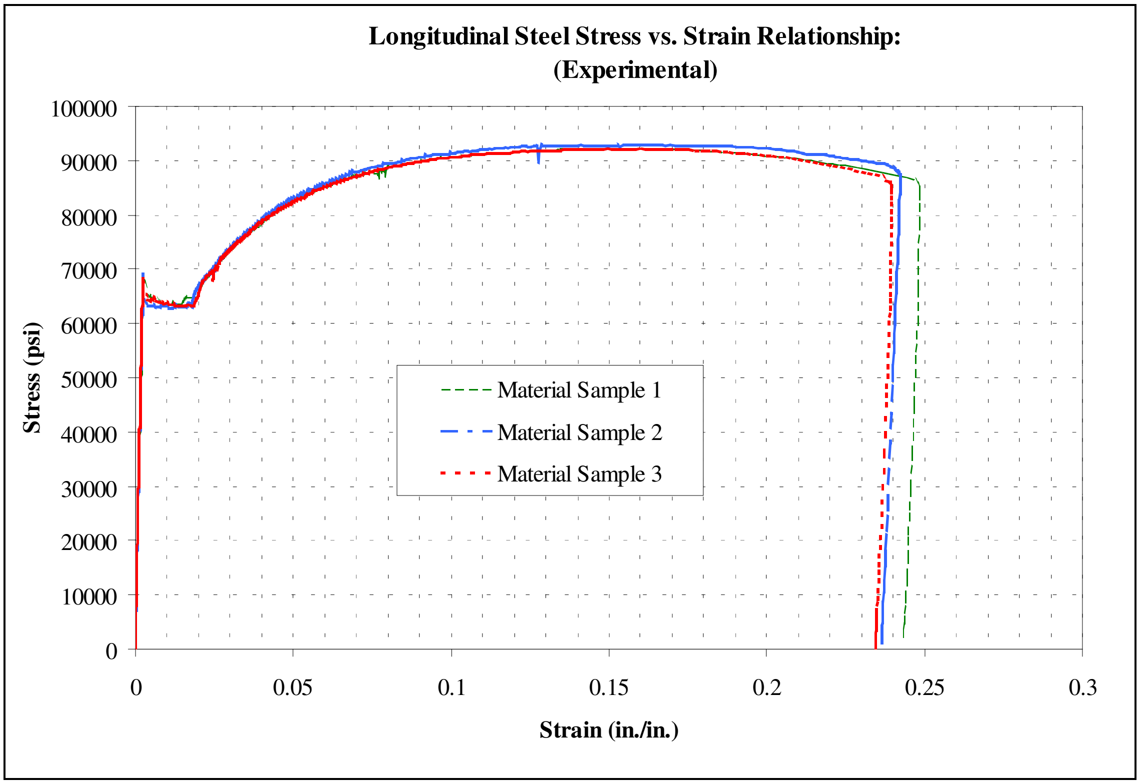

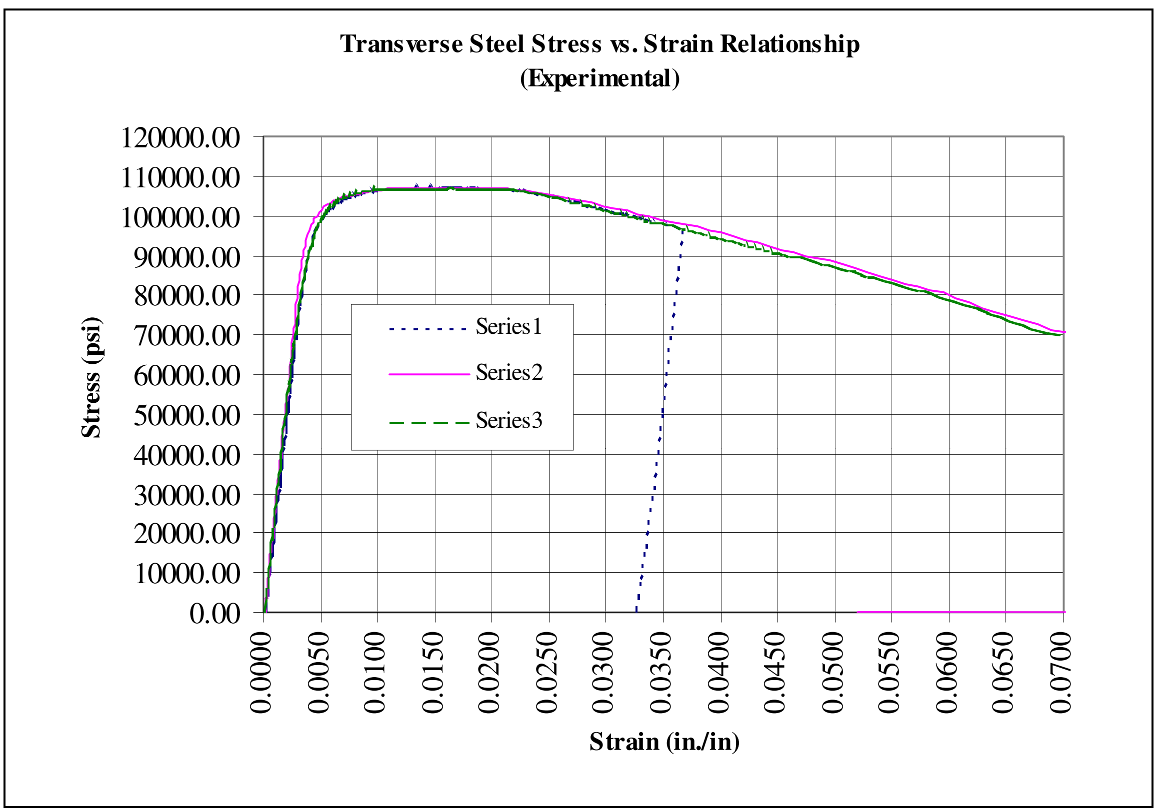

Figure A.2: Stress vs. Strain Relationship for Test Coupons of the Longitudinal and Transverse Steel Used to Construct Columns 328, 328T, 828, and 1028

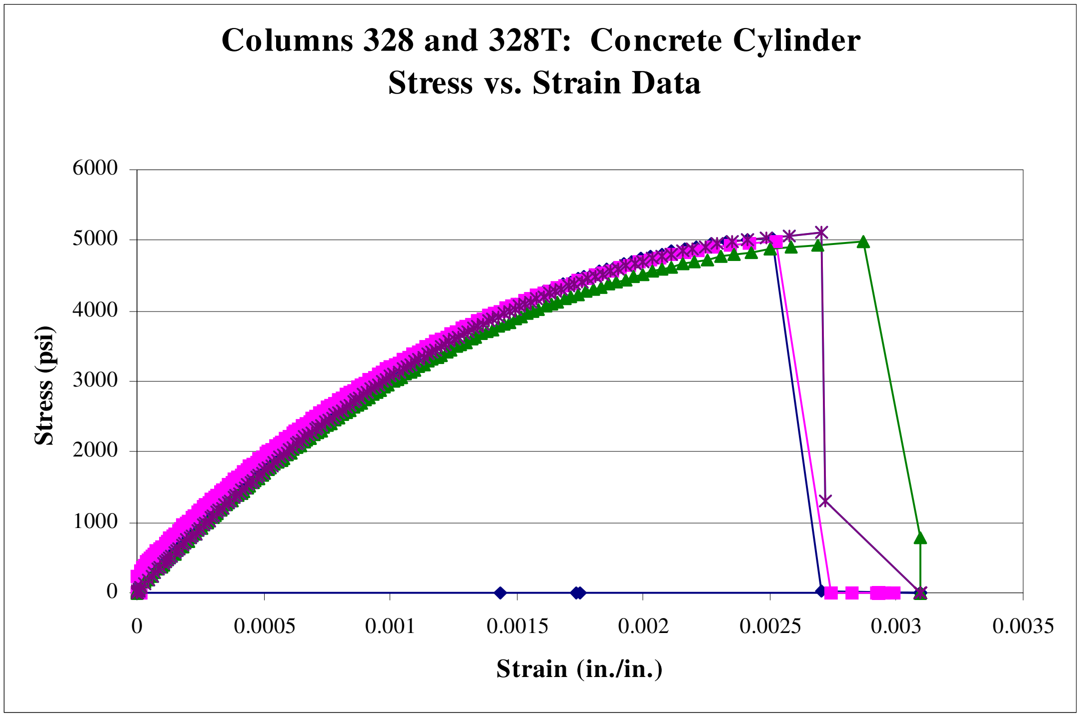

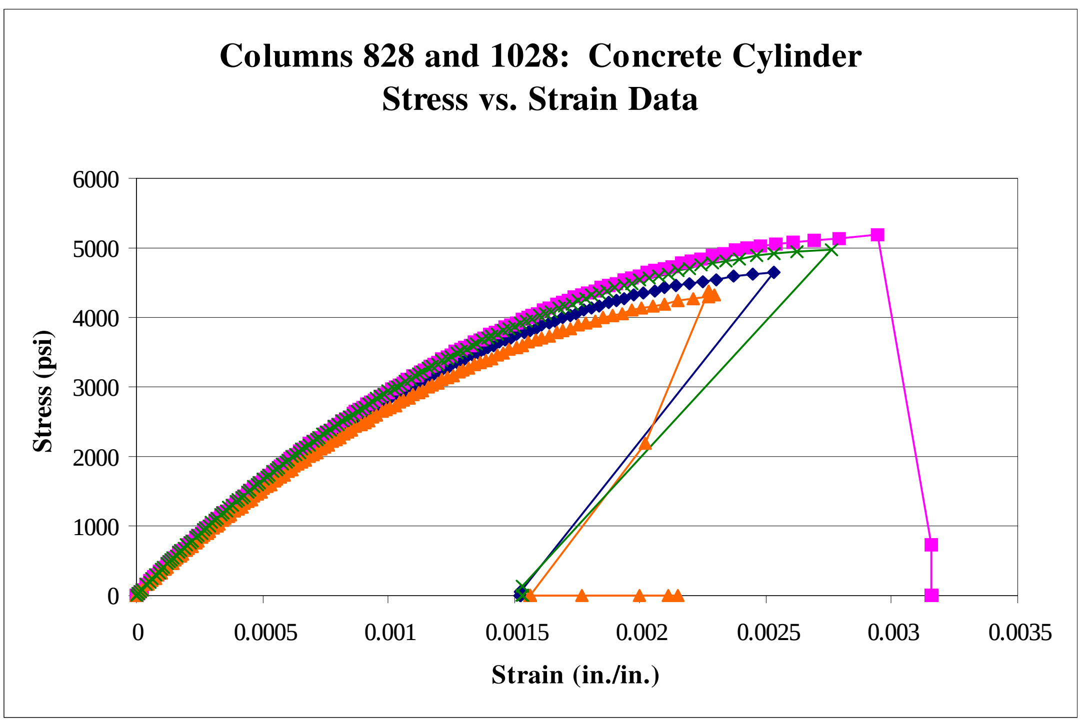

Figure A.3: **Compressive Stress-Strain Relationships of Concrete Cylinder Samples for Columns 328, 328T, 828, and 1028**

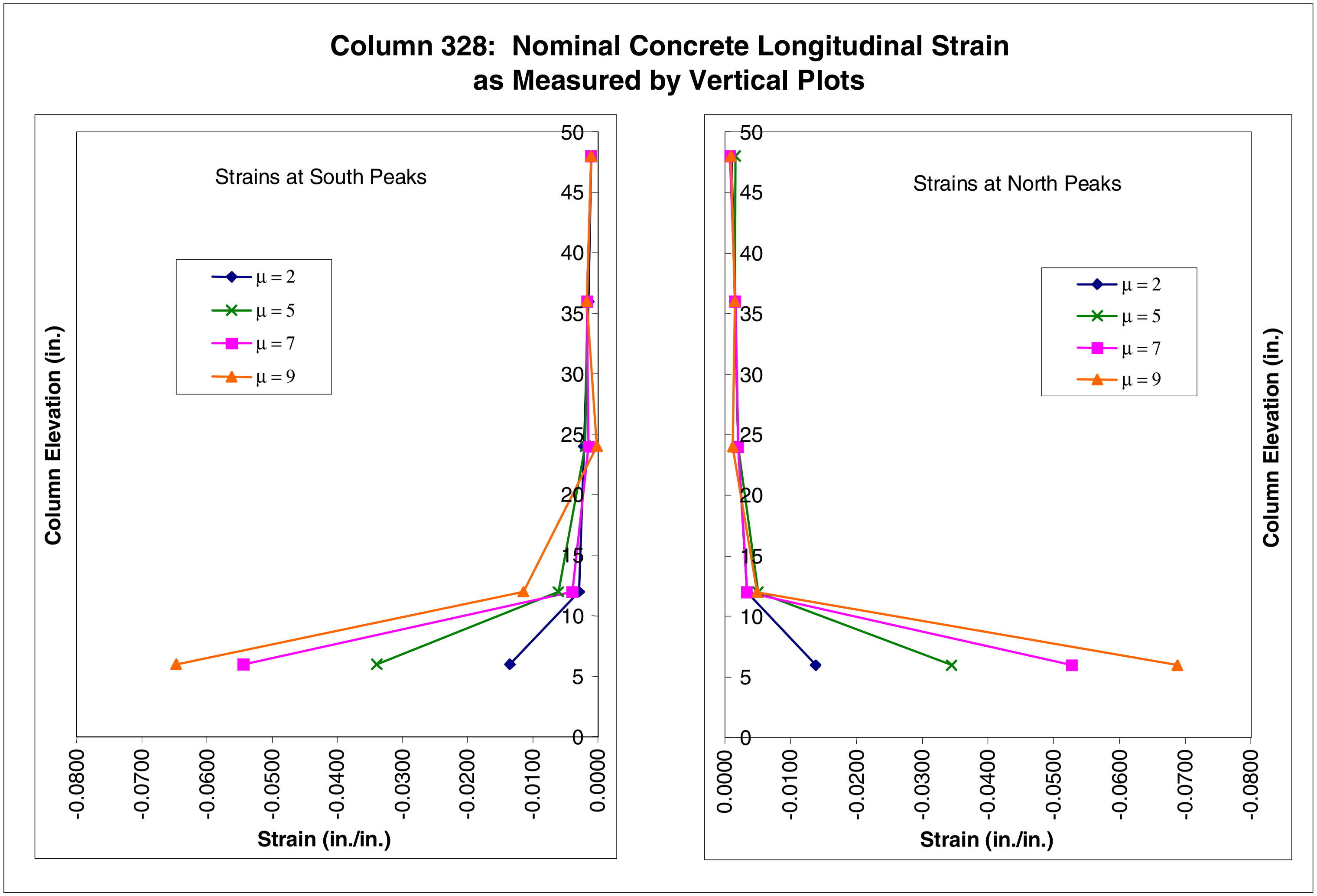

Figure A.4: Concrete Longitudinal Compressive Strains for Column 328 as Measured by Vertical Potentiometers during Testing

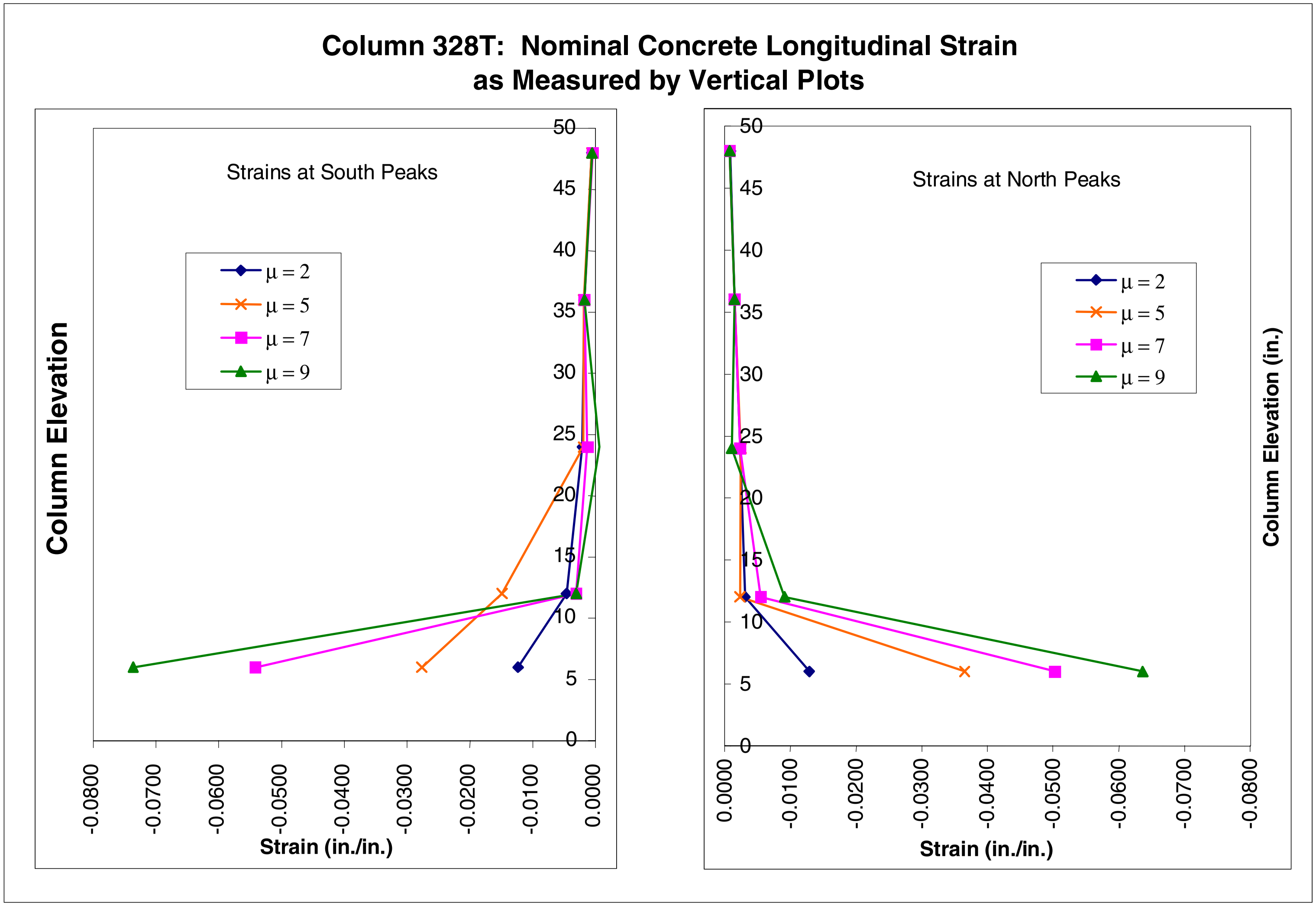

Figure A.5: **Concrete Longitudinal Compressive Strains for Column 328T as Measured by Vertical Potentiometers during Testing**

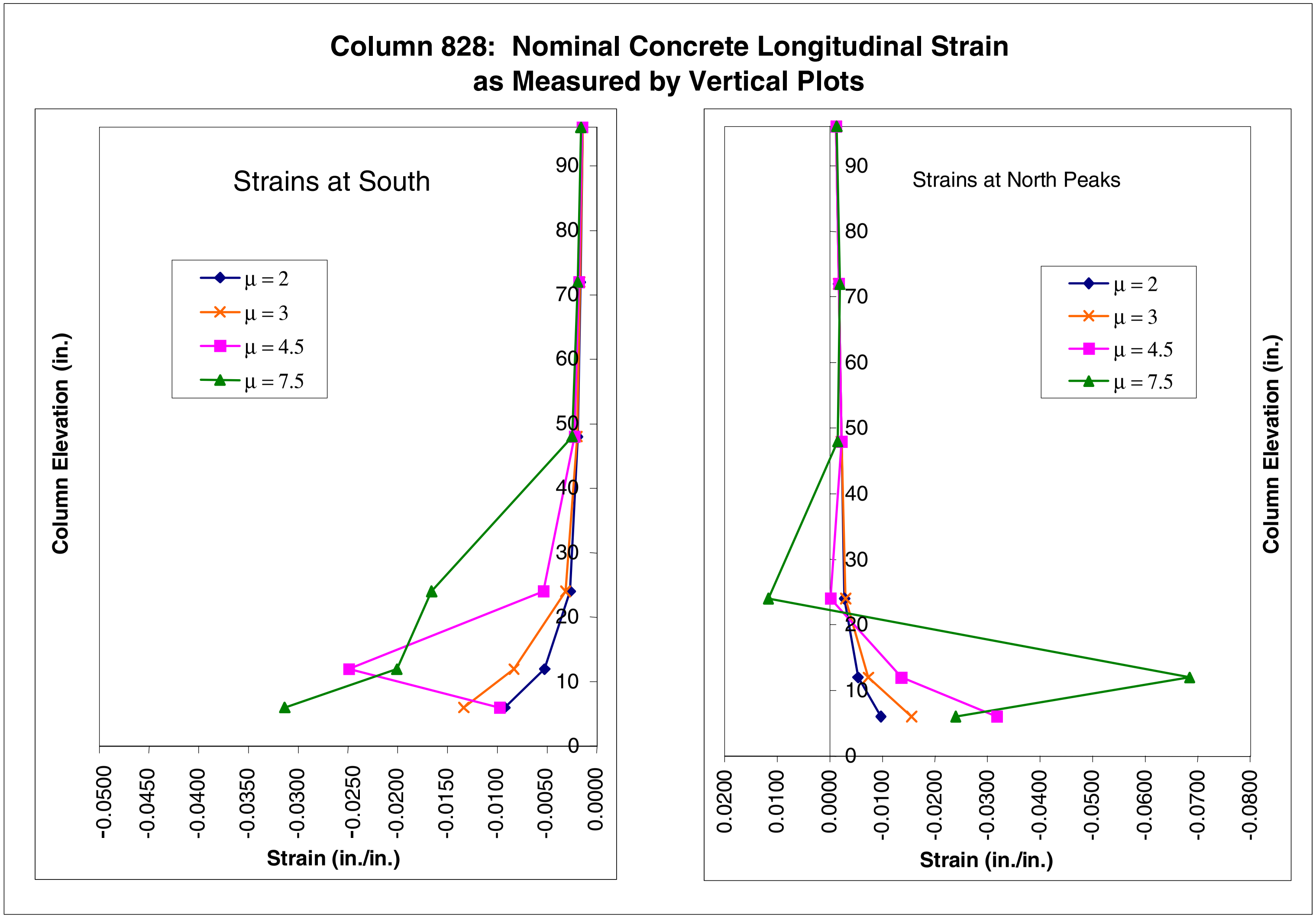

Figure A.6: Concrete Longitudinal Compressive Strains for Column 828 as Measured by Vertical Potentiometers during Testing

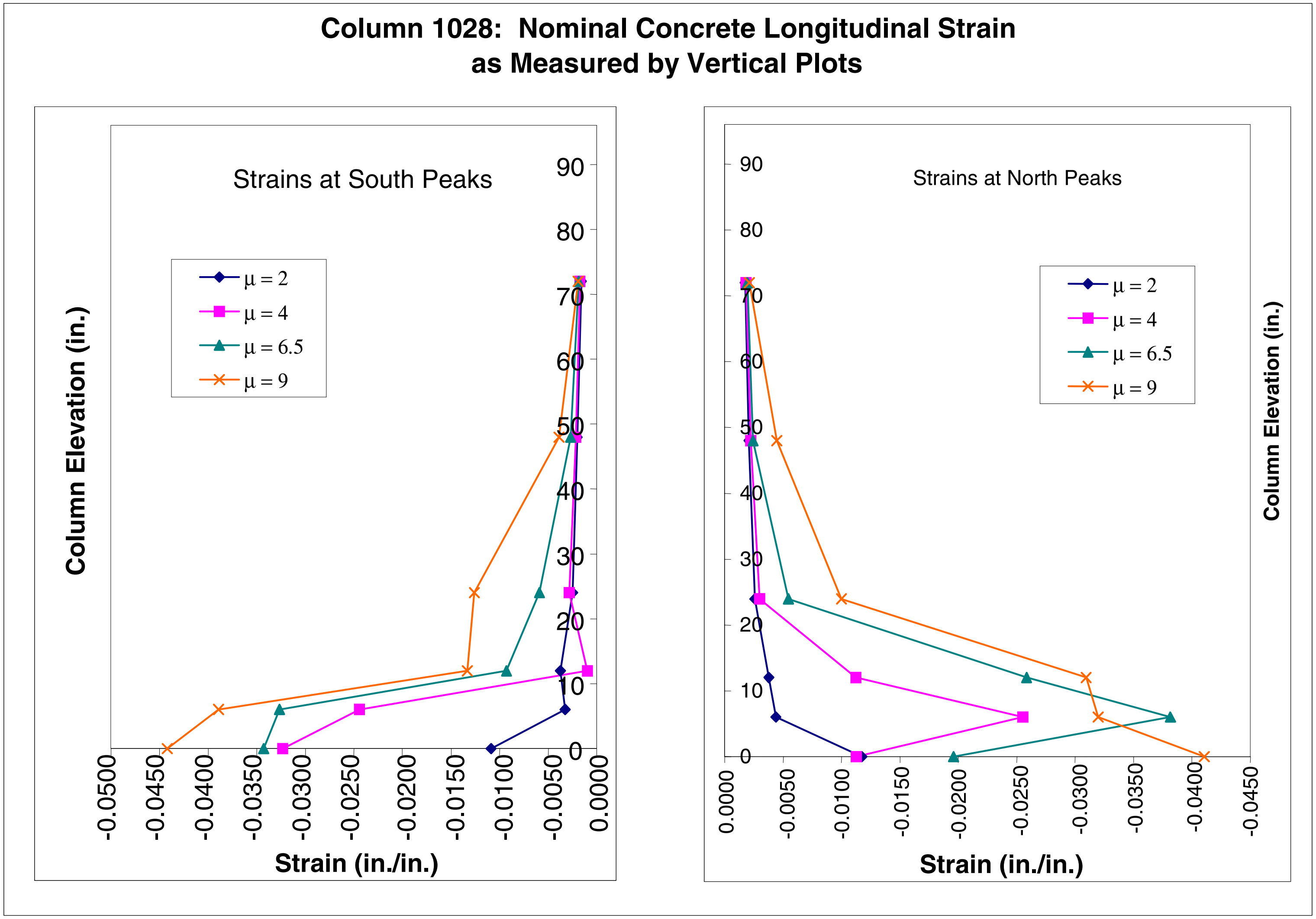

Figure A.7: Concrete Longitudinal Compressive Strains for Column 1028 as Measured by Vertical Potentiometers during Testing

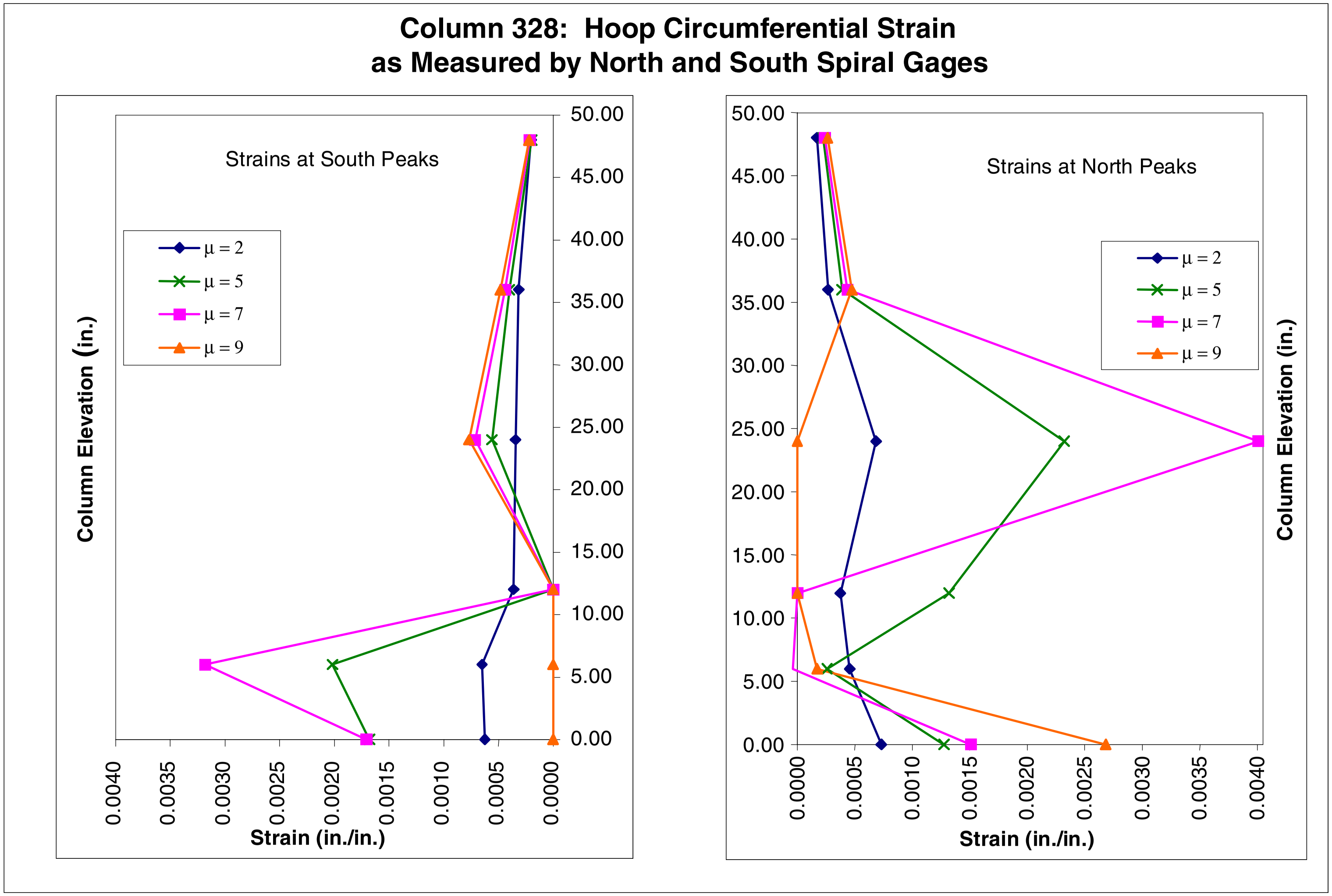

Figure A.8: Circumferential Tension Strains for Column 328 as Measured by North and South Spiral Gages at North and South Peak Displacements, Respectively

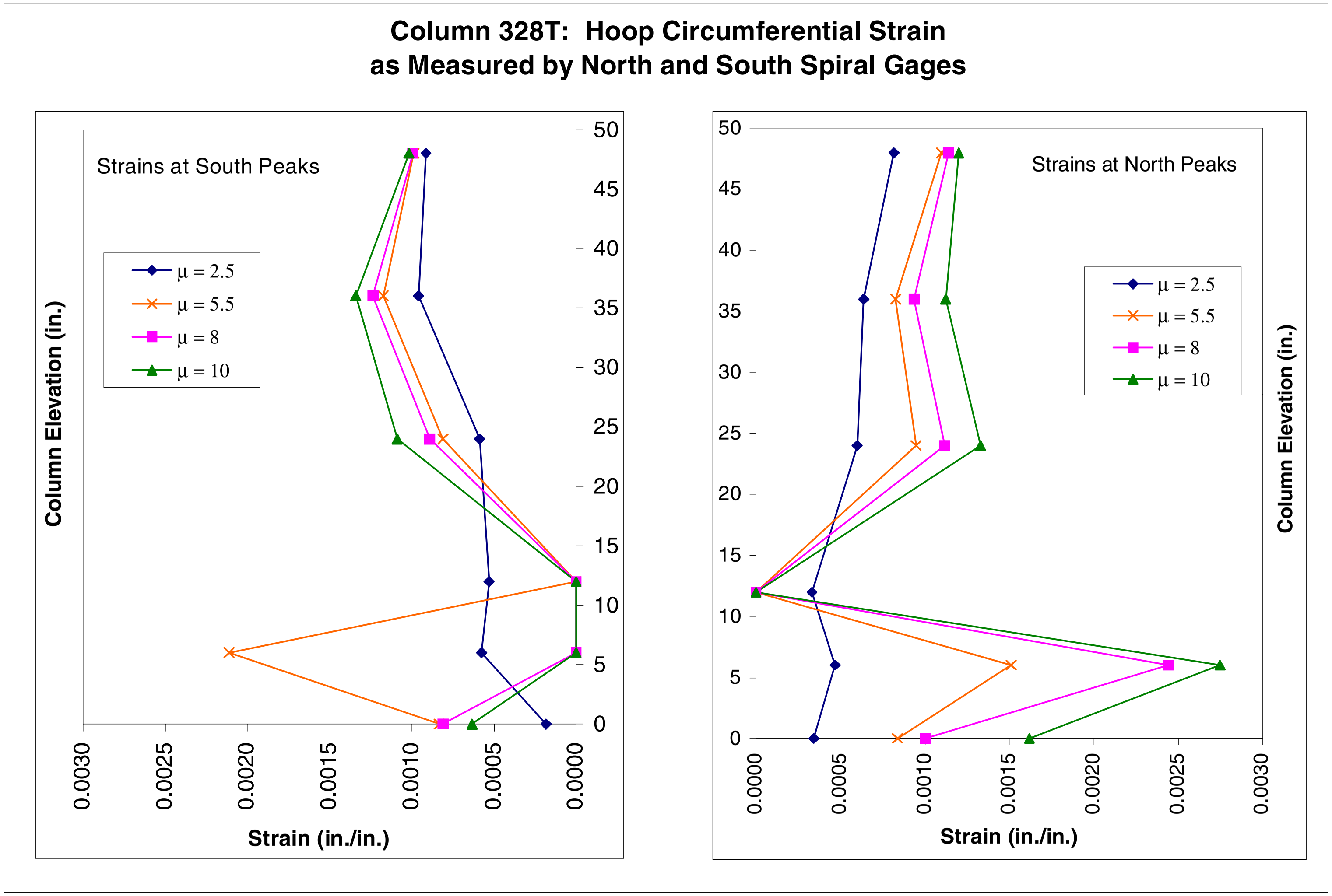

Figure A.9: Circumferential Tension Strains for Column 328T as Measured by North and South Spiral Gages at North and South Peak Displacements, Respectively

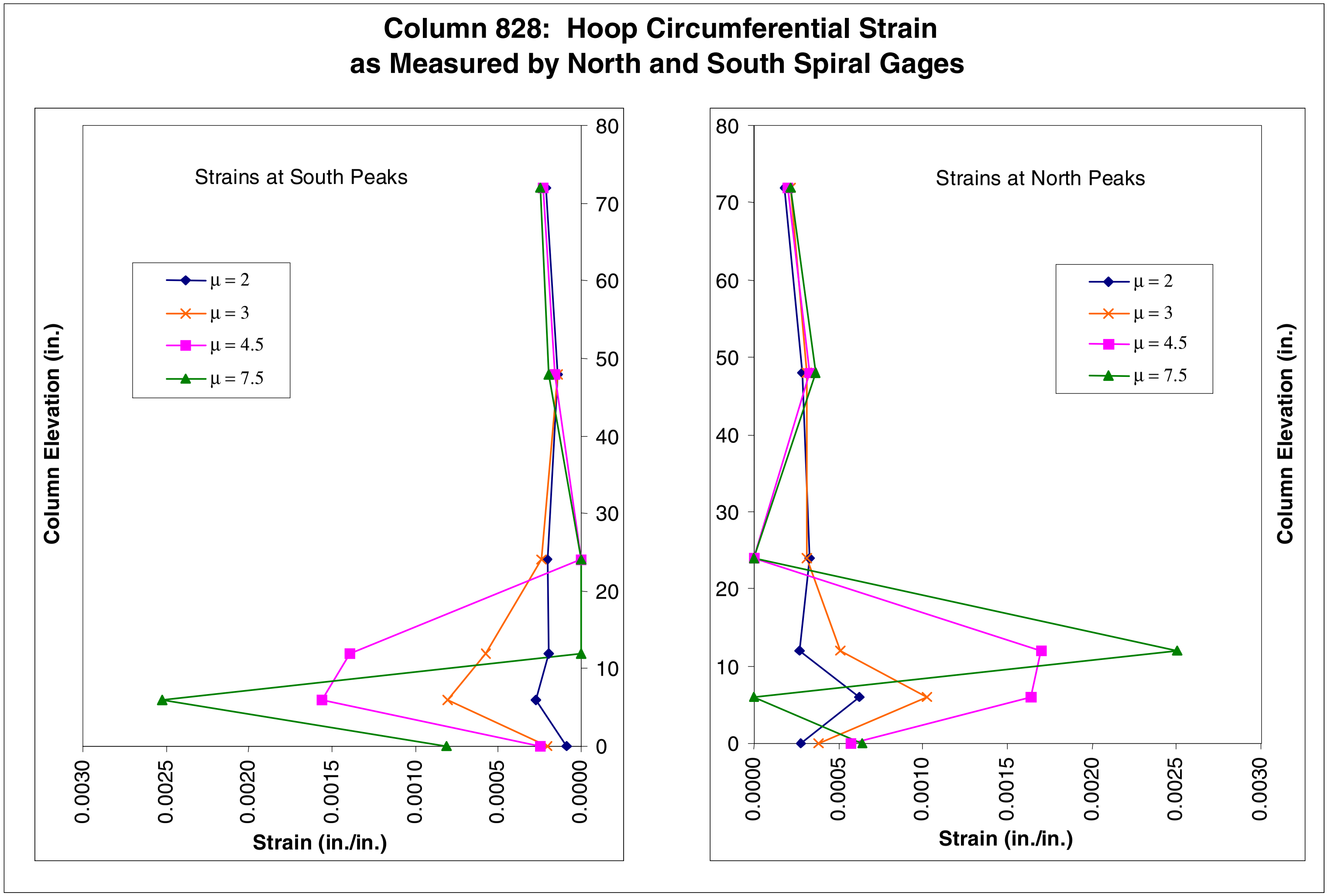

Figure A.10: Circumferential Tension Strains for Column 828 as Measured by North and South Spiral Gages at North and South Peak Displacements, Respectively

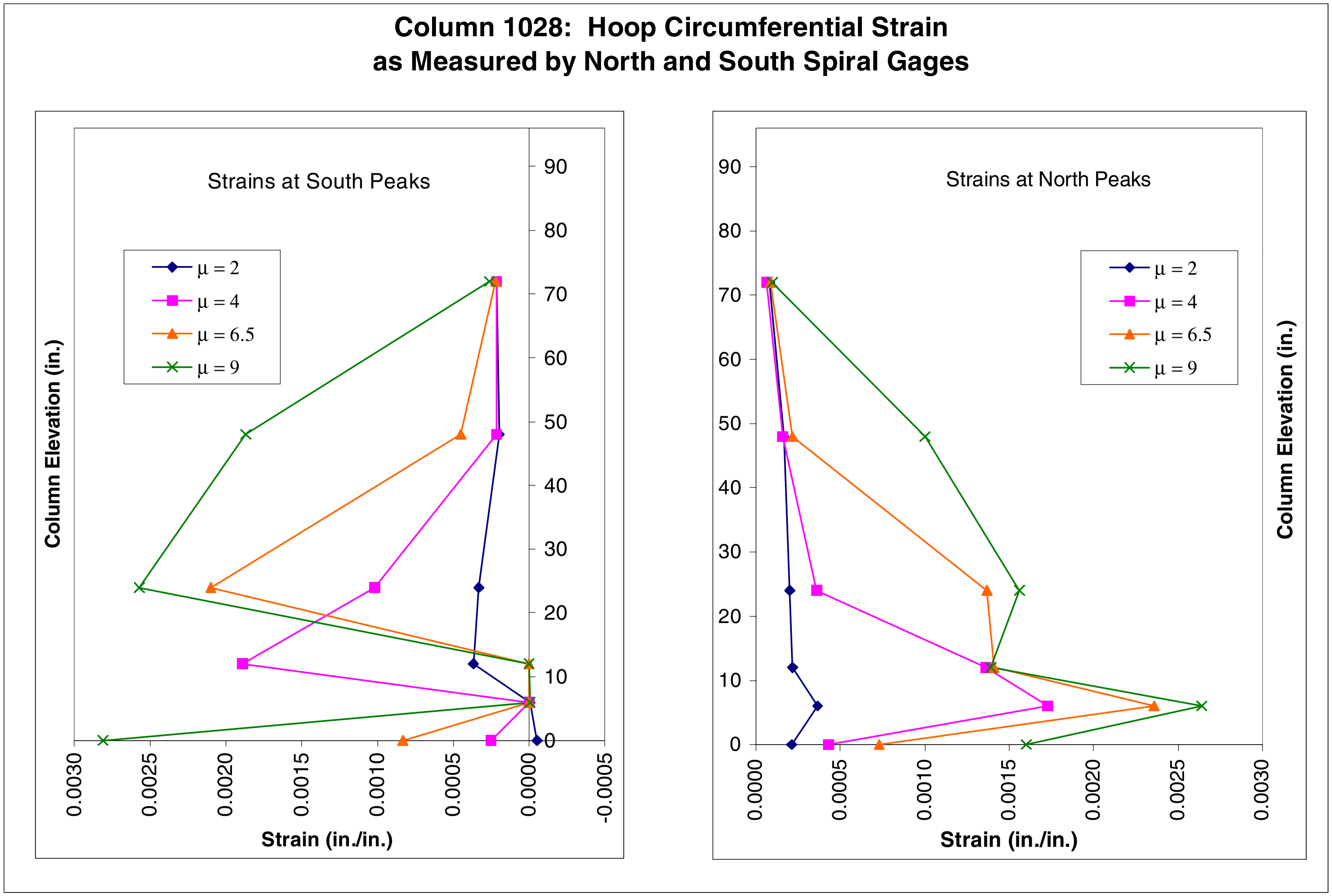

Figure A.11: Circumferential Tension Strains for Column 1028 as Measured by North and South Spiral Gages at North and South Peak Displacements, Respectively

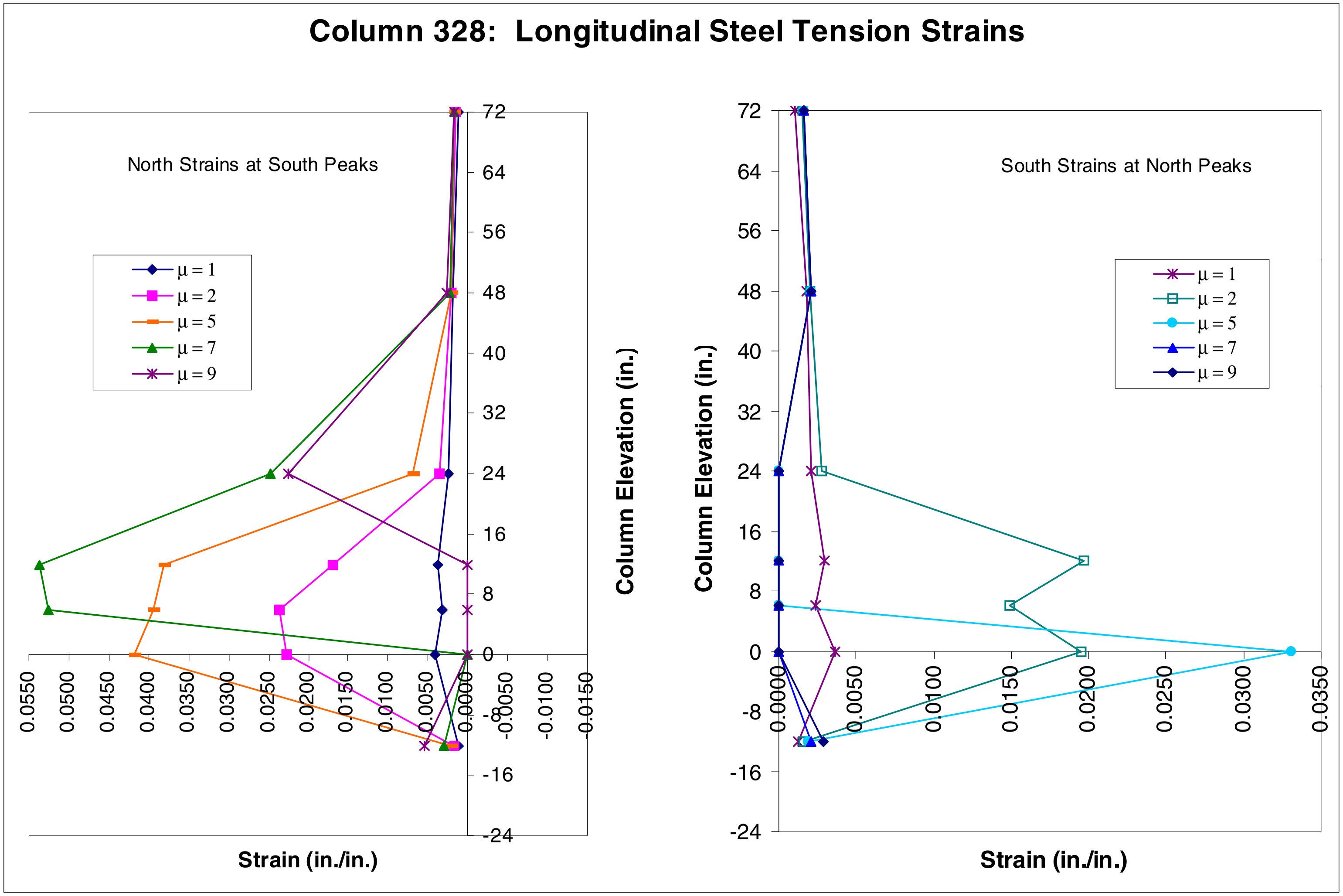

Figure A.12: Longitudinal Steel Tension Strains for Column 328 as Measured by North and South Gages at North and South Peak Displacements, Respectively

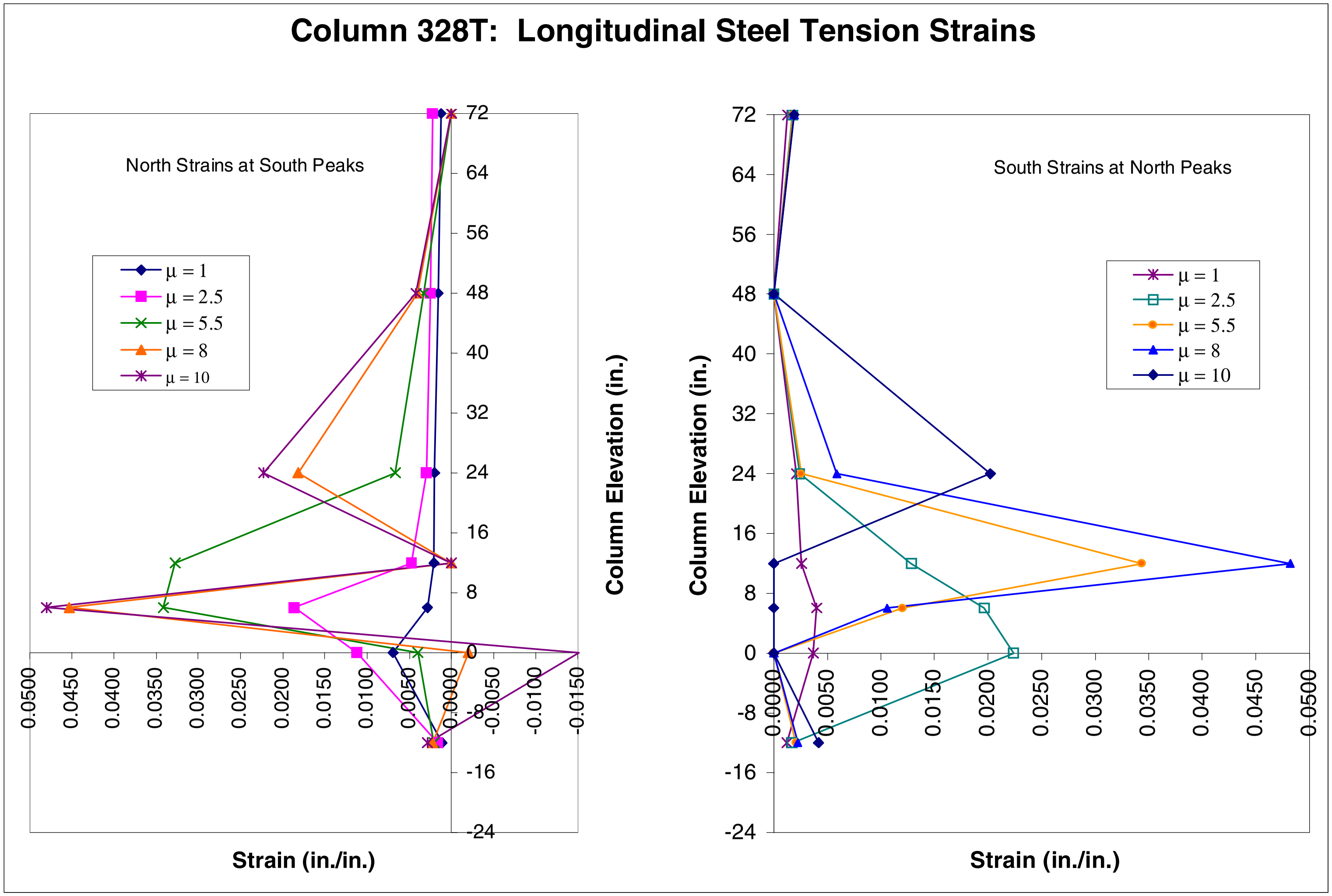

Figure A.13: Longitudinal Steel Tension Strains for Column 328T as Measured by North and South Gages at North and South Peak Displacements, Respectively

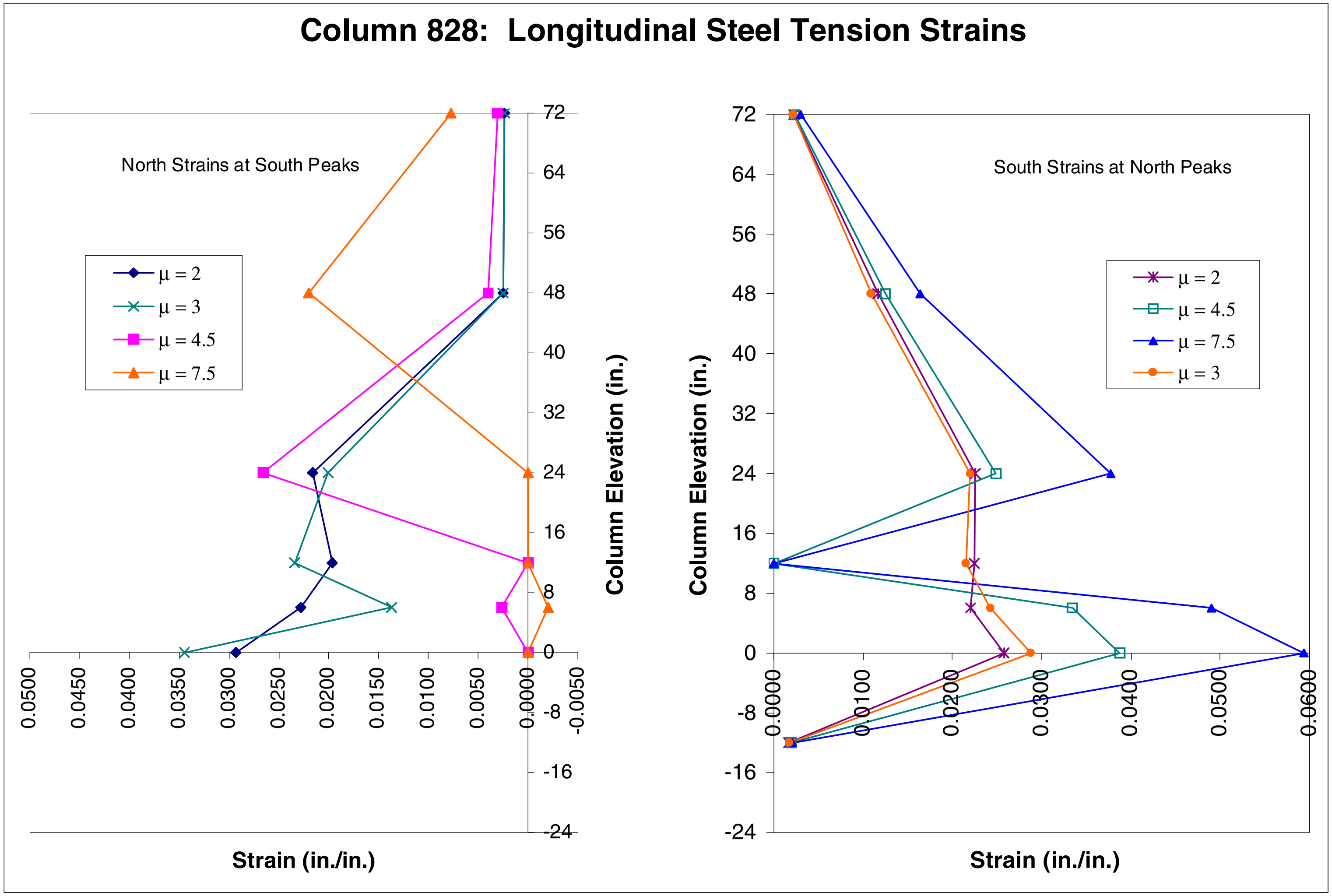

Figure A.14: Longitudinal Steel Tension Strains for Column 828 as Measured by North and South Gages at North and South Peak Displacements, Respectively

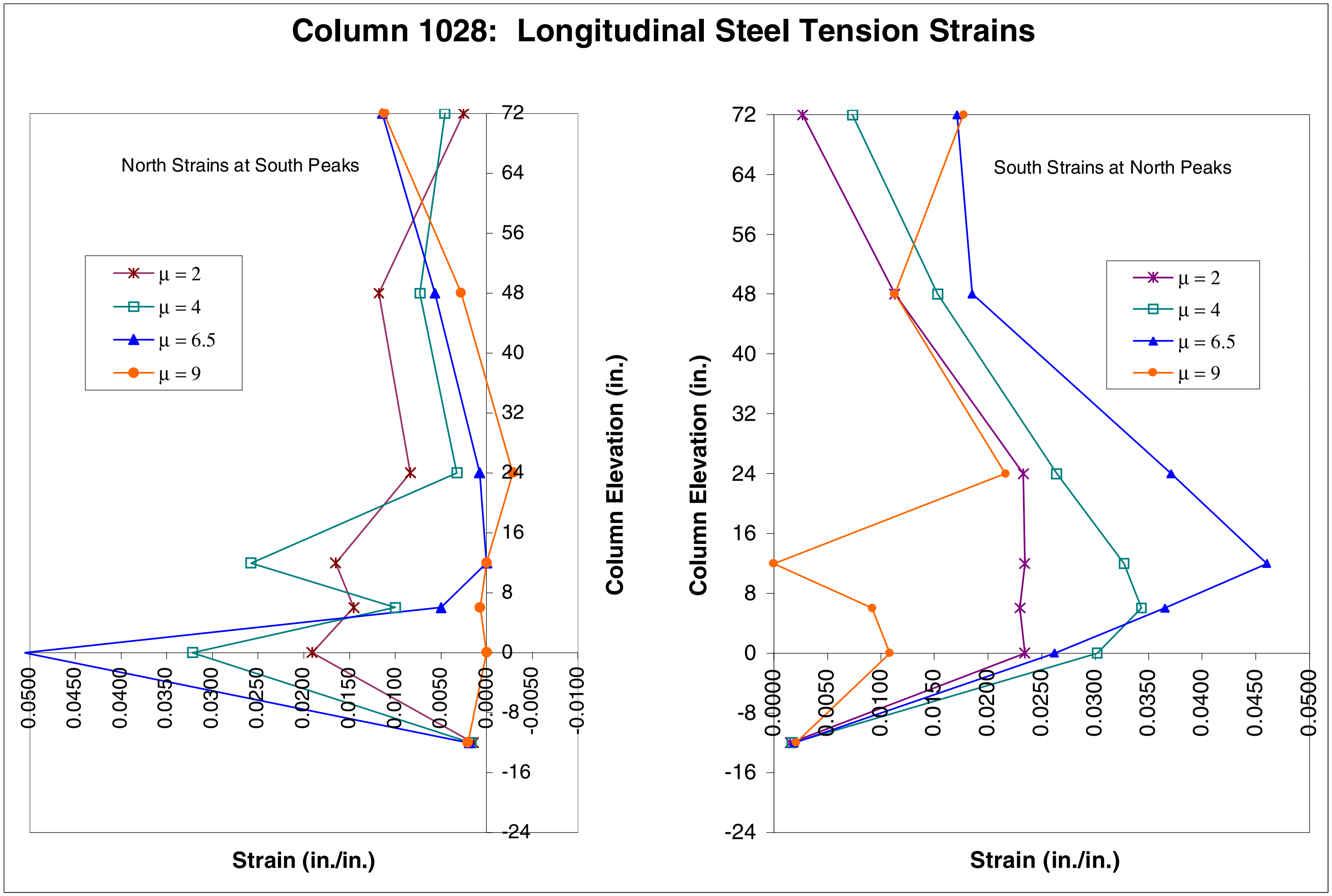

Figure A.15: Longitudinal Steel Tension Strains for Column 1028 as Measured by North and South Gages at North and South Peak Displacements, Respectively

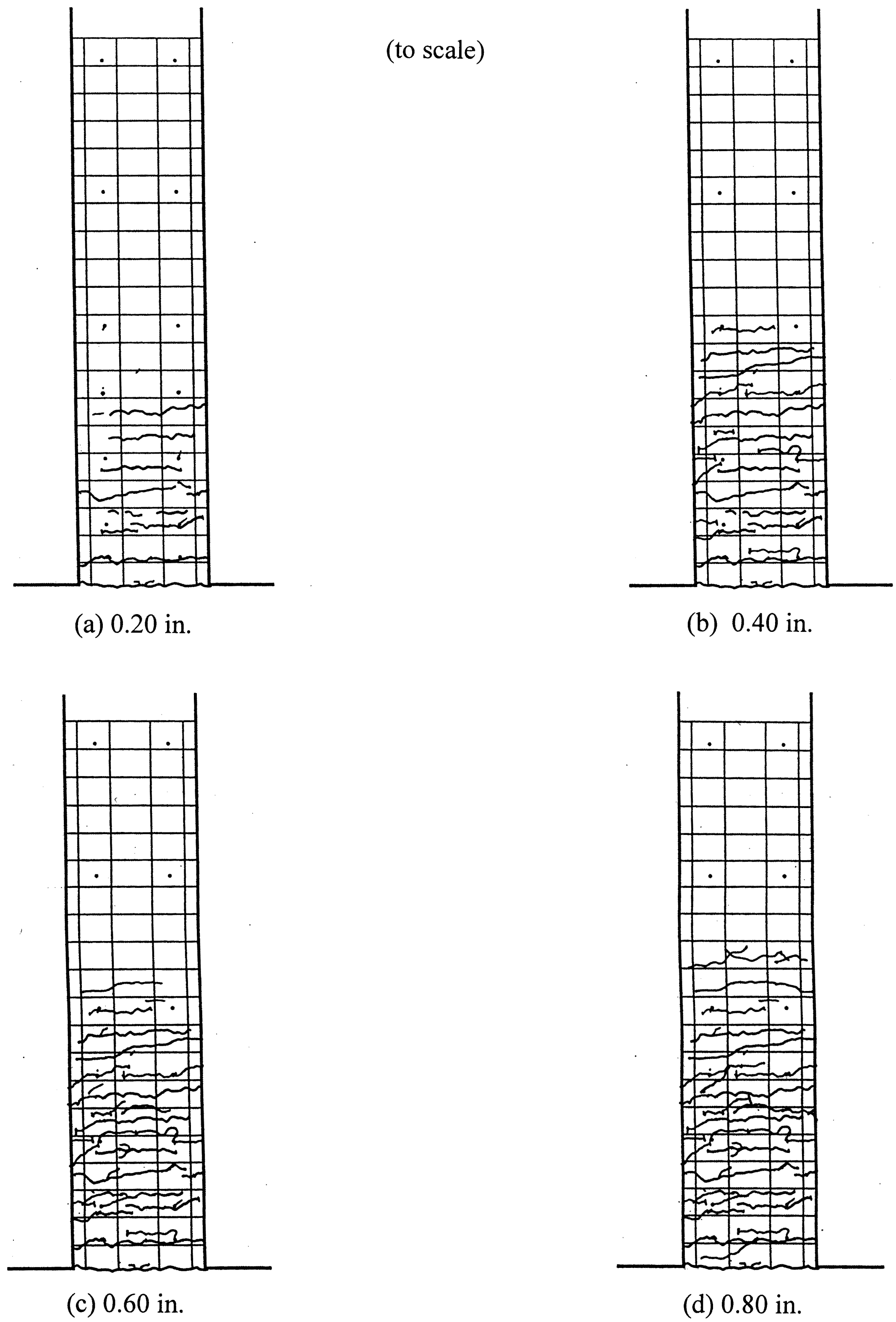

Figure A.16: Progression of Damage, Column 328, North Face

(to scale)

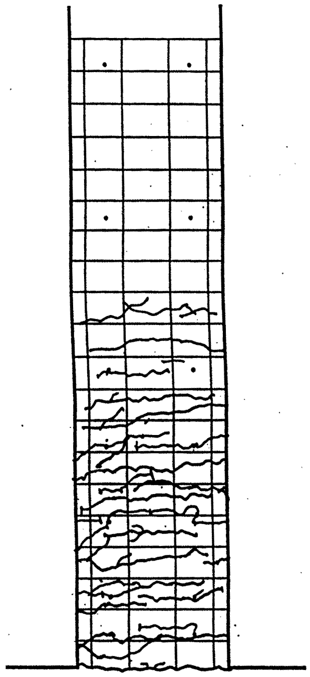

(e) 1.20 in.

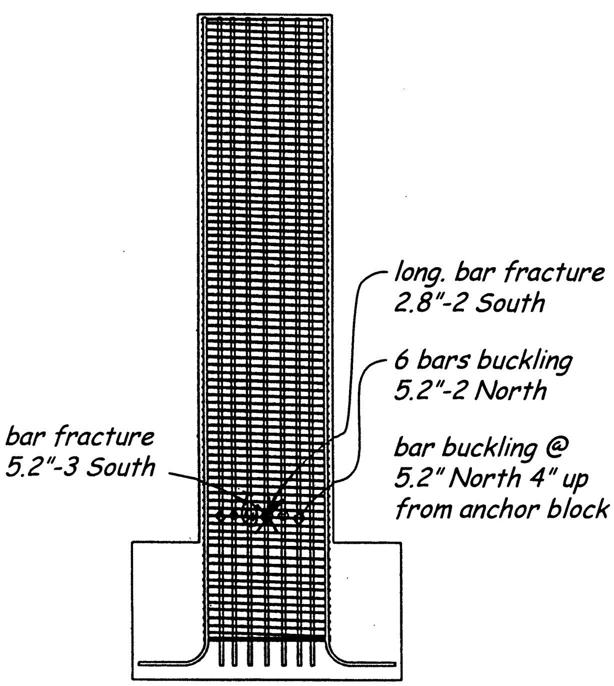

(f) end of test - rebar

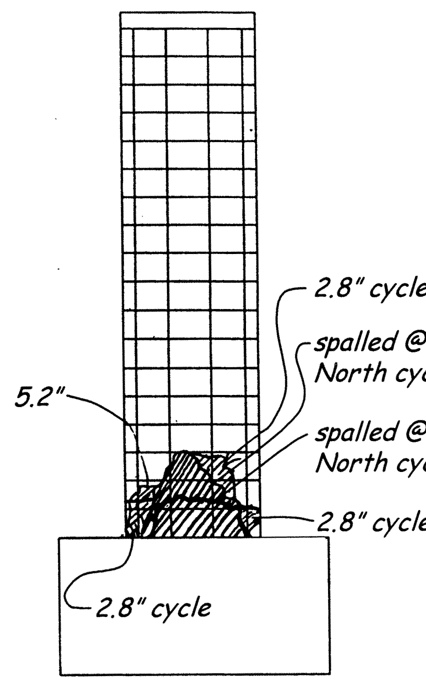

(g) end of test - spalling

Figure A.16 (continued): Progression of Damage, Column 328, North Face

(to scale)

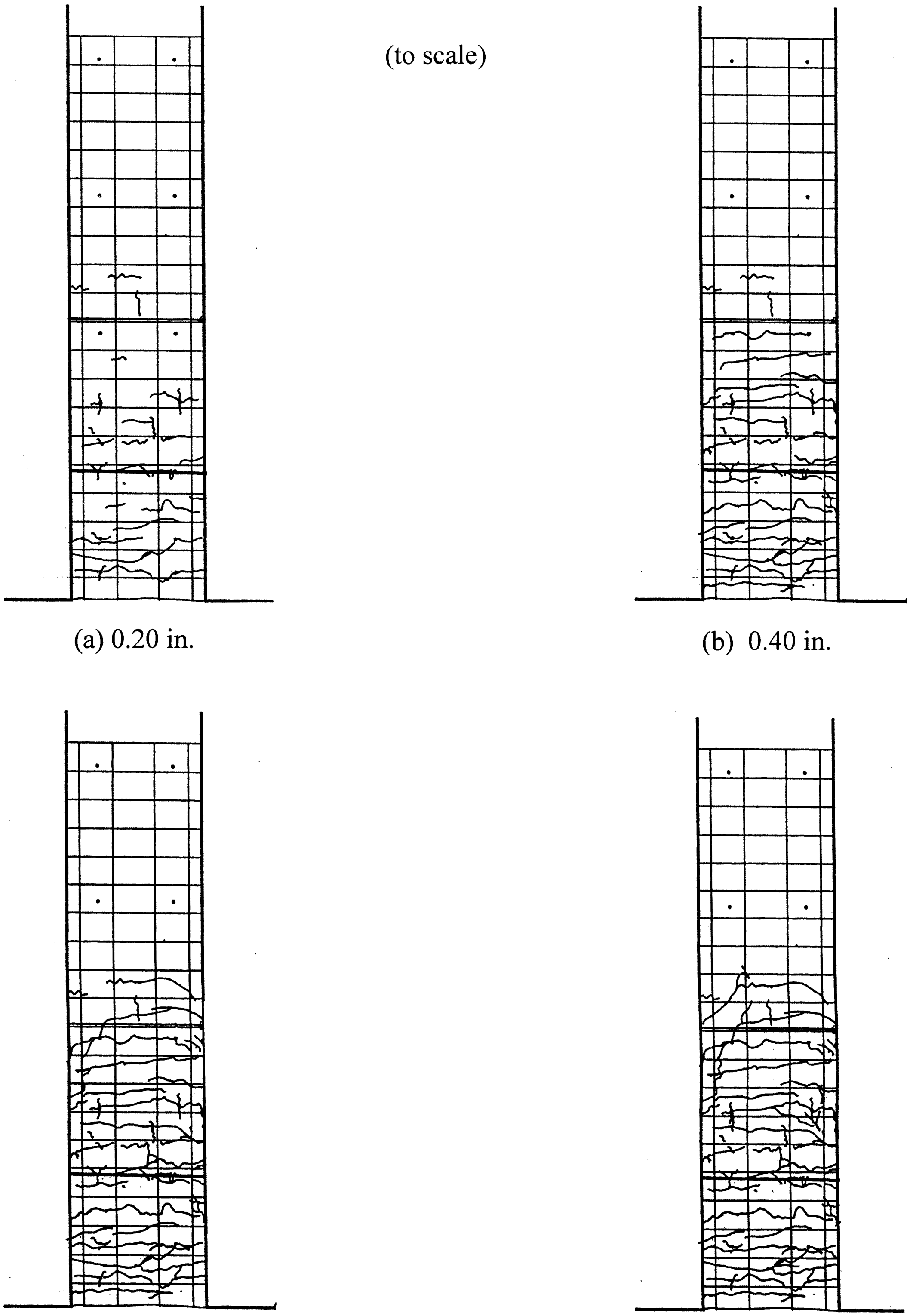

(a) 0.20 in.

(b) 0.40 in.

(c) 0.60 in.

(d) 0.80 in.

Figure A.17: Progression of Damage, Column 328T, North Face

(to scale)

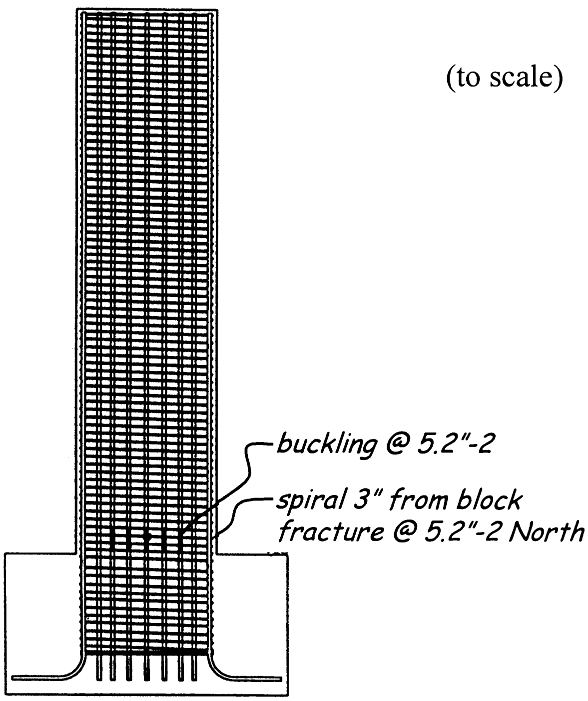

(e) end of test - rebar

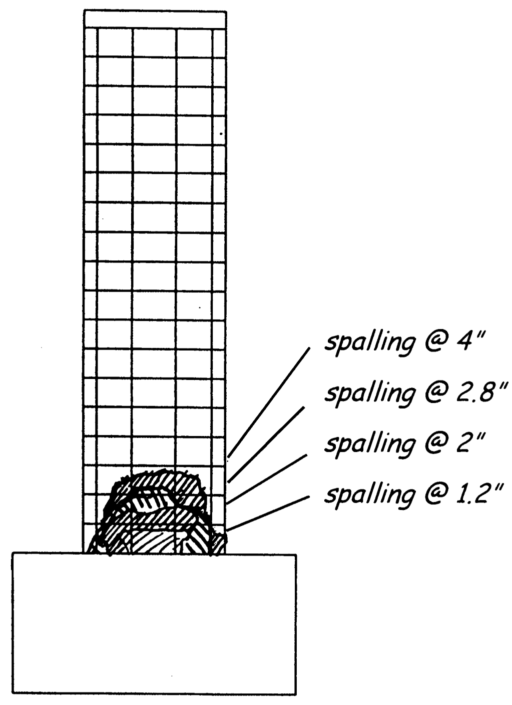

(f) end of test - spalling

Figure A.17 (continued): Progression of Damage, Column 328T, North Face

(to scale)

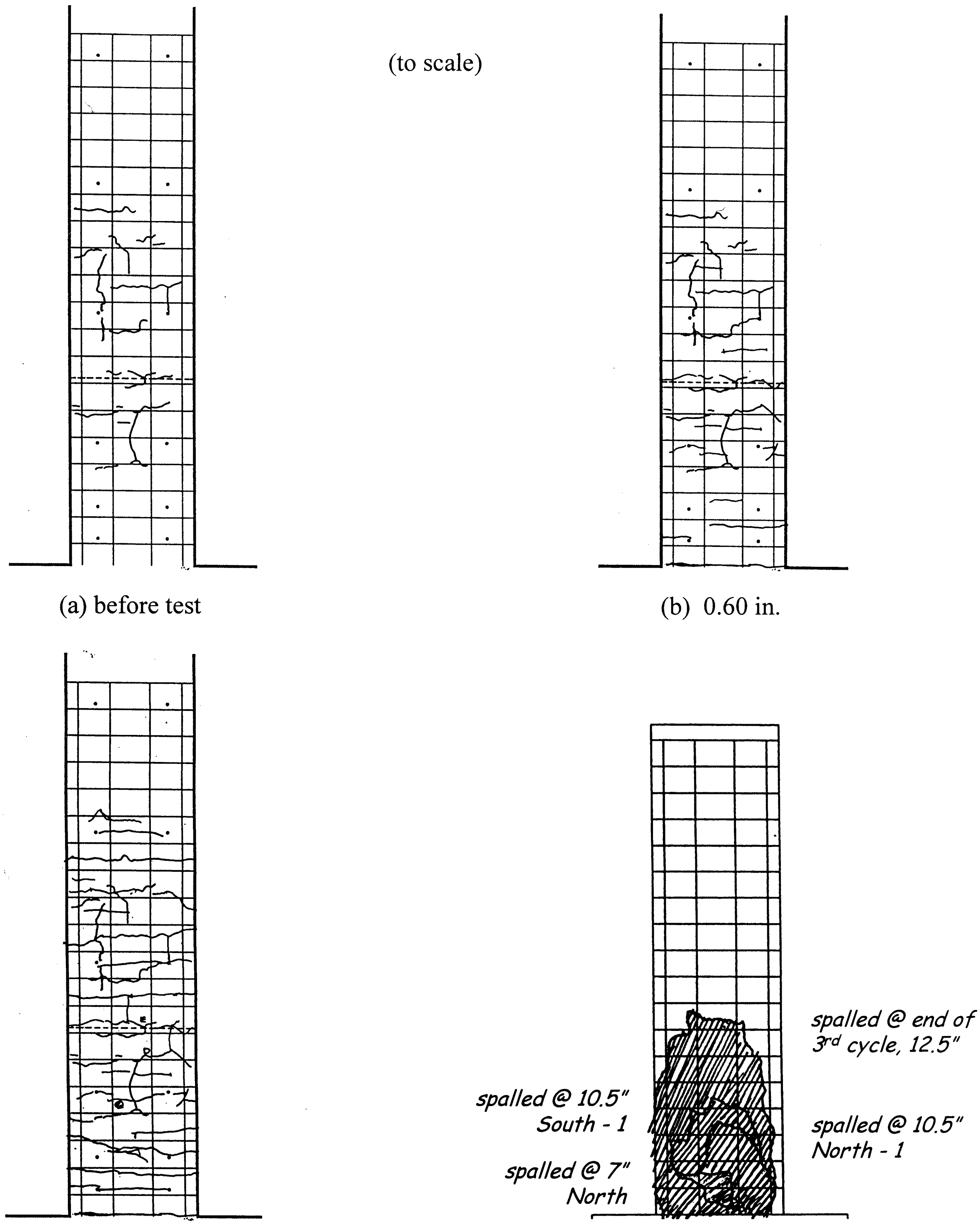

(a) before test

(b) 0.60 in.

(c) 3.5 in.

(d) end of test - spalling

Figure A.18: Progression of Damage, Column 828, North Face

(to scale)

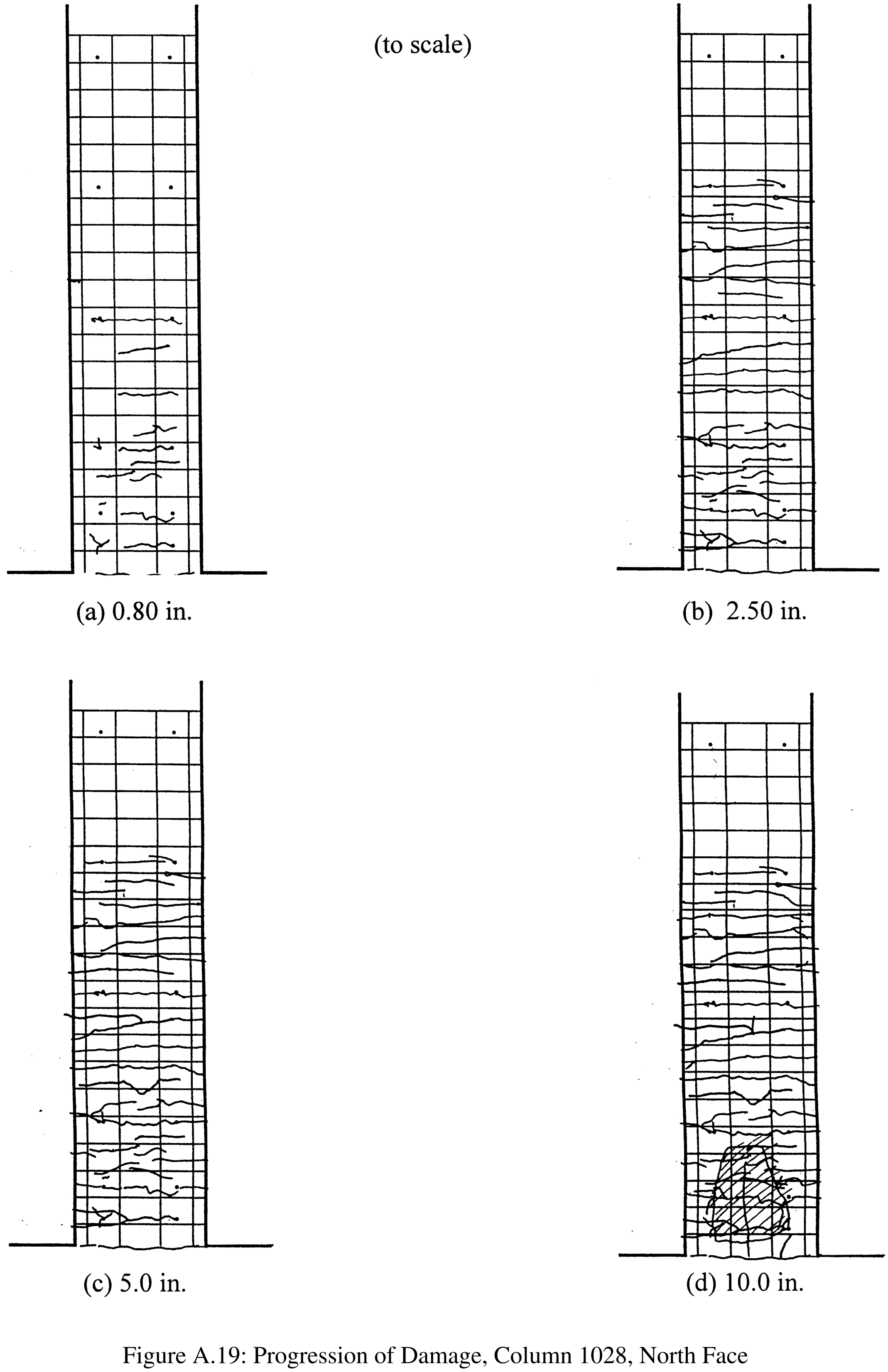

Figure A.19: Progression of Damage, Column 1028, North Face

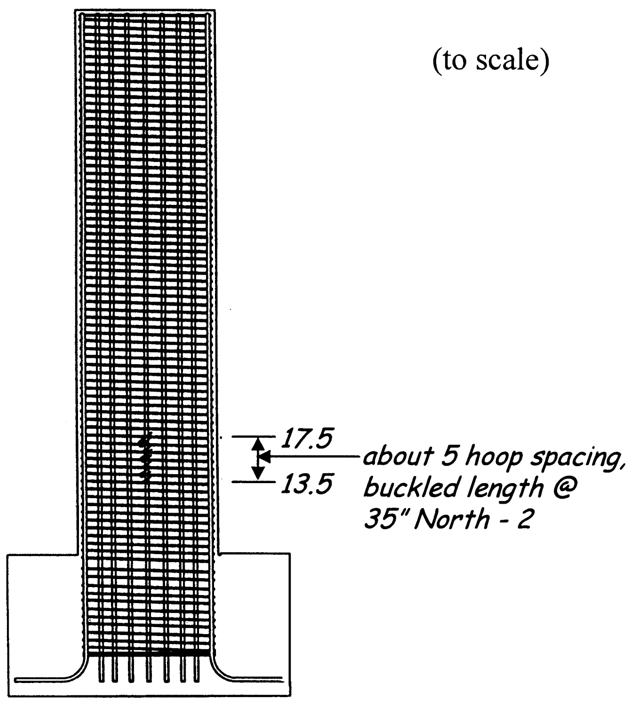

(to scale)

(e) end of test - rebar

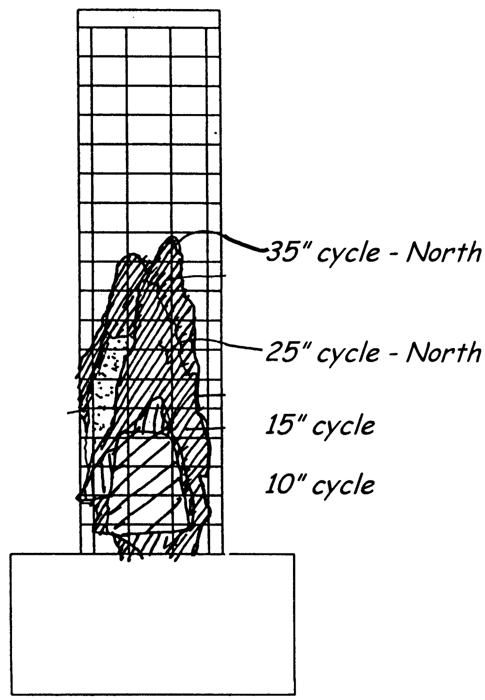

(f) end of test - spalling

Figure A.19 (continued): Progression of Damage, Column 1028, North Face

Table A.1: Measured Crack Widths (inches) for Column 328, North Face

Cycle	Elevation A		Elevation B		Elevation C		Elevation D		Elevation E	
	Peak	Zero	Peak	Zero	Peak	Zero	Peak	Zero	Peak	Zero
0.4”	0.016	0.003	0.009	0.0	0.007	0.0	0.005	0.0	0.003	0.0
0.6”	0.025	0.005	0.013	0.002	0.009	0.0	0.009	0.0	0.007	0.0
0.8”	0.04	0.007	0.02	0.005	0.01	0.0	0.01	0.0	0.007	0.0
1.2”	0.06	0.01	0.02	0.01	0.02	0.005	0.01	0.0	0.007	0.0
2.0”	0.125	0.02	0.013	0.02	0.025	0.013	0.01	0.0	0.005	0.0
2.8”	0.16	0.016	0.16	0.02	0.025	0.01	0.010	0.0	0.007	0.0
4.0”	0.187	-	0.03	0.04	0.04	0.02	0.025	0.005	0.007	0.0
5.2”	0.38	-	0.38	0.05	0.05	-	0.04	-	0.007	-

Notes:

1) Elevations A, B, C, D, and E are at 0, 5, 10.25, 21.75, and 33.25 inches, respectively, above the top of the foundation block.

2) For each cycle, readings are taken at the peak displacement at after the test specimen is returned to zero displacement.

Table A.2: Measured Crack Widths (inches) for Column 328T, North Face

Cycle	Elevation A		Elevation B		Elevation C		Elevation D		Elevation E	
	Peak	Zero	Peak	Zero	Peak	Zero	Peak	Zero	Peak	Zero
0.4”	0.013	0.002	0.003	0.0	0.003	0.0	0.005	0.0	0.002	0.0
0.6”	0.025	0.002	0.009	0.0	0.005	0.0	0.01	0.0	0.007	0.0
0.8”	0.03	0.007	0.01	0.002	0.007	0.002	0.013	0.0	0.007	0.0
1.2”	0.04	0.013	0.04	0.013	0.007	0.0	0.013	0.0	0.007	0.0
2.0”	0.156	0.02	0.016	0.016	0.007	0.0	0.013	0.0	0.007	0.0
2.8”	0.156	0.013	0.04	0.013	0.007	0.0	0.013	0.0	0.007	0.0
4.0”	0.187	-	0.02	0.013	0.02	0.007	0.016	0.002	0.007	0.0
5.2”	-	-	0.025	-	0.016	-	0.03	-	0.009	-

Notes:

1) Elevations A, B, C, D, and E are at 0, 7, 21, 24.25, and 36.25 inches, respectively, above the top of the foundation block.

2) For each cycle, readings are taken at the peak displacement at after the test specimen is returned to zero displacement.

Table A.3: Measured Crack Widths (inches) for Column 828, North Face

Cycle	Elevation A		Elevation B		Elevation C		Elevation D		Elevation E	
	Peak	Zero	Peak	Zero	Peak	Zero	Peak	Zero	Peak	Zero
1.75	0.016	0.005	0.009	0.0	0.005	0.0	0.005	0.002	0.003	0.002
3.5	0.03	0.009	0.009	0.002	0.007	0.0	0.010	0.002	0.010	0.002
5.25	0.13	0.025	0.04	0.009	0.02	0.003	0.013	0.0	0.016	0.002
7.0	0.15	0.035	0.06	0.025	0.025	0.005	0.016	0.0	0.02	0.002
10.5	0.16	0.04	0.12	0.04	0.06	0.01	0.01	0.002	0.016	0.002
17.5	0.19	-	-	-	-	-	-	-	0.06	-

Notes:

1) Elevations A, B, C, D, and E are at 0, 12, 25.5, 30.5, and 38.25 inches, respectively, above the top of the foundation block.

2) For each cycle, readings are taken at the peak displacement at after the test specimen is returned to zero displacement.

Table A.4: Measured Crack Widths (inches) for Column 1028, North Face

Cycle	Elevation A		Elevation B		Elevation C		Elevation D		Elevation E	
	Peak	Zero	Peak	Zero	Peak	Zero	Peak	Zero	Peak	Zero
5	0.03	0.005	0.02	0.003	0.01	0.0	0.013	0.002	0.013	0.0
7.5	0.06	0.016	0.04	0.013	0.015	0.0	0.025	0.005	0.016	0.003
10	0.09	0.04	0.125	0.013	0.01	0.0	0.03	0.002	0.016	0.0
15	0.14	0.06	0.03	-	0.05	0.01	0.04	0.005	0.027	0.0
25	0.16	-	0.04	0.007	0.02	0.009	0.03	0.009	0.05	0.002
35	0.19	-	0.04	-	0.04	-	0.02	-	0.03	-

Notes:

1) Elevations A, B, C, D, and E are at 0, 12.75, 23.5, 34.3 and 48 inches, respectively, above the top of the foundation block.

2) For each cycle, readings are taken at the peak displacement at after the test specimen is returned to zero displacement.

Appendix B

The following pages contain construction drawings, details, and specifications for the test specimens.

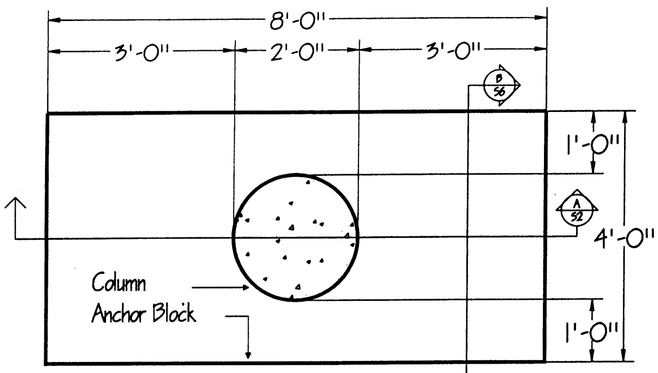

Plan of Specimen

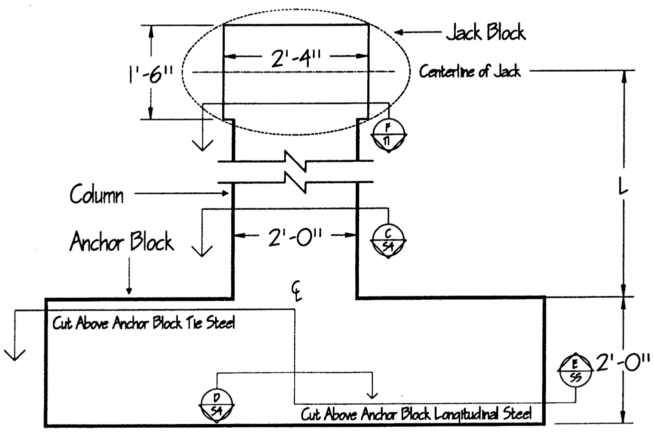

Elevation of Specimen

Notes:

1. Four specimens to be built.
2. Specimens differ only in length and in transverse steel provided
   Lengths of specimens are outlined in schedule below.
   L is measured from top of anchor block to center-line of Jack.
3. Column reinforcement layout : Section A-A, Section C-C, Section D-D
4. Anchor block reinforcement: Section A-A, Section B-B, Section E-E
5. Top 1'-6" of column is square block for Jack attachement
   Block is referred to as Jack Block. See Sheet 11.

Specimen Schedule

Specimen Number	Transverse Steel	Length
1	See Sheet 52	6'-0"
2	See Sheet 52	6'-0"
3	See Sheet 52	16'-0"
4	See Sheet 52	20'-0"

REVISIONS	BY
1	DL
2 - Oct. 24, 1996	AJC

U.C. BERKELEY COLUMN TESTS

Specimen Outline

Specimen Schedule

Date Mar. 5 1996

Scale 1":2'-0"

Drawn Dawn Lehman

Job

Sheet 51
Of Sheets

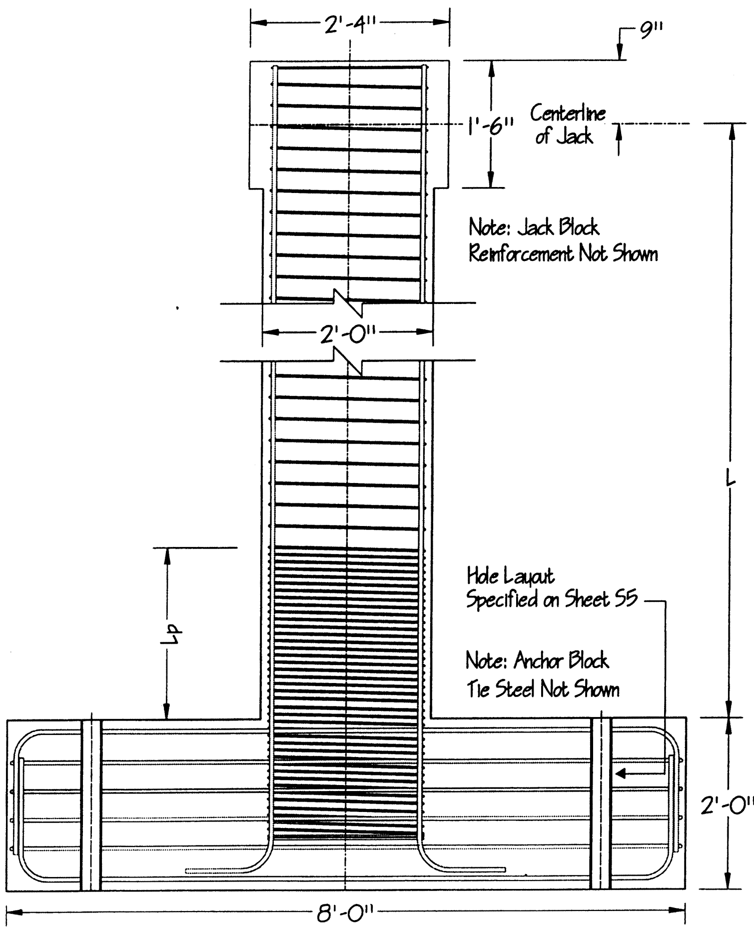

Notes:

1. Column transverse reinforcement varies as shown below.
2. Cross-section of Jack Block to be square, Sheet T1
3. Reinforcement for Jack Block Specified on Sheet T1
4. Anchor block reinforcement specified on Sheet S6
5. Spiral shall end with 1 1/2 turns anchored into cross-section. No splices shall be allowed in spiral reinforcement.
6. No splices will be allowed in column longitudinal reinforcement.
7. Spiral spacing changes above length Lp for column. Length Lp and spiral spacing are specified in schedule below.

Transverse Reinforcement Schedule

Specimen Number	Lp	Within Lp	Above Lp
1	2'-0"	No. 2 @ 1" o.c.	No. 2 @ 3" o.c.
2	2'-0"	No. 2 @ 1" o.c.	No. 2 @ 1" o.c.
3	3'-0"	No. 2 @ 1" o.c.	No. 2 @ 2" o.c.
4	4'-0"	No. 2 @ 1" o.c.	No. 2 @ 2" o.c.

REVISIONS	BY
1	DL
2 - Oct. 24, 1996	AJC

U.C. BERKELEY COLUMN TESTS

Section A-A
Column Elevation
Spiral Schedule and Anchor Detail

Date	Mar. 5 1996
Scale	1" : 1'-6"
Drawn	Dawn Lehman
Job	
Sheet	S2
Of	Sheets

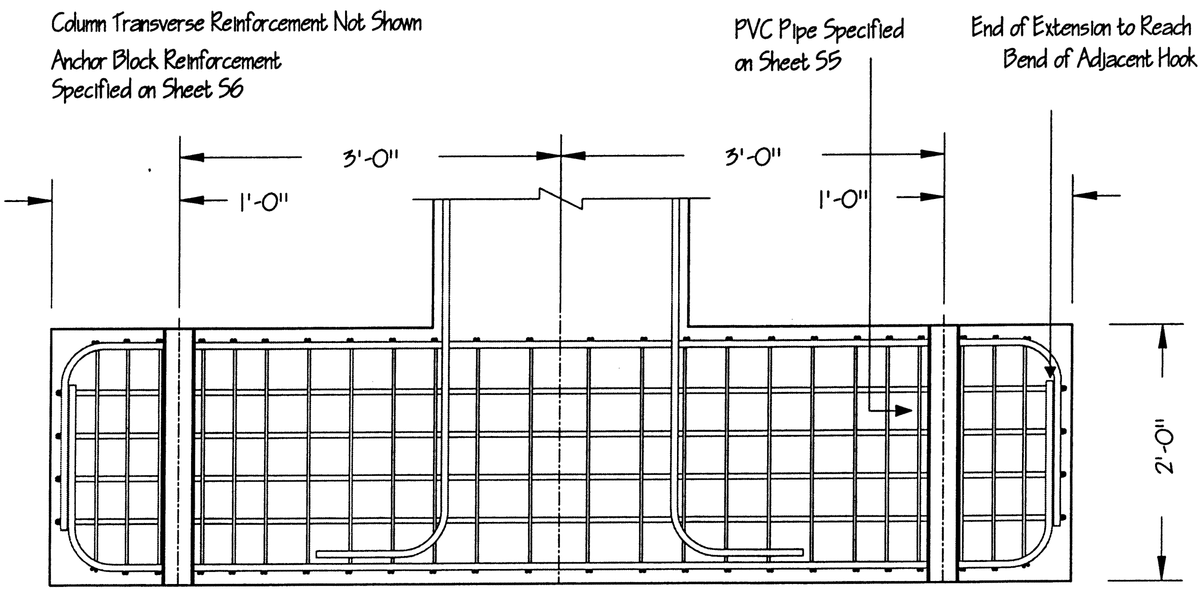

REVISIONS	BY
1 - Oct. 24, 1996	AJC

U.C. BERKELEY COLUMN TESTS

Section A-A

Anchor Block Elevation

Date	Feb. 12 1996
Scale	1" : 1'-0"
Drawn	Dawn Lehman
Job	
Sheet	53
Of	Sheets

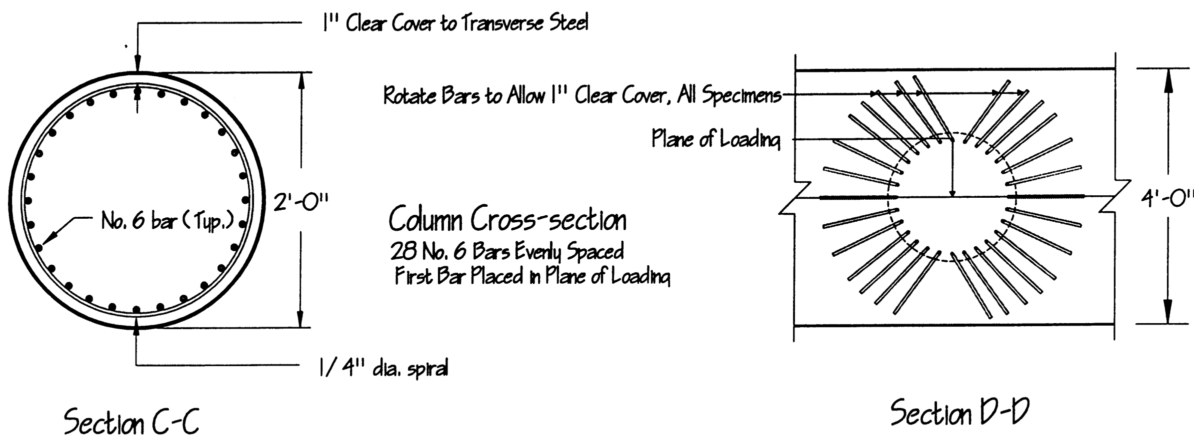

REVISIONS	BY
1 - Oct. 24, 1996	AJC

U.C. BERKELEY COLUMN TESTS

Section C-C
Column Cross-Section
Section D-D
Longitudinal Hook Layout

Date	Feb. 12 1996
Scale	Varies
Drawn	Dawn Lehman
Job	
Sheet	54
Of	Sheets

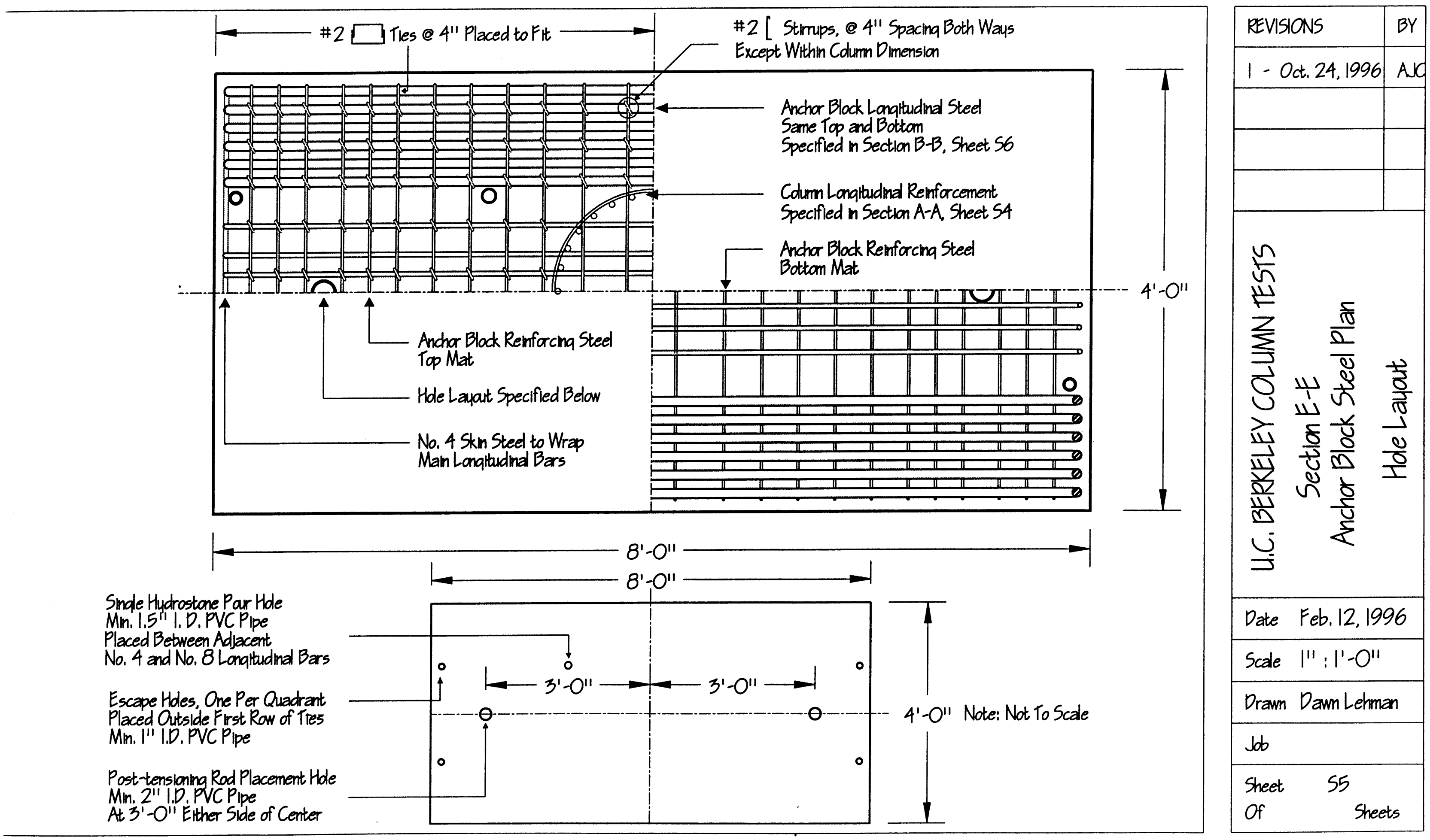

#2 Ties @ 4'' Placed to Fit
#2 [Stirrups, @ 4'' Spacing Both Ways
Except Within Column Dimension
Anchor Block Longitudinal Steel
Same Top and Bottom
Specified in Section B-B, Sheet 56
Column Longitudinal Reinforcement
Specified in Section A-A, Sheet 54
Anchor Block Reinforcing Steel
Bottom Mat
Anchor Block Reinforcing Steel
Top Mat
Hole Layout Specified Below
No. 4 Skin Steel to Wrap
Main Longitudinal Bars
4'-0''
8'-0''
8'-0''
Single Hydrostone Pour Hole
Min. 1.5'' I.D. PVC Pipe
Placed Between Adjacent
No. 4 and No. 8 Longitudinal Bars
Escape Holes, One Per Quadrant
Placed Outside First Row of Ties
Min. 1'' I.D. PVC Pipe
Post-tensioning Rod Placement Hole
Min. 2'' I.D. PVC Pipe
At 3'-0'' Either Side of Center
3'-0''
3'-0''
4'-0'' Note: Not To Scale
REVISIONS
BY
1 - Oct. 24, 1996
AJC
U.C. BERKELEY COLUMN TESTS
Section E-E
Anchor Block Steel Plan
Hole Layout
Date Feb. 12, 1996
Scale 1'' : 1'-0''
Drawn Dawn Lehman
Job
Sheet 55
Of Sheets

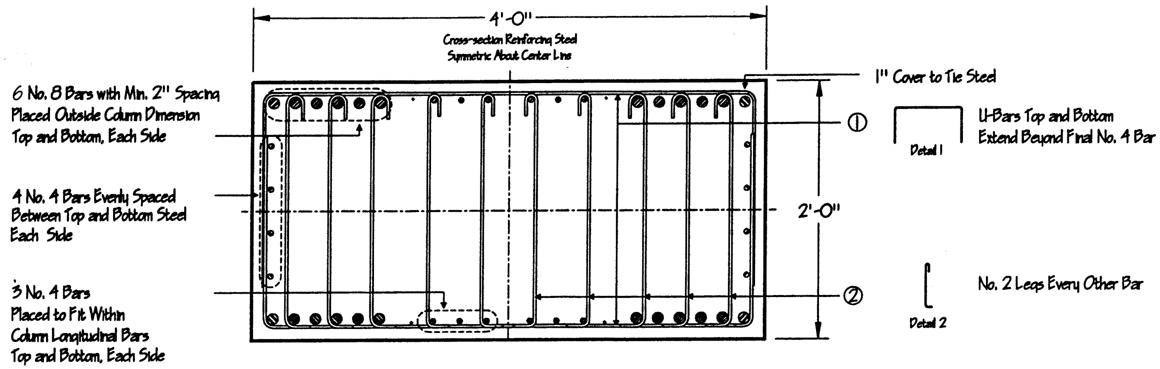

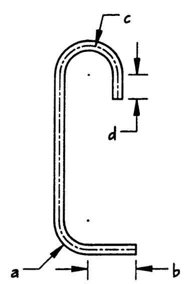

Note:
Bar Dimensions and Quantities Shall Be
Determined by the Contractor
Indicated on the Shop Drawings
And Approved by the Owner
* May be longer if necessary

Abbreviations:
B.S.L. : Based on Reinforcement Layout
See Drawings For Details
F.A.B. : To Fit Around Adjacent Bar
N.A. : Not Applicable

Location	Type	a	b	c	d
Column	Longitudinal No. 6 Bars	$5d_b$	$12d_b$	N.A.	N.A.
Anchor Block	Longitudinal No. 8 Bars	$3d_b$	B.S.L.	N.A.	N.A.
Anchor Block	Longitudinal No. 4 Bars	$3d_b$	B.S.L.	N.A.	N.A.
Anchor Block	Skin Steel No. 4 Bars	$3d_b$	B.S.L.	N.A.	N.A.
Anchor Block	U-Bars ① No. 2 Stirrups	F.A.B.	B.S.L.	N.A.	N.A.
Anchor Block	Legs ② No. 2 Stirrups	F.A.B.	$6d_b$*	F.A.B.	$4d_b$
Jack Block	No. 4 Hoops 135° hooks	N.A.	N.A.	F.A.B.	$6d_b$

REVISIONS	BY
1	DL
2 - Oct. 24, 1996	AJC
3 - Jan. 7, 1996	Ade

U.C. BERKELEY COLUMN TESTS

Section B-B
Anchor Block Cross-Section
Hook and Extension Schedule

Date Mar. 5 1996
Scale 1" : 1'-0"
Drawn Dawn Lehman
Job
Sheet 56
Of Sheets

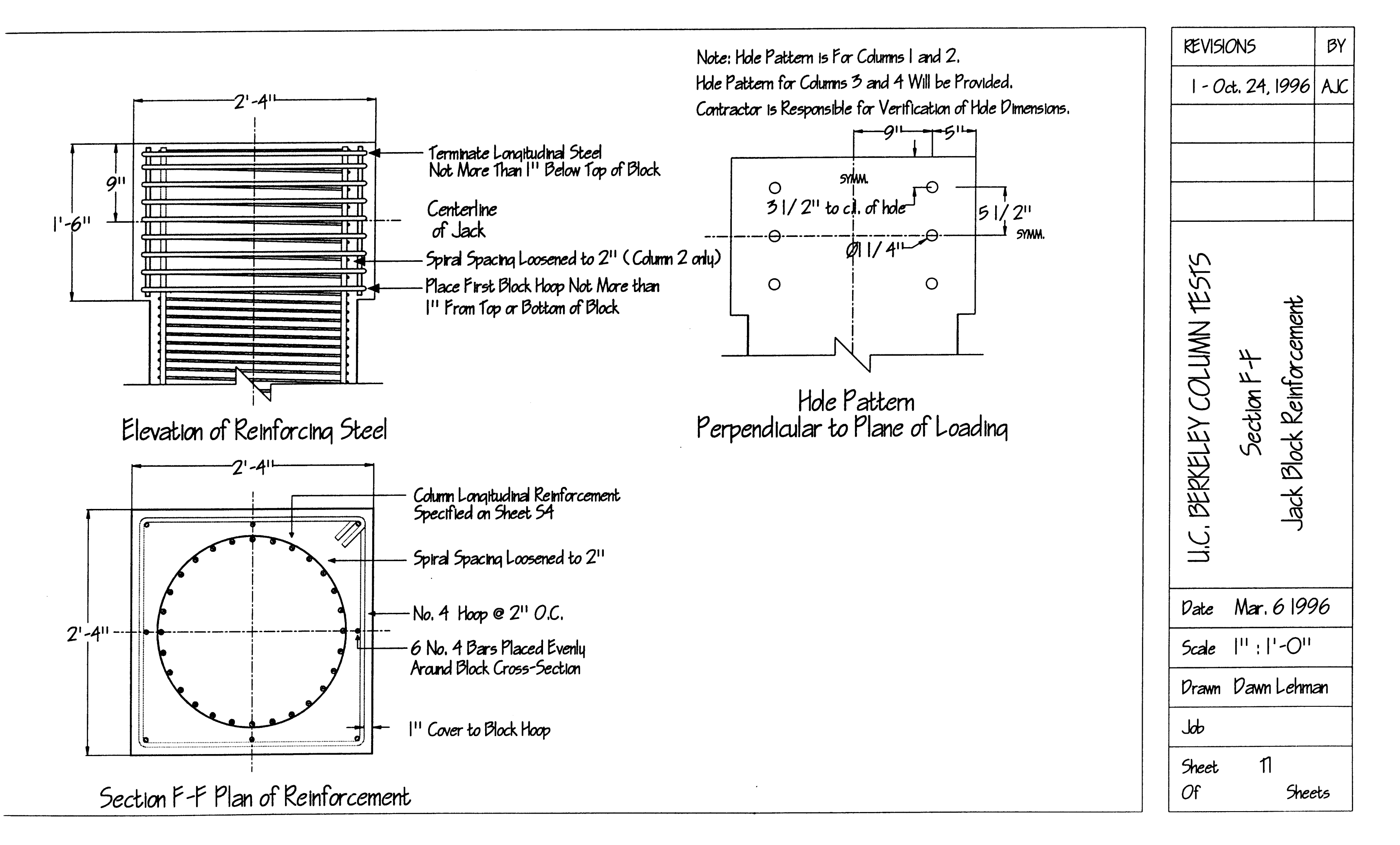
Note: Hole Pattern is For Columns 1 and 2.
Hole Pattern for Columns 3 and 4 Will be Provided.
Contractor is Responsible for Verification of Hole Dimensions.
2'-4"
9"
1'-6"
Terminate Longitudinal Steel Not More Than 1" Below Top of Block
Centerline of Jack
Spiral Spacing Loosened to 2" (Column 2 only)
Place First Block Hoop Not More than 1" From Top or Bottom of Block
Elevation of Reinforcing Steel
9"
5"
SYMM.
3 1/2" to c.l. of hole
5 1/2"
SYMM.
Ø1 1/4"
Hole Pattern
Perpendicular to Plane of Loading
2'-4"
2'-4"
Column Longitudinal Reinforcement Specified on Sheet S4
Spiral Spacing Loosened to 2"
No. 4 Hoop @ 2" O.C.
6 No. 4 Bars Placed Evenly Around Block Cross-Section
1" Cover to Block Hoop
Section F-F Plan of Reinforcement
REVISIONS
BY
1 - Oct. 24, 1996
AJC
U.C. BERKELEY COLUMN TESTS
Section F-F
Jack Block Reinforcement
Date Mar. 6 1996
Scale 1" : 1'-0"
Drawn Dawn Lehman
Job
Sheet 11
Of Sheets

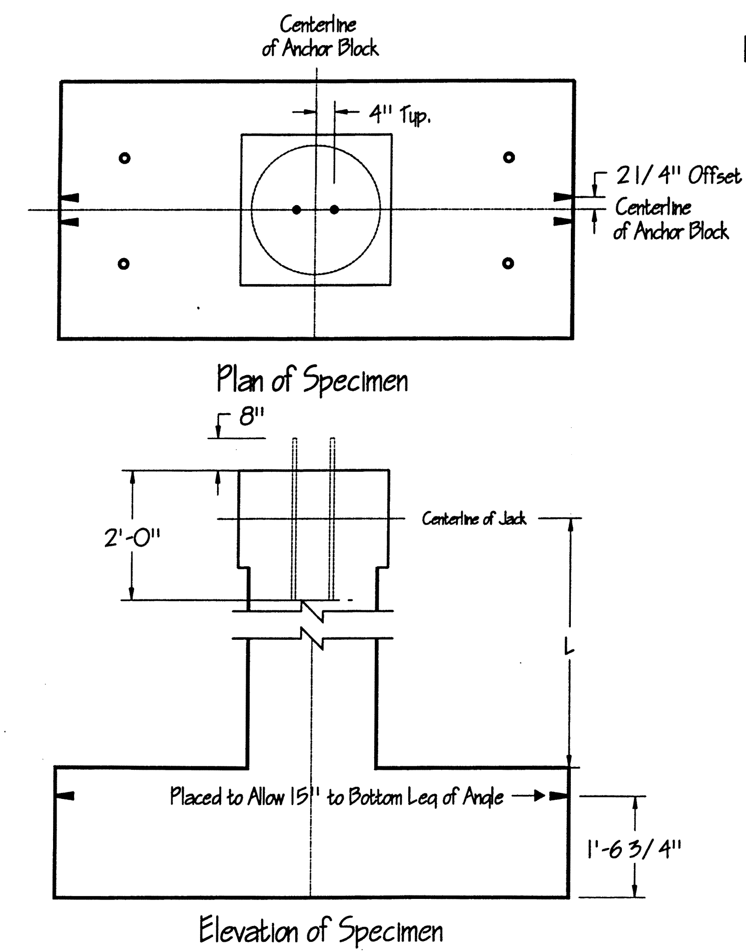

Notes:

1. 1" Burke Hi-tensile inserts to be placed in specimen.
   Approximate locations shown on drawings.
   Actual locations shall be determined by the contractor and verified by the owner.
2. Two inserts shall be embedded horizontally on each side of the anchor block.
   Locate inserts to correspond with location of angle holes.
   Actual locations shall be determined by the contractor and verified by the owner.
3. 1 insert shall be placed in each quadrant of the anchor block.
   Locate inserts to fit between last No. 8 bar and first No. 4 bar (Sheet 55).
   Actual locations shall be determined by the contractor and verified by the owner.
4. Two 3/ 4" diameter threaded rods to be embedded 24" into column.
   Extend 3/ 4" diameter rod 8" out of column.
   Approximate locations shown on drawings.
   Actual locations shall be determined by the contractor and verified by the owner.
5. The following key describes the symbols used

○	1" Hi tensile insert placed vertically
▶	1" Hi tensile insert placed horizontally
●	3/ 4" Threaded rod, embed 24", extend 6"

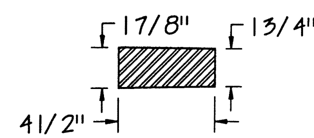

1" Burke Hi-Tensile Insert

REVISIONS	BY
1	DL
2 - Oct. 24, 1996	AJC

U.C. BERKELEY COLUMN TESTS

Specimen Lifting Devices

Date	Mar. 6 1996
Scale	1":2'-0"
Drawn	Dawn Lehman
Job	
Sheet	T2
Of	Sheets

PEER REPORTS

PEER reports are available from the National Information Service for Earthquake Engineering (NISEE). To order PEER reports, please contact the Pacific Earthquake Engineering Research Center, 1301 South 46th Street, Richmond, California 94804-4698. Tel.: (510) 231-9468; Fax: (510) 231-9461.

PEER 2001/05 *Stiffness Analysis of Fiber-Reinforced Elastomeric Isolators.* Hsiang-Chuan Tsai and James M. Kelly. May 2001. $20.00

PEER 2001/03 *A Modal Pushover Analysis Procedure to Estimate Seismic Demands for Buildings: Theory and Preliminary Evaluation.* Anil K. Chopra and Rakesh K. Goel. January 2001. $15.00

PEER 2001/02 *Seismic Response Analysis of Highway Overcrossings Including Soil-Structure Interaction.* Jian Zhang and Nicos Makris. March 2001. $20.00

PEER 2001/01 *Experimental Study of Large Seismic Steel Beam-to-Column Connections.* Egor P. Popov and Shakhzod M. Takhirov. November 2000. $15.00

PEER 2000/09 *Structural Engineering Reconnaissance of the August 17, 1999 Earthquake: Kocaeli (Izmit), Turkey.* Halil Sezen, Kenneth J. Elwood, Andrew S. Whittaker, Khalid Mosalam, John J. Wallace, and John F. Stanton. December 2000. $20.00

PEER 2000/08 *Behavior of Reinforced Concrete Bridge Columns Having Varying Aspect Ratios and Varying Lengths of Confinement.* Anthony J. Calderone, Dawn E. Lehman, and Jack P. Moehle. January 2001. $20.00

PEER 2000/07 *Cover-Plate and Flange-Plate Reinforced Steel Moment-Resisting Connections.* Taejin Kim, Andrew S. Whittaker, Amir S. Gilani, Vitelmo V. Bertero, and Shakhzod M. Takhirov. September 2000. $33.00

PEER 2000/06 *Seismic Evaluation and Analysis of 230-kV Disconnect Switches.* Amir S. J. Gilani, Andrew S. Whittaker, Gregory L. Fenves, Chun-Hao Chen, Henry Ho, and Eric Fujisaki. July 2000. $26.00

PEER 2000/05 *Performance-Based Evaluation of Exterior Reinforced Concrete Building Joints for Seismic Excitation.* Chandra Clyde, Chris P. Pantelides, and Lawrence D. Reaveley. July 2000. $15.00

PEER 2000/04 *An Evaluation of Seismic Energy Demand: An Attenuation Approach.* Chung-Che Chou and Chia-Ming Uang. July 1999. $20.00

PEER 2000/03 *Framing Earthquake Retrofitting Decisions: The Case of Hillside Homes in Los Angeles.* Detlof von Winterfeldt, Nels Roselund, and Alicia Kitsuse. March 2000. $13.00

PEER 2000/02 *U.S.-Japan Workshop on the Effects of Near-Field Earthquake Shaking.* Andrew Whittaker, ed. July 2000. $20.00

PEER 2000/01 *Further Studies on Seismic Interaction in Interconnected Electrical Substation Equipment.* Armen Der Kiureghian, Kee-Jeung Hong, and Jerome L. Sackman. November 1999. $20.00

PEER 1999/14 *Seismic Evaluation and Retrofit of 230-kV Porcelain Transformer Bushings*. Amir S. Gilani, Andrew S. Whittaker, Gregory L. Fenves, and Eric Fujisaki. December 1999. $26.00

PEER 1999/12 *Rehabilitation of Nonductile RC Frame Building Using Encasement Plates and Energy-Dissipating Devices.* Mehrdad Sasani, Vitelmo V. Bertero, James C. Anderson. December 1999. $26.00

PEER 1999/11 *Performance Evaluation Database for Concrete Bridge Components and Systems under Simulated Seismic Loads.* Yael D. Hose and Frieder Seible. November 1999. $20.00

PEER 1999/10 *U.S.-Japan Workshop on Performance-Based Earthquake Engineering Methodology for Reinforced Concrete Building Structures.* December 1999. $33.00

PEER 1999/09 *Performance Improvement of Long Period Building Structures Subjected to Severe Pulse-Type Ground Motions*. James C. Anderson, Vitelmo V. Bertero, and Raul Bertero. October 1999. $26.00

PEER 1999/08 *Envelopes for Seismic Response Vectors.* Charles Menun and Armen Der Kiureghian. July 1999. $26.00

PEER 1999/07 *Documentation of Strengths and Weaknesses of Current Computer Analysis Methods for Seismic Performance of Reinforced Concrete Members.* William F. Cofer. November 1999. $15.00

PEER 1999/06 *Rocking Response and Overturning of Anchored Equipment under Seismic Excitations.* Nicos Makris and Jian Zhang. November 1999. $15.00

PEER 1999/05 *Seismic Evaluation of 550 kV Porcelain Transformer Bushings.* Amir S. Gilani, Andrew S. Whittaker, Gregory L. Fenves, and Eric Fujisaki. October 1999. $15.00

PEER 1999/04 *Adoption and Enforcement of Earthquake Risk-Reduction Measures.* Peter J. May, Raymond J. Burby, T. Jens Feeley, and Robert Wood. $15.00

PEER 1999/03 *Task 3 Characterization of Site Response General Site Categories*. Adrian Rodriguez-Marek, Jonathan D. Bray, and Norman Abrahamson. February 1999. $20.00

PEER 1999/02 *Capacity-Demand-Diagram Methods for Estimating Seismic Deformation of Inelastic Structures: SDF Systems*. Anil K. Chopra and Rakesh Goel. April 1999. $15.00

PEER 1999/01 *Interaction in Interconnected Electrical Substation Equipment Subjected to Earthquake Ground Motions.* Armen Der Kiureghian, Jerome L. Sackman, and Kee-Jeung Hong. February 1999. $20.00

PEER 1998/08 *Behavior and Failure Analysis of a Multiple-Frame Highway Bridge in the 1994 Northridge Earthquake.* Gregory L. Fenves and Michael Ellery. December 1998. $20.00

PEER 1998/07 *Empirical Evaluation of Inertial Soil-Structure Interaction Effects.* Jonathan P. Stewart, Raymond B. Seed, and Gregory L. Fenves. November 1998. $26.00

PEER 1998/06 *Effect of Damping Mechanisms on the Response of Seismic Isolated Structures.* Nicos Makris and Shih-Po Chang. November 1998. $15.00

PEER 1998/05 *Rocking Response and Overturning of Equipment under Horizontal Pulse-Type Motions.* Nicos Makris and Yiannis Roussos. October 1998. $15.00

PEER 1998/04 *Pacific Earthquake Engineering Research Invitational Workshop Proceedings, May 14–15, 1998: Defining the Links between Planning, Policy Analysis, Economics and Earthquake Engineering.* Mary Comerio and Peter Gordon. September 1998. $15.00

PEER 1998/03 *Repair/Upgrade Procedures for Welded Beam to Column Connections.* James C. Anderson and Xiaojing Duan. May 1998. $33.00

PEER 1998/02 *Seismic Evaluation of 196 kV Porcelain Transformer Bushings.* Amir S. Gilani, Juan W. Chavez, Gregory L. Fenves, and Andrew S. Whittaker. May 1998. $20.00

PEER 1998/01 *Seismic Performance of Well-Confined Concrete Bridge Columns.* Dawn E. Lehman and Jack P. Moehle. December 2000. $33.00